

The Penikat Intrusion, Finland: Geochemistry, Geochronology, and Origin of Platinum–Palladium Reefs

W. D. Maier^{1*}, T. Halkoaho², H. Huhma³, E. Hanski⁴ and S.-J. Barnes⁵

¹School of Earth and Ocean Sciences, Cardiff University, Cardiff, UK; ²Geological Survey of Finland, Kuopio, Finland; ³Geological Survey of Finland, Espoo, Finland; ⁴Oulu Mining School, Oulu, Finland; ⁵Université du Québec à Chicoutimi, Quebec, Canada

*Corresponding author. E-mail: MaierW@cardiff.ac.uk

Received November 21, 2016; Accepted May 8, 2018

ABSTRACT

The Palaeoproterozoic Penikat layered ultramafic–mafic intrusion in northern Finland is one of the most richly mineralized layered intrusions on Earth, containing at least six platinum-group element (PGE) enriched horizons exposed along >20 km of strike, amongst them the SJ reef, which at ~3–7 ppm Pt + Pd over a width of ~1–2 m is surpassed by few other PGE reefs globally in terms of its endowment in PGE. Important PGE enrichments also occur in the PV reef (average 2.6 ppm Pd, 4 ppm Pt over 1.1 m) and AP1 reef (average 6.2 ppm Pd, 1.7 ppm Pt over 0.7 m). Here we present new major and high-precision trace element and Nd isotope data from a traverse across the intrusion, and a new U–Pb age of 2444 ± 8 Ma for the intrusion. We show that the PGE reefs formed by predominantly orthomagmatic processes as, for example, reflected by well-defined positive correlations between Pt + Pd and Os + Ir + Ru contents. Late-magmatic fluids played no significant role in concentrating PGE. There are at least six cyclic units in the intrusion, displaying a progressive upward decrease in differentiation indices Mg# and Cr/V. Subdued stratigraphic variations in incompatible trace element ratios (Ce/Sm mostly 5–10) and Nd isotope compositions (ϵ_{Nd} –3 to –1) indicate that mixing of magmas of distinct lineage, or *in situ* contamination with country rocks, was not required to form the PGE reefs. There is also no evidence for addition of external sulphur to the magma, based on S/Se ratios at, or below, primitive mantle levels. Instead, we propose that sulphide melt saturation at Penikat was reached in response to fractionation of a siliceous, high-magnesium basalt, and that the sulphides were concentrated through hydrodynamic phase sorting, consistent with bonanza-style PGE grades in large potholes.

Key words: platinum-group elements; chromite; Palaeoproterozoic; layered intrusion; Finland

INTRODUCTION

Layered intrusions host the bulk of global resources in platinum-group elements (PGE) that are crucial in the production of vehicle exhaust catalytic converters and many other applications in, for example, the chemical and electrical industry. However, at present only four intrusions globally are mined for PGE as the main product, namely Bushveld (South Africa), Great Dyke (Zimbabwe), Stillwater (USA) and Lac des Iles (Canada). Among sub-economic intrusions, the Penikat intrusion is perhaps the most richly mineralized, yet it remains

relatively little studied, with few contributions having appeared in the literature since the early 1990s, following the discovery of the mineralization in the late 1980s. In this study, we first review the geology and PGE mineralization styles of the Penikat intrusion. We then present new U–Pb zircon data to refine the age of the intrusion using *in situ* laser ablation inductively coupled plasma mass spectrometry analysis, and new whole-rock major and trace element as well as Nd isotopic data to propose a new model for the origin of the PGE reefs.

2.44–2.50 Ga layered intrusions in the Fennoscandian Shield

The northeastern part of the Fennoscandian Shield hosts more than two dozen Palaeoproterozoic layered mafic–ultramafic intrusions (Fig. 1). Uranium–lead zircon and Sm–Nd whole-rock data have yielded a mean age for the Finnish intrusions of ~2440 Ma (Huhma *et al.*, 1990, 2018). In Russia, the ages of the intrusions span a wider range, from c. 2450 to 2500 Ma (for a summary, see Hanski & Melezhik, 2012), possibly reflecting two distinct mantle plume events, analogous to the 2445–2490 Ma Matachewan and 2510 Ma Mistassini events of the Superior craton (Ernst & Bleeker, 2010), which was probably attached to Fennoscandia at the time.

The intrusions were formed by bimodal igneous activity, resulting in mafic and felsic, plutonic and extrusive rocks in Finland and NW Russia. Magnesian basaltic to dacitic volcanic rocks are exposed in the Vetreny belt, whereas felsic volcanic rocks (Hanski, 2012) and rapakivi-type granite batholiths (Rämö & Luukkonen, 2001) occur in the Imandra Varzuga belt

and greenstone belts in northeastern Finland, closely associated with the coeval 2.44 Ga Koillismaa and Akanvaara layered intrusions. Magmatism was triggered by plume-driven aborted break-up of the Archaean Kenorland supercontinent (Amelin *et al.*, 1995; Hanski *et al.*, 2001; Hanski & Huhma, 2005) and was concentrated in linear belts tracing intracratonic rift zones (Fig. 1). In Finland and neighbouring Sweden, several intrusive belts or clusters can be distinguished (Alapieti *et al.*, 1990; Iljina & Hanski, 2005), including those in central Lapland (Koitelainen and Akanvaara intrusions), northwestern Lapland (Tsohkoivi, Kelottijärvi, Kurkovare, Keukiskero), and in north-central Finland. The last is the most mineralized, comprising an ~300 km long, west–east-trending belt named the Tornio–Näränkäväära belt (TNB), which includes Penikat, the target of this study, as well as the Tornio, Kemi, Portimo, Koillismaa and Näränkäväära intrusions. The compositions of the intrusions vary from ultramafic dominated (Tornio and Näränkäväära) to mafic–ultramafic interlayered (Kemi, Penikat, Portimo), to

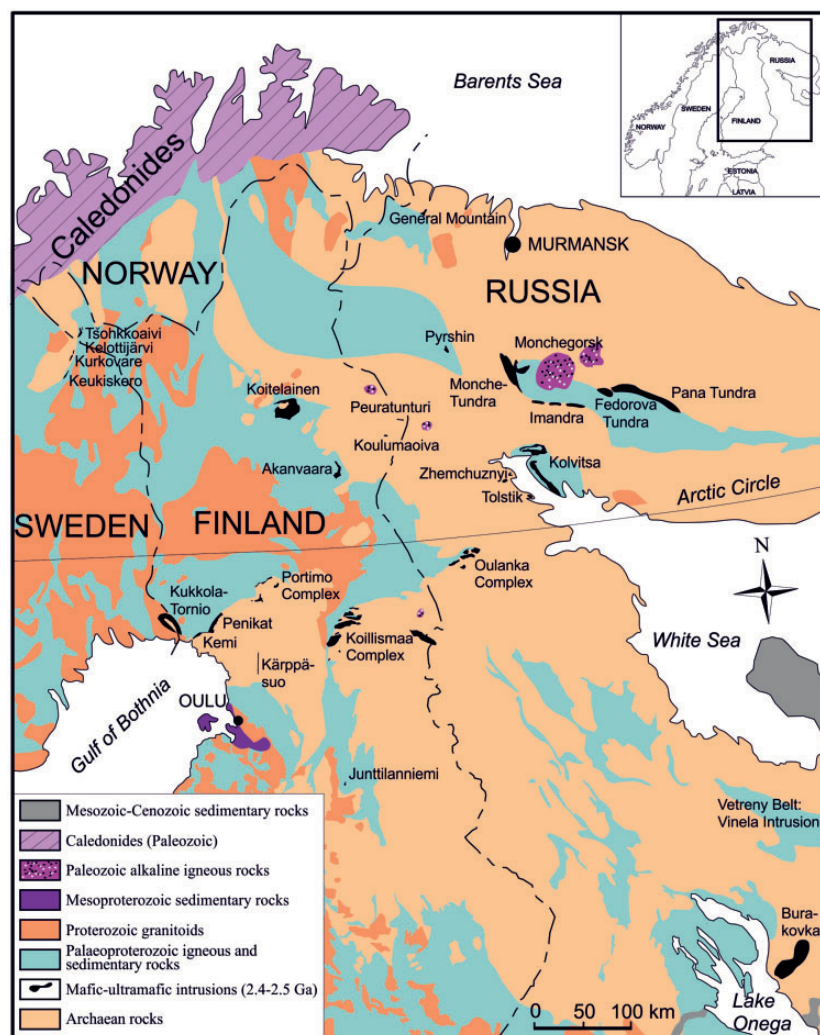


Fig. 1. Simplified geological map of part of the Fennoscandian Shield, highlighting location of 2.44–2.5 Ga layered intrusions. Figure modified after Alapieti & Lahtinen (1989).

predominantly mafic (Koillismaa). Based on similarities in their stratigraphy (Iljina & Hanski, 2005; Karinen *et al.*, 2015), some of the intrusions, or parts of them, may represent dismembered fragments of one or several larger magmatic bodies. The footwall to most of the intrusions consists of Archaean granite gneiss basement rocks, whereas the hanging-wall rocks consist of Palaeoproterozoic metavolcanic rocks or younger supracrustal sequences deposited on a Palaeoproterozoic erosional unconformity (e.g. Alapieti *et al.*, 1989, 1990; Karinen, 2010). This may imply a relatively shallow emplacement depth followed by tilting, faulting, rapid uplift and partial erosion of the intrusions. Gravity and seismic surveys indicate that the intrusions plunge underneath the Proterozoic cover rocks for several kilometres (Kukkonen *et al.*, 2010; Iljina & Salmirinne, 2011).

The Finnish layered intrusions contain a wide range of PGE mineralization styles, including narrow silicate-hosted reefs at Penikat and Portimo that are analogous to the Merensky Reef of the Bushveld Complex, wide contact-style reefs at Portimo and Koillismaa, analogous to the Platreef of the Bushveld, PGE-bearing chromitite layers at Kemi, Koitelainen, Akanvaara and Penikat, analogous to those in many other layered intrusions, and an unusual style of vein-hosted footwall mineralization (i.e. the Kilvenjärvi offset veins at Portimo; Andersen *et al.*, 2006), that has rarely been identified in other layered intrusions. None of the intrusions is currently exploited for PGE, but an exploration programme in the Suhanko block of the Portimo intrusion is at an advanced feasibility stage (Puritch *et al.*, 2007).

Geology and lithostratigraphy of the Penikat intrusion

The Penikat intrusion is a SW–NE-trending body located ~20–30 km to the NE of Kemi, in southern Lapland (Fig. 1). Its exposed portion is 23 km long and 1.5–3.5 km wide (Halkoaho, 1993). The deepest boreholes intersecting rocks of the intrusion, drilled by the Arctic Platinum Project, reach ~500 m, and the seismic reflection data of Kukkonen *et al.* (2010) indicate that the intrusion and its PGE reefs extend to a depth of about 2.5 km, consistent with the gravity model of Lerssi (1990). Layering is mostly not overturned and dips 40–70° to the NW, constituting what appears to be a sheet-like body. However, its SW and NE contacts are faults and thus the original size and shape of the intrusion remain unknown. Major faults also occur within the intrusion, resulting in five structurally offset blocks, named, from the north to the south, Sompujärvi, Kilka, Ylipenikka, Keski-Penikka and Ala-Penikka (Fig. 2).

The lithological variation in the Penikat intrusion is illustrated in a NW–SE-trending drillcore fence located in the Sompujärvi block (Supplementary Data Electronic Appendix 1; supplementary data are available for downloading at <http://www.petrology.oxfordjournals.org>) and in a plot of CIPW norms against height

(Fig. 3). As a whole, the intrusion is relatively mafic, with ultramafic rocks (i.e. those containing >90% dark minerals) making up <10% of the stratigraphy (Fig. 3). Most of the rocks are gabbro-norites with about 40–60% plagioclase and 10–20% orthopyroxene and clinopyroxene each, as well as accessory Cr-spinel, magnetite, quartz, and phlogopite. Trace phases include sulphides, K-feldspar, apatite, lövringite and others (Alapieti & Lahtinen, 1989; Halkoaho, 1993). The paucity of ultramafic rocks constitutes a major difference from the Kemi intrusion, located immediately to the SW, which contains c. 1000 m of massive lherzolite, plagioclase-bearing websterite–olivine websterite and plagioclase-bearing clinopyroxenite, in addition to gabbroic rocks (Alapieti *et al.*, 1986, 1989). Further major differences from Kemi include the relatively low abundance of chromitite seams, measuring centimetres to decimetres at Penikat versus tens of metres at Kemi, and the relative enrichment in PGE (up to tens of ppm at Penikat versus <500 ppb at Kemi; Linkermann, 2011). In comparison with many other layered intrusions such as Bushveld and Stillwater, anorthosites are rare at Penikat and mostly consist of thin, centimetre- to decimetre-wide bands. However, these can be traced along the entire strike of the intrusion. Massive ilmenomagnetite or apatite-rich seams are absent.

Based on CIPW norms, the intrusion has been subdivided into five megacyclic units (MCU I–V) that can be traced across most blocks, with the exception of MCU III (discontinuous in the Ala-Penikka block), and MCU V (largely absent in the Keski-Penikka and Sompujärvi blocks, probably owing to erosion) (Fig. 2). All units are characterized by relatively pyroxene-rich rocks at the base and gabbroic rocks in their upper portions (Fig. 3 and Supplementary Data Electronic Appendix 1). Olivine is absent in MCU I, but forms an important phase at the base of MCU II, III and IV, within mainly lherzolites and olivine websterites. At the base of MCU V, no olivine is seen in thin section, but it is present in the CIPW norm. Olivine may also occur as a minor to major normative phase (up to ~20 normative %) within the central to upper portions of some MCUs.

The exposed and inferred thickness of the layered series is ~3000 m. It has a sharp, magmatic basal contact with Archaean K-rich granite (Fig. 4a) locally containing abundant fluorite and galena. The contact is defined by a chilled margin at least 40 cm wide (Supplementary Data Electronic Appendix 2), which has a relatively evolved composition (6.5–8.0 wt % MgO, Table 1) and is notably enriched in biotite (reflected by 4.6–5.7 wt % K₂O in the whole-rock), interpreted to be the result of *in situ* contamination (Halkoaho, 1993). Xenoliths of the country rocks (as e.g. in the basal portions of the Portimo and Koillismaa intrusions; Iljina, 1994; Karinen, 2010), are rarely observed, but this could simply reflect paucity of exposure.

The chilled margin is overlain by ~10–20 m of rocks of the marginal series consisting of sub-ophitic gabbro at the base grading upwards into gabbro-norite and then

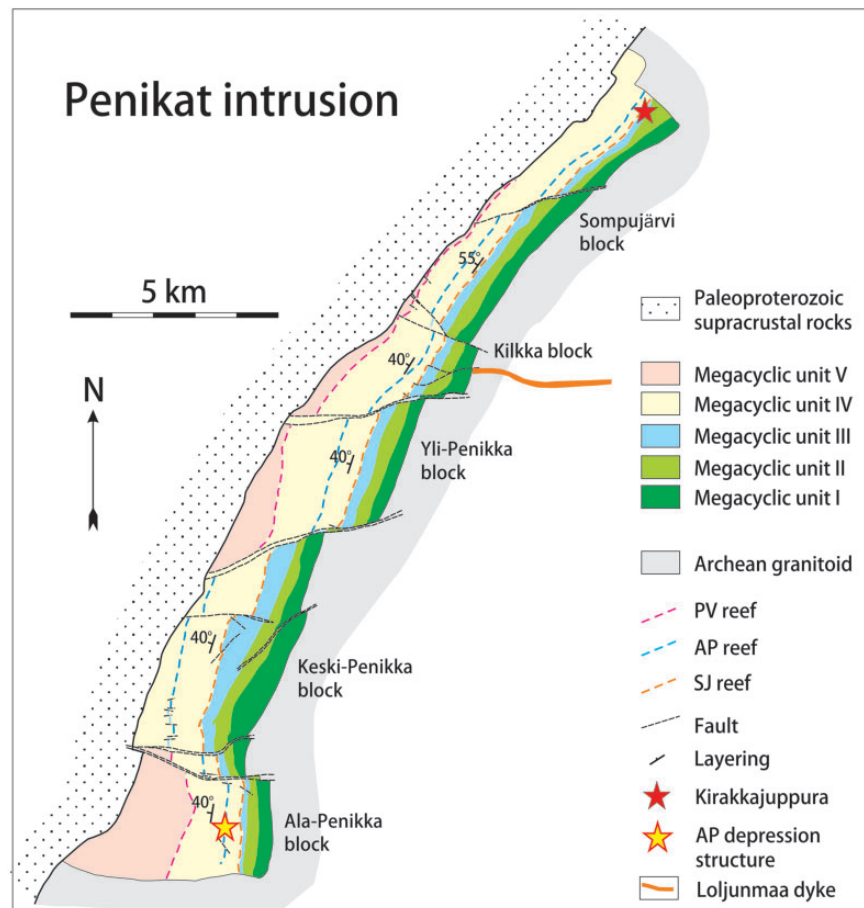


Fig. 2. Geological map of the Penikat intrusion (modified after Halkoaho *et al.*, 2005).

plagioclase-bearing websterite, all of which may be injected by rheomorphic granite veins (Halkoaho, 1993).

The first megacyclic unit, MCU I, is between 270 and 410 m thick. Its base is defined by a thin (up to a few centimetres) chromite-rich zone characterized by a fine grain size of <0.1 mm. This is overlain by plagioclase- and chromite-bearing websterite (Fig. 4b and c; 100–350 m) containing significant (up to 20%) intercumulus plagioclase and clinopyroxene. Horizons enriched in disseminated chromite occur in the centre of the interval, and above these there is a 0.5 m, laterally continuous, massive chromitite. The websterite contains granophyric material (Fig. 4b) as well as biotite, ilmenite, apatite and loveringite concentrated in the intercumulus space. It grades into norite, in which augite is initially mainly an intercumulus phase before attaining cumulus status in gabbronorite further up. Strong chromite disseminations can occur in the centre of the noritic–gabbronoritic interval, notably in the Sompujärvi block, whereas at the analogous stratigraphic level in the Kilkka block there are several thin anorthosite layers overlain by pegmatoids.

MCU II has a thickness of 160–230 m and shows more lithological variability than MCU I, particularly in its lower part where lherzolite and websterite are inter-layered (Huhtelin *et al.*, 1989b). In most parts of the

intrusion the base of MCU II is formed by a websterite a few metres thick that hosts a thin (a few centimetres wide) chromitite layer near its base (see fig. 3.3 of Huhtelin *et al.*, 1989b). This is overlain by 20 m of lherzolite (Fig. 4d) with clino- and orthopyroxene as intercumulus phases. It contains several thin layers and disseminations of chromitite. Next are 20–30 m of websterite and then 30–70 m of lherzolite containing several thin (decimetre-wide) layers of websterite. At the top of the ultramafic sequence is a sequence of alternating lherzolite, websterite and gabbronorite, with the last being locally chromite-bearing. The upper portion of MCU II consists of gabbronorite. In the Kilkka Block this may contain four 20 cm wide mottled anorthosite layers (i.e. rocks consisting predominantly of cumulus plagioclase, but with abundant oikocrysts of clino- and/or orthopyroxene) near its base, whereas in the Yli-Penikka Block the gabbronorite contains narrow lherzolite and websterite layers in addition to anorthosite (Huhtelin *et al.*, 1989b). In the Yli-Penikka block there is a 100 m wide ‘depression structure’, in which MCU II transgresses through most of the gabbronoritic upper portion of MCU I. This and other depression structures at Penikat are probably analogues of the so-called ‘pot-holes’ of the Bushveld Complex. The top of MCU I is here formed by 0.5 m of mottled anorthosite, and the

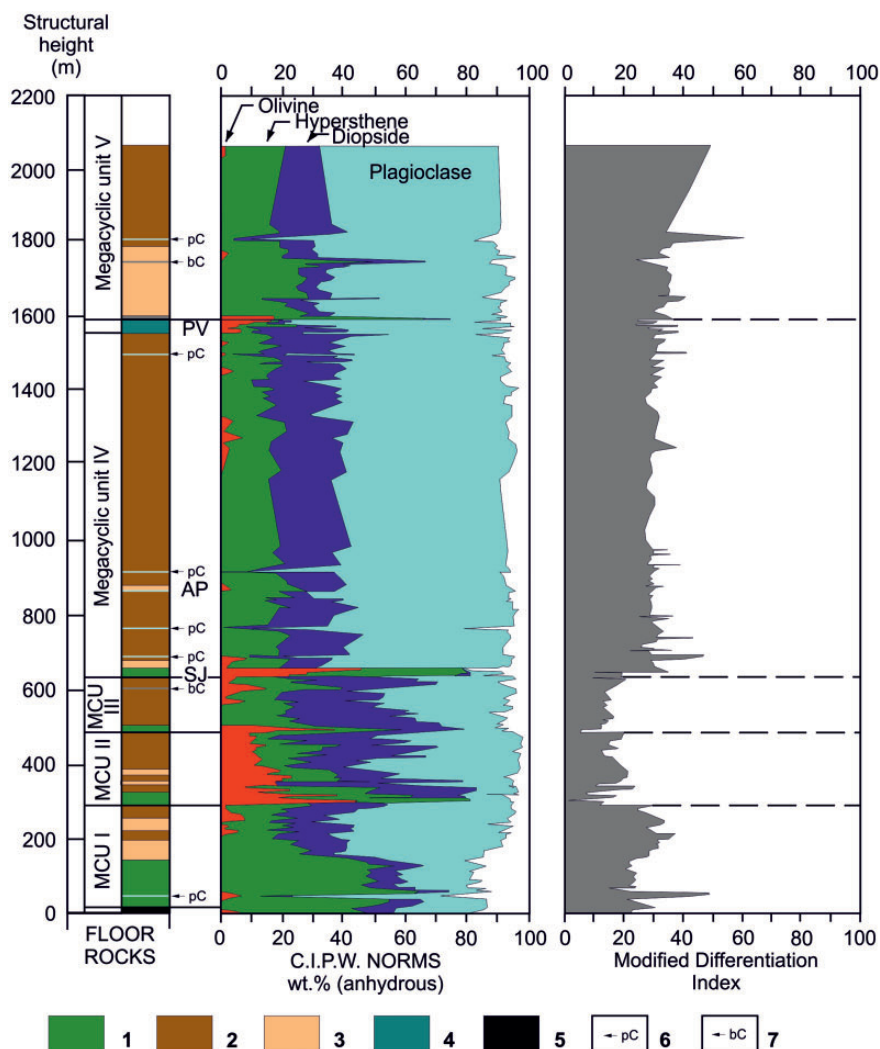


Fig. 3. Stratigraphy, CIPW norms and modified differentiation index (MDI) in a profile through the Penikat intrusion in the Ala-Penikka block (modified after Alapieti & Halkoaho, 1995). It should be noted that > 400 m of MCU V is preserved in this block. MDI is the sum of normative ocl + ab + qtz + ferroan diopside + fayalite + ferrosilite, normalized to the total whole-rock norm from which the normative proportions of chromite + magnetite + ilmenite + apatite have been subtracted (von Gruenewaldt, 1973). Rock types: 1, peridotite + pyroxenite; 2, gabbro-norite (with cumulus opx and cpx); 3, gabbro-norite (with intercumulus augite); 4, Transition Zone; 5, contact zone; 6, anorthosite; 7, bronzite cumulate layer.

potholed MCU II succession consists of a 1–2 cm thick chlorite schist overlain by a 0.5 cm undulating chromite stringer, and then Iherzolite (Fig. 5a and b). In the Ala-Penikka block, the basal ultramafic portion of MCU II is either missing or very thin.

MCU III is 75–330 m thick. It appears to pinch out near the exposed southern margin of the intrusion (Fig. 2). The unit consists of basal chromite-bearing websterite that measures several metres in thickness, followed by 30 m of chromite-bearing Iherzolite. In the middle of the latter is an ~10 m rhythmically layered sequence in which the Iherzolite contains thin (centimetre-scale) harzburgite bands (Fig. 5c). Several thin (centimetre-scale) chromitite layers occur above this zone. The Iherzolites are overlain by a few metres of websterite that may contain two thin (decimetre-scale) gabbro-norite interlayers near the top. This is overlain by

several tens of metres of gabbro-norite, and poikilitic gabbro-norite. Towards the top of the unit occur gabbro-noritic pegmatoids, as well as disseminations of corroded chromite grains, with locally very high PGE contents.

MCU IV is 760–1110 m thick and hosts the bulk of the PGE mineralization in the form of three reefs, named, from the bottom to the top, the Sompujärvi (SJ, Fig. 5d), Ala-Penikka (AP, Fig. 6a-d) and Paasivaara (PV) reefs. The base of MCU IV hosting the SJ reef is transgressive relative to MCU III and consists of a 10–20 m thick ultramafic layer that can be as thin as 20–50 cm near the margins of the intrusion. At its base is a centimetre to 1 m wide basal hybrid rock or chlorite schist that can be enriched in chromite, the latter occurring as layers, schlieren, clasts and disseminations (Fig. 5e). Based on elevated MgO and Al₂O₃ contents, the chlorite schist

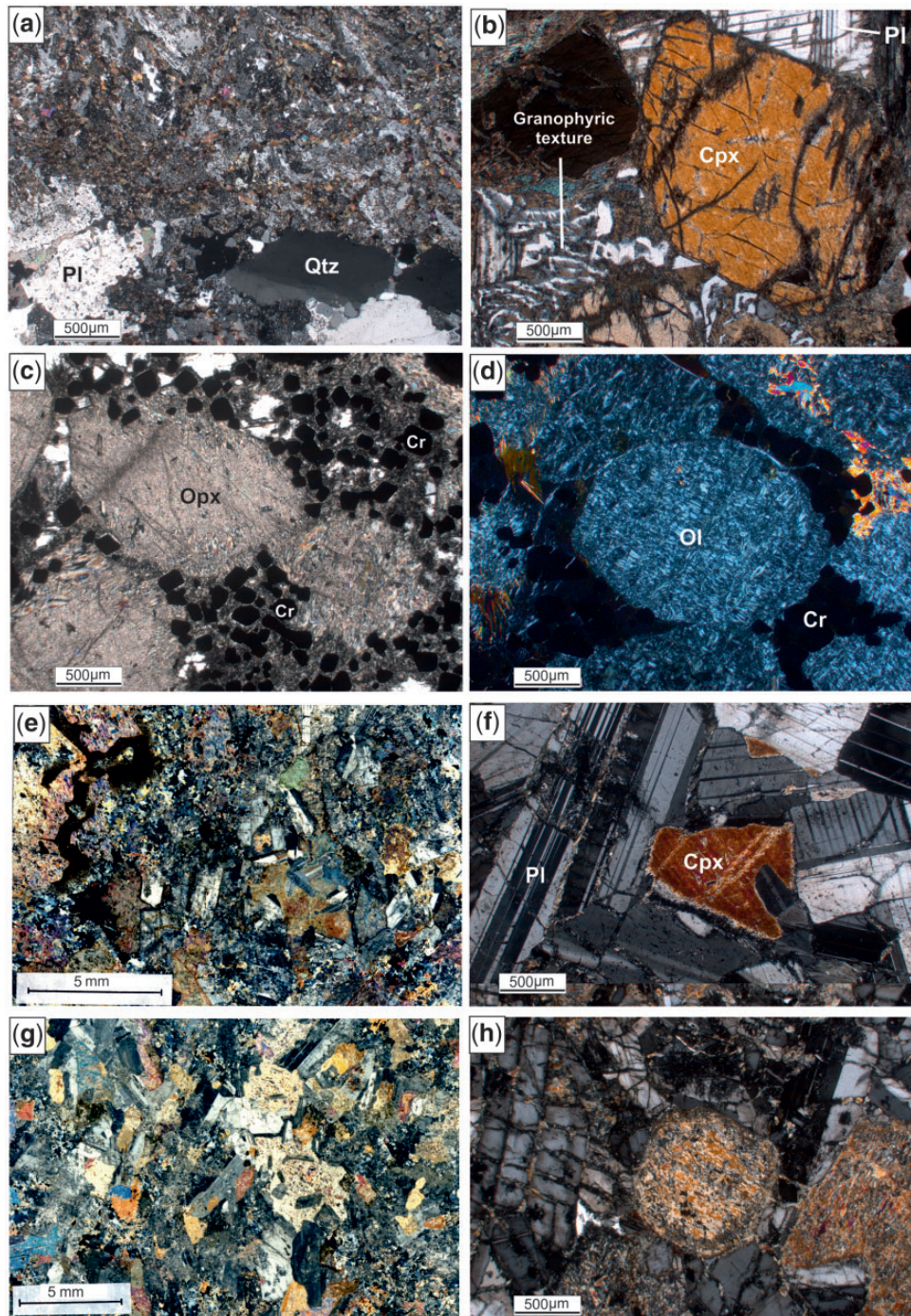


Fig. 4. Photomicrographs of Penikat rocks. (a) Basal contact of the Penikat intrusion, drillcore SiKi 6 (172 m), Lower portion of the image shows the basement and the upper portion shows the chilled margin of the intrusion. (b) Websterite orthocumulate, sample Pen 12, MCU I, 90 mab. (c) Orthopyroxenite–websterite with disseminated chromite, drillcore SiKi 6 (110.6 m), MCU II, ~60 mab. (d) Lherzolite with interstitial chromite, drillcore SiKi 7 (252 m), MCU II, ~170 mab. (e) AP1 reef gabbro-norite orthocumulate with intercumulus magnetite and 5% sulphide. Silicates are strongly altered to epidote and chlorite. Sample 52A-PAT, 802.2 mab. (f) Norite in hanging wall of AP1 reef, sample Pen 30, MCU IV, 804 mab. (g) AP2 reef gabbro-norite orthocumulate, strongly altered to epidote and chlorite. Rock contains ~2% sulphide. Sample 9383-7202, 891 mab. (h) Norite, sample Pen 39, MCU V, 1920 mab.

has been interpreted as a highly altered and sheared pyroxenite or melanorite (Halkoaho *et al.*, 1989a). The chlorite schist is overlain by about 1 m of websterite in which clinopyroxene is an intercumulus phase, lherzolite and then again websterite with intercumulus

clinopyroxene. Next follow gabbro-noritic cumulates in which orthopyroxene has a cumulus habit, whereas clinopyroxene has a poikilitic intercumulus texture; these are overlain by gabbro-norite in which clinopyroxene shows a cumulus habit. In the lower portion of the

Table 1: Composition of potential Penikat parent magmas and Bushveld parent magmas

	2.44 Ga Finnish dykes					Penikat and Koitelainen chilled rocks and dykes				Bushveld magmas		
	Bon 1	GN 1	OPX 1	Tho 1	Fe-Tho 1	2	3	4	5	B1 6	B2 6	B3 6
SiO ₂	53.38	53.22	56.71	50.35	48.56	51.74	50	57.31	53.69	55.74	50.79	51.33
TiO ₂	0.63	0.99	0.66	1.49	2.57	0.61	0.86	0.27	0.57	0.34	0.76	0.37
Al ₂ O ₃	12.32	12.81	14.34	13.68	13.62	13.17	11.7	14.7	14.24	11.82	15.70	16.14
Fe ₂ O ₃	11.19	11.77	9.76	15.03	15.78	10.30	11.80	10.21	10.38	10.50	12.54	10.45
MnO	0.16	0.19	0.16	0.21	0.23	0.15	0.16	0.09	0.12	0.18	0.19	0.18
MgO	11.30	8.52	5.68	6.08	6.24	8.40	11.20	6.49	8.04	11.85	6.91	7.69
CaO	8.06	9.24	8.68	10.18	9.77	10.10	9.12	3.24	5.26	6.50	10.70	11.25
Na ₂ O	2.24	2.16	2.58	2.27	2.16	2.80	1.77	3.91	2.76	1.63	1.94	1.91
K ₂ O	0.63	0.98	1.30	0.58	0.74	0.72	0.92	4.57	5.73	0.98	0.25	0.28
P ₂ O ₅	0.09	0.12	0.12	0.14	0.34	0.06	0.12	0.04	0.08	0.08	0.16	0.03
Mg#	0.67	0.59	0.53	0.44	0.44	0.62	0.65	0.56	0.60	0.69	0.52	0.59
Ba	204	262	165	152	157	188	223	490	530	364	192	139
Ce	18.35	27.71	43.26	26.22	42.70	17.2	22.7	n.a.	n.a.	34.80	31.74	11.55
Co	44	44	39	54	43	n.a.	51	n.a.	n.a.	59	53	52
Cr	962	488	72	122	259	466	992	470	440	965	201	408
Cs	0.86	0.96	1.85	0.32	0.90	n.a.	n.a.	n.a.	n.a.	2.55	0.31	0.38
Cu	67	83	73	184	387	n.a.	123	n.a.	n.a.	51	76	13
Dy	1.65	3.32	4.02	5.15	6.38	2	2.57	n.a.	n.a.	1.90	3.21	1.62
Er	0.99	1.92	2.27	3.01	3.81	1.34	1.6	n.a.	n.a.	1.05	1.79	0.96
Eu	0.67	1.02	1.54	1.36	1.82	0.73	0.87	n.a.	n.a.	0.82	1.31	0.76
Ga	15.01	17.11	18.54	18.96	17.24	n.a.	24	n.a.	n.a.	18.14	14.16	14.00
Gd	1.70	3.44	5.05	4.94	6.15	2.37	3.07	n.a.	n.a.	2.40	3.61	1.63
Hf	1.68	2.13	3.09	2.47	4.35	n.a.	1.14	n.a.	n.a.	1.91	1.33	0.66
Ho	0.33	0.63	0.72	1.01	1.25	0.49	0.57	n.a.	n.a.	0.38	0.66	0.35
La	9.05	13.06	20.08	11.53	18.28	8.63	10.3	n.a.	n.a.	18.00	14.97	5.66
Lu	0.19	0.31	0.41	0.48	0.73	0.2	0.22	n.a.	n.a.	0.17	0.26	0.15
Nb	2.26	5.54	6.18	7.40	12.78	2	2.85	n.a.	n.a.	4.15	3.87	1.42
Nd	8.75	14.17	21.11	15.61	25.92	9.63	11.7	n.a.	n.a.	15.47	17.15	6.29
Ni	308	152	60	71	131	104	354	90	104	284	106	133
Pb	3.44	8.26	8.24	5.24	3.04	n.a.	<20	n.a.	n.a.	13.92	4.27	2.75
Pr	1.75	3.51	5.36	3.20	4.51	2.27	2.8	n.a.	n.a.	4.16	4.04	1.49
Rb	23	29	12	19	24	20	31	n.a.	n.a.	40	4	9
S	144	280	153	548	1965	n.a.	417	180	270	396	178	107
Sc	n.a.	n.a.	n.a.	n.a.	n.a.	31	30	n.a.	n.a.	30	33	31
Sm	2.00	3.52	4.84	4.39	6.69	2.21	2.89	n.a.	n.a.	2.80	3.76	1.54
Sr	179	212	273	208	136	337	238	260	220	198	348	337
Ta	0.17	0.33	0.00	0.69	0.64	n.a.	<0.2	n.a.	n.a.	0.48	0.34	0.20
Tb	0.30	0.53	0.82	0.86	1.20	0.38	0.47	n.a.	n.a.	0.34	0.55	0.26
Th	1.98	2.67	4.53	1.70	1.84	1.3	2.13	n.a.	n.a.	3.46	0.68	0.76
Tm	0.16	0.29	0.31	0.43	0.60	0.21	0.23	n.a.	n.a.	0.16	0.26	0.15
U	0.39	0.61	0.93	0.33	0.54	0.24	0.35	n.a.	n.a.	0.99	0.23	0.18
V	189	238	190	326	324	199	206	130		164	239	173
Y	14.0	21.6	17.6	30.1	52.6	13.6	15.7	n.a.	n.a.	11.7	19.4	9.9
Yb	1.15	2.20	3.19	3.56	4.58	1.23	1.59	n.a.	n.a.	1.10	1.73	0.98
Zn	80	98	80	106	129	65	94	530		80	90	63
Zr	69	108	123	119	200	51	41	130	40	77	54	23
Os	0.29	0.20	n.a.	0.13	0.08	n.a.	<1	n.a.	n.a.	0.61	0.11	0.23
Ir	0.54	0.26	n.a.	0.05	0.13	n.a.	0.36	n.a.	n.a.	0.54	0.21	0.30
Ru	2.19	1.05	n.a.	0.07	0.68	n.a.	<2	n.a.	n.a.	1.90	0.89	1.23
Rh	1.57	1.12	n.a.	0.09	1.14	n.a.	1.58	n.a.	n.a.	1.78	0.77	0.74
Pt	7.11	8.26	n.a.	8.14	12.34	n.a.	8.6	b.d.l.	b.d.l.	19.36	9.54	12.71
Pd	6.17	6.48	n.a.	7.54	13.69	n.a.	6.27	14	12	13.99	5.41	3.85
Au	0.88	0.85	n.a.	1.97	2.26	n.a.	1.57	n.a.	n.a.	2.72	1.90	0.89

Bon, boninite; GN, gabbro-norite; OPX, orthopyroxenite; Tho, tholeiite; Fe-Tho, Fe-tholeiite. 1, F. Guo (unpublished data); 2, Koitelainen chilled margin (from [Ijjina & Hanski, 2005](#)); 3, Loljunmaa dyke (sample 1-LOL-2009); 4, Penikat chilled margin, sample Ki6 171.82 (from [Halkoaho, 1993](#)); 5, Penikat chilled margin, sample Ki 171.49 (from [Halkoaho, 1993](#)); 6, [Barnes et al. \(2010\)](#). n.a., not analysed; b.d.l., below detection limit.

gabbro-norite, ~100 m above the base of MCU IV, pronounced rhythmic layering is seen, including a thin (up to a few centimetres) anorthosite layer with sharp contacts ([Fig. 5g](#)), locally with elevated PGE contents of up to 1 ppm. Above the anorthosite is about 1 m of websterite and about 20 m above this occurs a mottled

anorthosite marker horizon that defines the boundary between zones 1 and 2 of MCU IV ([Fig. 5f](#)). Some 250 m above the base of MCU IV is a thin (2–10 cm), but laterally continuous mottled anorthosite layer that has sharp but undulating contacts to its hanging-wall and footwall gabbro-noritic host rocks ([Fig. 6a](#)). A further, very similar

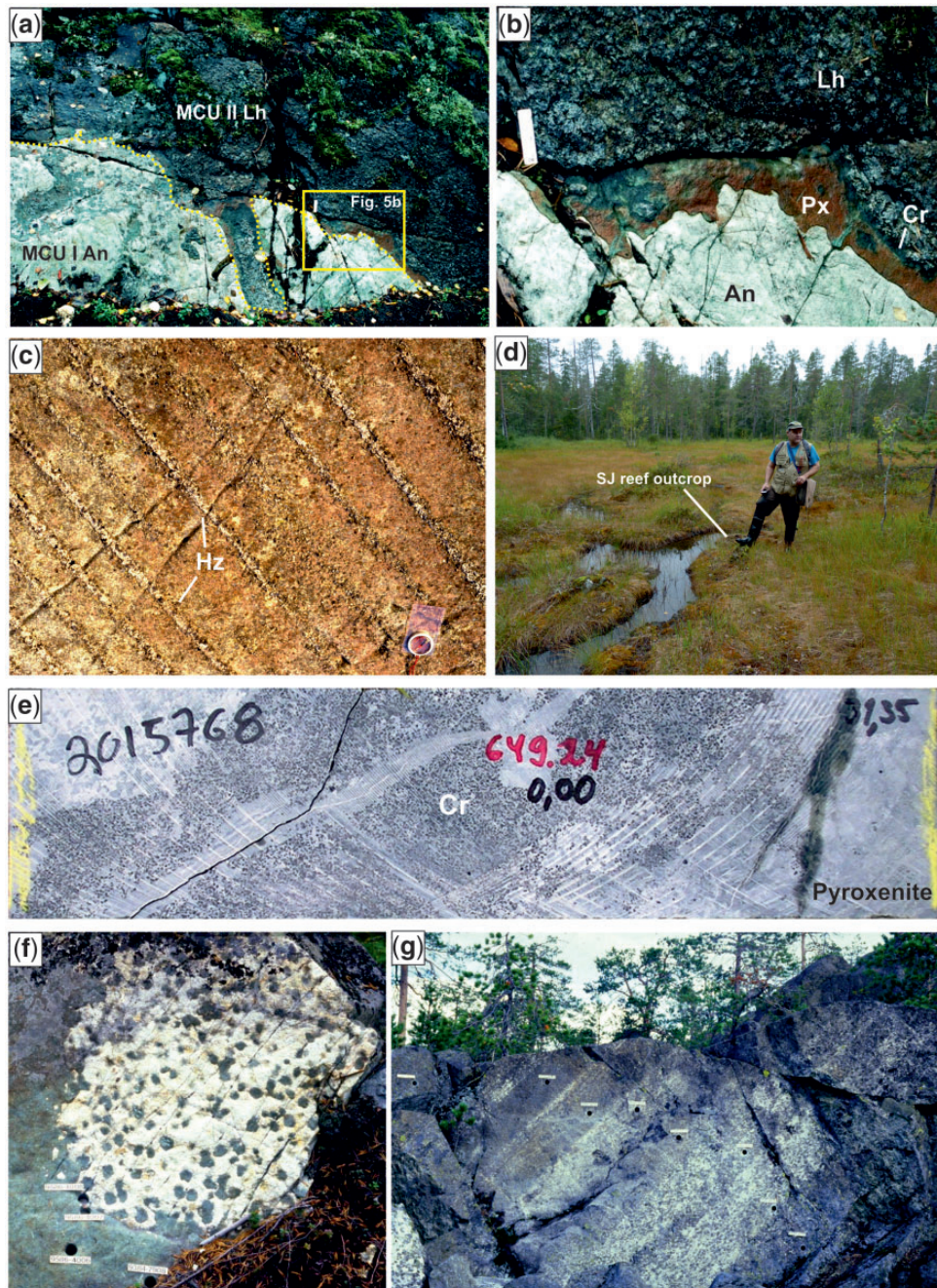


Fig. 5. (a, b) Contact between MCU I and MCU II at depression structure in Yli-Penikka block. Dip of layering is $\sim 40^\circ$ towards the viewer, whereas the exposure is inclined at a slightly steeper angle. At the top of MCU I is an anorthositic plagioclase orthocumulate layer (white). At the base of the overlying olivine mesocumulate (with poikilitic opx and cpx) of MCU II (dark green) is a narrow (1–2 cm) layer of metapyroxenite (now chlorite schist; brown and green), which is overlain by a chromitite (black) layer 0.5 cm in thickness. Ultramafic transgressive channel within anorthosite in lower portion of (a), in which Iherzolite is bracketed by chromitite and chlorite schist, should be noted. Length of the white scale is about 6.5 cm. (c) Layering in the ultramafic sequence of MCU III, consisting of alternating layers of bronzite-bearing and bronzite-free Iherzolite, Penikanjänkä, Keski-Penikka block. Length of the compass is 12 cm. (d) Outcrop of the MCU IV Iherzolite layer (the host-rock of the SJ Reef), Ala-Penikka block. (e) Chromitite type of the SJ Reef exposed in drillcore Pen-475, Sompujärvi block. The diffuse Cr stringer is ~ 5 cm wide. It should be noted that sample contains 650 ppm PGE. (f) Near-plan view of anorthosite layer (poikilitic plagioclase adcumulate, with clinopyroxene oikocrysts) ~ 80 m above base of MCU IV, Ala-Penikka block. The anorthosite and the overlying 1 m thick websterite layer (poikilitic bronzite mesocumulate) form a prominent marker horizon throughout the Penikat intrusion. Length of the white scales is 10 cm. (g) Anorthosite (poikilitic plagioclase mesocumulate) layers at the contact between zones 1 and 2 of MCI IV, Ala-Penikka Block (~ 100 m above base of MCU IV). This interval forms the most prominent marker horizon in the Penikat intrusion and can be traced along the entire strike length. Length of the white scales is 10 cm.

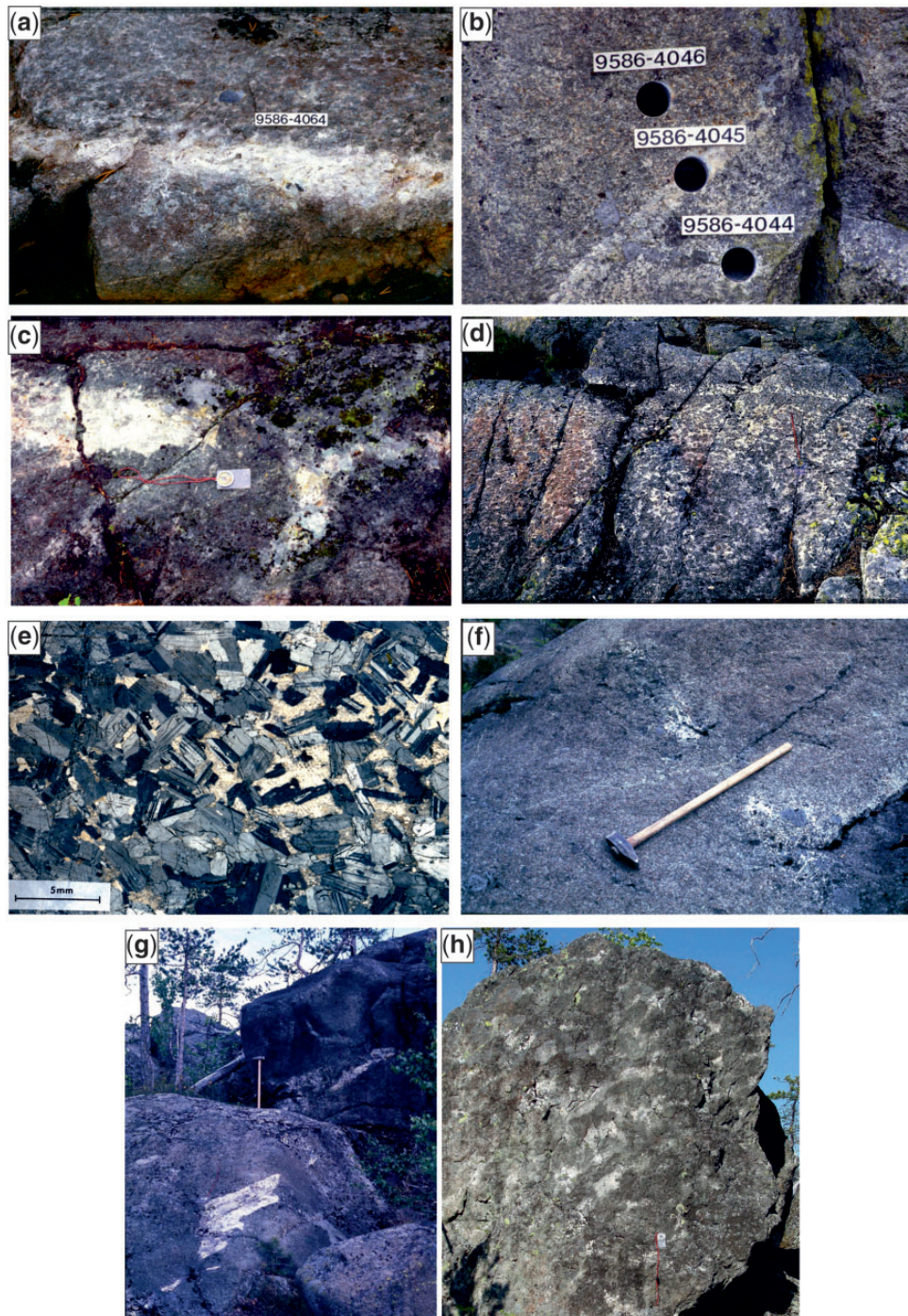


Fig. 6. (a) AP1 Reef poikilitic anorthosite with intercumulus augite, bronzite and accessory sulphides. Below the anorthosite is a plagioclase–augite–bronzite adcumulate with accessory sulphides and intercumulus ilmenomagnetite and above is a spotted plagioclase–bronzite mesocumulate with poikilitic intercumulus augite. Ala-Penikka block, ~250 m above base of MCU IV. Length of the white scale is 10 cm. (b) The AP2 Reef is closely associated with a thin (2–3 cm) anorthosite (poikilitic plagioclase adcumulate). The anorthosite is hosted by gabbro-norite (plagioclase–augite–bronzite adcumulates). Ala-Penikka block, ~345 m above base of MCU IV. Length of the white scales is 10 cm. (c) Slumped AP1 reef anorthosite, Length of compass is 12 cm. (d) Poikilitic gabbro-norite mesocumulate forming thick ‘mottled anorthosite’ in centre of AP1 pothole. Height of exposure is 1.5 m. (e) Photomicrograph of ‘mottled anorthosite’ in (d). (f) Pegmatoidal pods located above AP1 pothole, ~20 m below AP2 reef. (g) Mottled anorthositic (plagioclase orthocumulate) fragments located about 180 m above the base of the AP1 depression structure, ~300 m above base of MCU IV, Ala-Penikka block. Length of the hammer is 65 cm. (h) Mixed rock of the Transition Zone (PV reef) in the upper part of MCU IV (~980 m above base of MCU IV) The mixed rock is composed of white patches of plagioclase adcumulate and darker patches of plagioclase and/or plagioclase–bronzite cumulate in which intercumulus augite occurs as oikocrysts.

thin anorthosite occurs another 100 m up-section (Fig. 6b). The anorthosite layers and their immediate footwall rocks host the AP1 and AP2 PGE reefs (Halkoaho, 1989, 1993; Halkoaho *et al.*, 1990b). The reefs are strongly altered relative to their hanging-wall rocks. The AP1 anorthosite can locally be disrupted and may slump into its footwall (Fig. 6c). In places, the AP1 anorthosite and its hanging-wall norite are transgressive relative to their footwall, forming a large pothole, somewhat analogous to the large anorthosite potholes in the Bushveld Complex (Maier *et al.*, 2016). Within the pothole, the anorthosite is markedly thickened, and the pyroxene oikocrysts appear to have become larger and more abundant, essentially resulting in a poikilitic gabbro-norite (Fig. 6d,e). Numerous pegmatoidal pods are also developed (Fig. 6f).

Decimetre-sized anorthosite fragments (Fig. 6g) commonly occur between the two AP reefs, notably above the main AP1 depression structure. Approximately 900 m above the base of MCU IV is a further mottled anorthosite layer, and 100 m above this, at the top of MCU IV, is a 40–60 m thick, highly complex zone termed the Transition Zone (Huhtelin, 1989; Huhtelin *et al.*, 1989a, 1990; Halkoaho *et al.*, 2005). This consists of layers and lenses of gabbro-norite, norite, mottled anorthosite, pegmatoid, and a 10–15 m thick 'mixed rock' composed of irregular, up to 0.5 m wide patches or fragments of poikilitic gabbro and 1–2 m sized autoliths of gabbro-norite in anorthosite adcumulate (Fig. 6h). This mixed rock layer has a thin anorthosite layer at its base, and both can be transgressive to the gabbroic floor rocks (fig. 21 of Halkoaho *et al.*, 2005). It has been compared with the Mixed Rock of the J-M reef of the Stillwater Complex (Turner *et al.*, 1985) and possibly represents a magmatic breccia of anorthosite and gabbro-norite (Huhtelin *et al.*, 1990). This zone hosts the PV reef, which is described in more detail below.

MCU V has a highly variable thickness. The unit is up to 900 m thick in the Ala-Penikka block, but entirely absent in the Keski-Penikka and most of the Sompujärvi blocks, probably owing to erosion. At the base of the unit is 4–10 m of websterite (with intercumulus clinopyroxene) displaying a basal contact that undulates relative to the underlying Transition Zone on a scale of metres. The websterite grades upwards into norite. Towards the top of MCU V occur norite (Fig. 4h), gabbro-norite, gabbro, leucogabbro, anorthosite, and plagioclase-quartz-biotite rocks containing minor ilmenomagnetite throughout. The uppermost exposed rocks resemble the granophyre in the roof of the Koillismaa intrusion (Iljina & Hanski, 2005). Based on geophysical data, these lithologies are overlain by at least a further 500 m of intrusive rocks under cover.

MINERALOGY AND MINERAL CHEMISTRY

The petrography and mineral chemistry of the intrusion have been studied in detail by Halkoaho (1989, 1993), Halkoaho *et al.* (1989a, 1989b, 1990a, 1990b) and

Alapieti & Halkoaho (1995), and only a brief summary of the data is given here. Prior to pervasive greenschist- to amphibolite-facies alteration to pseudomorphs of serpentine, amphibole and carbonate, olivine formed euhedral or subhedral grains of up to several millimetres in diameter. Owing to its alteration (Fig. 4d) its primary composition could generally not be determined.

Orthopyroxene occurs throughout the intrusion and tends to be strongly uralitized (Fig. 4c, e and g), but some unaltered grains of euhedral and subhedral habit could be analysed in most units, ranging in composition from En 80.9 to 67.3, and containing up to 0.56 wt % Cr₂O₃. Clinopyroxene is also present throughout the intrusion and could be analysed in most units. It has an intercumulus habit in most ultramafic rocks, notably in MCU I, II, IV and V, and in the basal parts of the mafic portions of all megacyclic units, but attains cumulus status towards the top of most megacyclic units. Clinopyroxene is less altered than orthopyroxene, thus its composition has been particularly useful in constraining the compositional cyclicity of the intrusion (Halkoaho, 1993; Alapieti & Halkoaho, 1995). In MCU I, II and III, the data show normal differentiation trends of decreasing Mg# with height, with sharp reversals towards elevated Mg# at the base of units. The most primitive grains occur in MCU II, where Mg# reaches 90%, with up to 1.3 wt % Cr₂O₃. One of the most notable features evident in the clinopyroxene data is the markedly lower Mg# and Cr content in clinopyroxenes of MCU IV, relative to the under- and overlying units. This pattern has led a number of researchers to propose two distinct magmatic lineages for the intrusion, one being relatively Cr-rich and the other Cr-poor (Halkoaho, 1993; Alapieti & Halkoaho, 1995), as discussed in more detail below.

Plagioclase is the least altered of the major silicates and is present throughout the intrusion. Its composition ranges from An 60 to 82%, with the highest values observed in norites and gabbro-norites of MCU II and III. The anorthite contents of intercumulus plagioclase in the ultramafic rocks can be as low as 55%.

Cumulus chromite occurs in most rocks of MCU I and II, and in the peridotites and pyroxenites of MCU III, IV and V. The grain size of the chromite shows a broadly progressive coarsening with height. In the peridotites and pyroxenites, euhedral and subhedral grains are mostly confined to the intercumulus domains between cumulus olivine and orthopyroxene (Fig. 4c and d), whereas chromite grains at the base of, and below, MCU IV typically are strongly annealed, analogous to those in the Merensky Reef of the Bushveld Complex (Eales & Reynolds, 1986), and may form inclusions within augite. Chromite has relatively constant Cr₂O₃ contents in the peridotites, pyroxenites and norites, with a maximum of just over 40 wt %.

Cumulus ilmenite and magnetite are relatively minor phases, but may occur in MCU IV and V, with ilmenite being more abundant.

Apatite is a trace phase throughout the intrusion, but may be common in MCU I and V. The grains can reach

up to 1 mm in length and are mostly of intercumulus habit, except in the upper parts of MCU IV and V. Halkoaho (1993) studied apatite compositions in four blocks of the Penikat intrusion and showed that F contents generally increase with height, but show a particularly pronounced increase across the MCU III–IV boundary. Cl contents tend to be highest near the base of the intrusion, but in the Ala-Penika block, there is an additional strong increase in Cl (in excess of 2%) in the lower portions of MCU IV and MCU V.

Sulphides are trace phases throughout much of the intrusion, comprising mainly pyrrhotite, chalcopyrite, and pentlandite. Elevated pyrite contents, as well as trace bornite, sphalerite, galena, millerite and violarite, are found in some of the reefs. The SJ and AP reefs contain abundant platinum-group minerals (PGM) (Halkoaho, 1993), with diameters between 1 and 300 μm . These are described in more detail below.

DESCRIPTION OF PGE-ENRICHED ZONES

Chromitites in MCU I–IV

Chromitite seams occur throughout the lower portion of the Penikat intrusion. The seams are mostly relatively thin (<10 cm), except for one 0.5–0.8 m wide seam within MCU I. The lateral continuity of most chromitites is not well established, owing to poor exposure and the low number of drillcore intersections in the basal portion of the intrusion, mainly confined to the Sompujärvi block (Supplementary Data Electronic Appendix 1). Chromitite seams, stringers or disseminations occur within websterite or lherzolite at the base of cyclic units (MCU I, II, IV) or within norite or gabbro-norite in the centre and towards the top of units (MCU I, II, III). The seams tend to be sulphide poor (<240 ppm S, <130 ppm Cu, Huhtelin *et al.*, 1989b). They show a broad trend of increasing grain size, PGE contents and PGE fractionation with height; seams in MCU II contain <300 ppb PGE, with Pt/Pd \sim 1 and Pd/Ir 4–5, whereas seams in MCU III have up to 3 ppm total PGE, with Pt/Pd >2 and Pd/Ir up to 10 (Huhtelin *et al.*, 1989b).

The SJ (Sompujärvi) reef

The SJ reef is a classical PGE reef sharing many similarities with, for example, the Merensky Reef of the Bushveld Complex: in both cases a relatively narrow zone of PGE-rich sulphide mineralization (thickness typically \sim 1 m) is closely associated with one, or in the case of Bushveld, several chromitite stringers, predominantly along, or near the lower contact of an ultramafic layer that forms the base of a cyclic unit. The ultramafic and mafic rocks below and above the reefs are mostly strongly PGE depleted.

The detailed stratigraphy of the SJ reef interval is highly complex, with several distinct PGE mineralization styles being described by Halkoaho *et al.* (1989a, 1990a) and Halkoaho (1993) (Supplementary Data Electronic Appendix 3). The mineralization is

concentrated within the lowermost ultramafic rocks of MCU IV, typically consisting of a centimetre to metre thick chlorite schist, which is commonly enriched in chromite occurring as disseminations or stringers and schlieren. Above the chlorite schist can sometimes occur an orthopyroxenite or olivine orthopyroxenite layer, typically up to 1 m in thickness, but locally reaching 3 m in thickness. More usually, the chlorite schist is overlain by a thick (10–20 m) lherzolite. In places, mineralization can extend, in patchy form, for several decimetres or metres into the gabbro-noritic footwall, where it can be associated with chromite disseminations and pyroxenite lenses and layers (Fig. 7).

A typical profile across the reef is shown in Fig. 7c. Of note is that the increase in MgO and decrease in Al_2O_3 , reflecting the appearance of ultramafic rocks, is accompanied by sharply lower Mg# and Cr contents in the whole-rocks and augite than in the footwall gabbro-norites, suggesting that the sulphides of the reef precipitated from relatively evolved magma.

The MCU IV ultramafic rocks are laterally of variable thickness, and they may pinch out and form channels or so-called ‘depression structures’ that are transgressive relative to the footwall layers. They probably are analogues to the potholes of the Bushveld Complex (Maier *et al.*, 2016, and references therein). The depression structures in the SJ reef tend to be enriched in disseminated chromite (e.g. at Kirakkajuppura) and can be extensive. For example, in the northern part of the Sompujärvi block, MCU III is just 30 m thick, suggesting several tens of metres of magmatic erosion. At the northern and southern edges of the intrusion the ultramafic portion of MCU IV can be very thin and may pinch out altogether. It remains unclear whether these are large-scale erosional structures or reflect a distal facies of the intrusion relative to a feeder zone (see Eales *et al.*, 1988).

Halkoaho (1993) distinguished four types of PGE mineralization in the SJ reef. (1) In the sulphide-dominated type the PGE are associated with sulphide enrichments of up to several per cent (Supplementary Data Electronic Appendix 3). This type of mineralization tends to be located in the basal chlorite schist or websterite of MCU IV and sometimes in the overlying lherzolite. The peak sulphide abundance tends to occur near the base of the lherzolite, whereas the peak PGE values are usually in the underlying websterite and schist. (2) In the chromite type, sulphides are rare (usually <0.1 modal %), but PGE are closely associated with disseminations of up to \sim 10 modal % chromite (Supplementary Data Electronic Appendix 4) in MCU IV websterite, chlorite schist or their gabbro-noritic footwall. This type has markedly higher PGE grade than the other types. (3) The silicate type can occur in all rock types. PGE occur as PGM within silicates, whereas sulphides and chromite are sparse (<0.1%), to the effect that the mineralization is macroscopically invisible (Supplementary Data Electronic Appendix 5). (4) In the composite type, PGE enrichments occur in

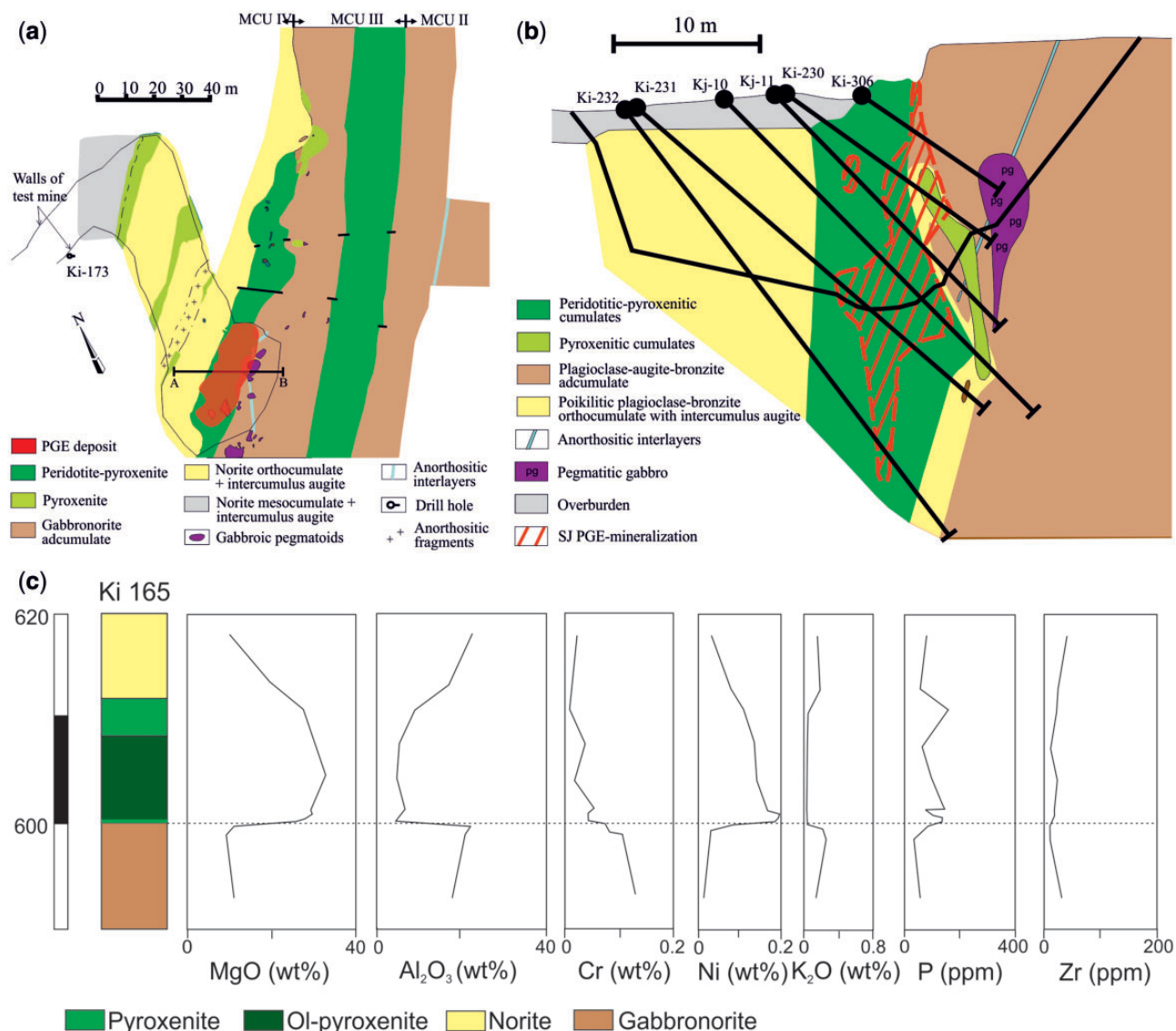


Fig. 7. (a) Outcrop map of the SJ reef sequence at Kirakkajuppura, Sompujärvi block. The poor lateral continuity and irregular basal contact of ultramafic rock at base of MCU IV, contrasting with planar contacts of the MCU III ultramafic layer, should be noted. Also noteworthy is the pod-like nature of the PGE deposit, and abundance of pegmatoidal patches below the SJ reef. Outline of test pit is shown by black continuous line. Modified after Halkoaho *et al.* (2005). (b) Cross-section through the SJ reef at Kirakkajuppura where the reef is locally thickened. Potholing and the irregular nature of the SJ reef should be noted. Modified after Halkoaho *et al.* (2005). (c) Compositional variation across the SJ reef intersected by drillcore SiKi 165 (modified from Halkoaho *et al.*, 1990a). The sharp decrease in Cr content, and lack of enrichment in incompatible elements, should be noted. (See text for further discussion.)

sulphide + chromite-enriched intervals, as well as in zones enriched in either chromite or sulphide (Supplementary Data Electronic Appendix 6). In all reef types, the rocks are strongly altered, rendering recognition of primary textures near impossible.

PGE grades are locally extremely variable, and spectacular grades of >100 ppm PGE over several decimetres are not uncommon (Supplementary Data Electronic Appendices 4 and 7). The highest grade recorded is from drillcore SiKi 308 at a depth interval of 4.57–4.75 m (18 cm) in the Kirakkajuppura area, northern Sompujärvi block (Fig. 2), where concentrations of 501 ppm Pt, 1350 ppm Pd, 58.2 ppm Rh, and 12 ppm Au are found in the uppermost gabbronorite of MCU III,

peridotite of MCU IV and, in particular, a tremolite-chlorite rock between the gabbronorite and peridotite. In the drillcore, the average grade over a height of 11.2 m is 46.4 ppm Pd and 18 ppm Pt (i.e. ~520 ppm Pd and ~200 ppm Pt normalized to a thickness of 1 m, about 100 times that of a typical Merensky Reef intersection). However, notwithstanding the local-scale variation in grade, mineralization style and stratigraphic setting, on a larger scale the grade of the mineralization is remarkably consistent. Our compilation of the available drillcore data until 1990 indicates that of 400 holes drilled through the SJ reef along the strike of the intrusion, only 20 (5%) were 'unmineralized' (i.e. contained less than ~100 ppb PGE, the analytical detection limit at

the time). The SJ reef has the following average grades in the individual blocks of the intrusion: Ala-Penikka (3.06 ppm over 1.38 m, 13 holes), Keski-Penikka (4.54 ppm over 1.28 m, 35 holes), Yli-Penikka (5.96 ppm over 1.78 m, 22 holes), Kilka (4.82 ppm over 1.09 m, 32 holes), Sompujärvi North excluding Kirakkajuppura (5.84 ppm over 1.31 m, 113 holes), and Sompujärvi South (7.28 ppm over 1.36 m, 185 holes). Because drilling density is highly heterogeneous between blocks, the calculated average grades for some of the blocks are probably approximate. As mentioned above, highly enriched grades occur at Kirakkajuppura at the northern edge of the Sompujärvi block, and the bulk grade of this 115 000 t ore body is 11.3 ppm Pt, 19.8 ppm Pd, 1.42 ppm Rh and 0.15 ppm Au over an average reef thickness of 2.4 m. The data further indicate that chromite-hosted mineralization dominates at Kilka and Sompujärvi (25–35% of all intersections), whereas this type of mineralization is nearly absent at Ala-Penikka, Keski-Penikka and Yli-Penikka, where sulphide-hosted and composite mineralization dominates (30–68% of all intersections). The published mineral resource (to a depth of 100 m) for the entire Sompujärvi block stands at 6.7 Mt at a grade of 5.36 ppm Pd and 3.08 ppm Pt over 0.97 m (Eerola *et al.*, 1990). For the sulphide type of the SJ reef (across the entire Penikat intrusion), Pt and Pd contents are 2.7 ppm each (Pt/Pd is close to unity) and Pd/Ir is 27 (Halkoaho *et al.*, 2005). Average sulphur contents of the sulphide-type reef are 0.13 wt % and for the chromite-type reef 0.03 wt % (Halkoaho *et al.*, 2005). The tenors of the sulphides are thus extremely high (~1500 ppm Pt + Pd in sulphide-type).

The PGM in the chromite-type of the SJ reef comprise predominantly Pd–As–Sb minerals (49% of all grains), sperrylite (12.7%), PGE–Fe–Cu–Mn hydroxides (9%), PGE sulphides (except laurite, 9%), PGE alloys (7.3%), Sn and/or Pb-bearing PGM (3.6%, particularly at Kirakkajuppura), laurite (1.8%) and Pd–Te– (Bi) minerals (1.8%) (Halkoaho, 1993). Most of the PGMs occur in association with silicates, and a small amount on the edge of chromite or magnetite. Only laurite has been encountered as inclusions in chromite. In the Kirakkajuppura area, PGE sulphides dominate, whereas in the base metal sulphide type of the SJ reef, sperrylite is dominant (31%), followed by Pd–As–Sb minerals (29.3%), Pd–Te– (Bi) minerals (12.1%), RhAsS–IrAsS minerals (12.1%), laurite (6.9%) alloys (3.4%) and Au–Ag minerals (5.2%). The base metal sulphide type mineralization has PGMs associated with both silicates and base metal sulphides.

The AP (Ala-Penikka) reefs

The AP reefs are present along most of the strike length of the intrusion. They occur in a thick gabbro-noritic interval, specifically within and below (but never above) two narrow, but laterally highly continuous anorthosite seams. The closest known analogues are PGE mineralized anorthosites in the Vurechuaivench block of the

Monche pluton, Russia (Pripachkin *et al.*, 2018). A commonality with many other PGE reefs elsewhere is that the AP reefs occur at a stratigraphic level marked by enhanced compositional layering interpreted by most researchers to reflect magma replenishment. However, contrary to most other global reefs, the AP (and SJ) reefs are at the base of reversals towards more fractionated compositions, as expressed by lower Mg# and Cr content. At the same time, the An content of plagioclase in the few AP traverses examined is higher than in the footwall; that is, pyroxene and plagioclase compositions are decoupled (Fig. 8a).

AP1 is normally 20–40 cm thick and of erratic grade. The PGE mineralization is associated with interstitial sulphides (on average 0.52 wt % sulphur; Eerola *et al.*, 1990). Average grades are 7 ppm Pd and 2 ppm Pt, and average metal tenors are 750 ppm Pt + Pd (Halkoaho *et al.*, 2005). The Outokumpu Company established a resource of 3.5 mt at 6.16 ppm Pd and 1.68 ppm Pt, 0.11 ppm Rh, 0.28 ppm Au, and 0.21 wt % Cu (average reef thickness 73 cm; Eerola *et al.*, 1990). In a detailed traverse across the AP1 reef interval, Halkoaho (1989) showed locally elevated P, Zr and K contents in some, but not all reef samples (Fig. 8a and b). An analogous enrichment in P and Zr occurs in a sample of gabbro-norite immediately above the AP2 reef.

Where the AP1 reef is potholed (Fig. 8b), it may be up to 20 m thick at an average grade of 4 ppm Pt + Pd + Au (Fig. 8a), representing a remarkable 80 ppm PGE normalized to 1 m (Supplementary Data Electronic Appendices 9 and 10). The pothole is characterized by a number of lithological and compositional anomalies, as follows. (1) The AP1 anorthosite thickens from a few centimetres to ~20 m, but at the same time, the plagioclase content of the rock decreases from >90% to <80%, constituting a gabbro-norite. The rock has a 'mottled' texture, with large (up to > 10 cm) oikocrysts of pyroxene in a matrix of plagioclase (Fig. 6d) and contains abundant lenses of pegmatoid (Fig. 6f). (2) The density of faults appears to be higher in the vicinity of the pothole (Fig. 8b). (3) Abundant subvertical pegmatoid veins and anorthosite fragments occur ~200 m above the pothole (Fig. 6g). (4) A dolerite dyke trends through the centre of the pothole (Fig. 8b). (5) Apatite in the vicinity of the pothole has elevated Cl contents (Halkoaho, 1993). (6) VLF-R and IP-DC measurements indicate a lenticular conductivity anomaly located ~5–10 m below the pothole and following its contours. The anomaly is 30 m wide, 100 m long and up to 200 m deep (Lerssi, 1990). (7) Some, but not all samples of mineralized anorthosite and some of the roof rocks show a relative enrichment in P and Zr (Fig. 8a; Halkoaho *et al.*, 1989b). (8) The hanging wall to the pothole contains barite and Ni-rich chlorite not observed elsewhere in the Penikat intrusion.

The AP2 reef is normally very sulphide-poor and almost barren, but sulphide-rich areas may occur. In one of these areas the reef has an average grade of 11.4 ppm Pd and 3.4 ppm Pt over a width of several tens

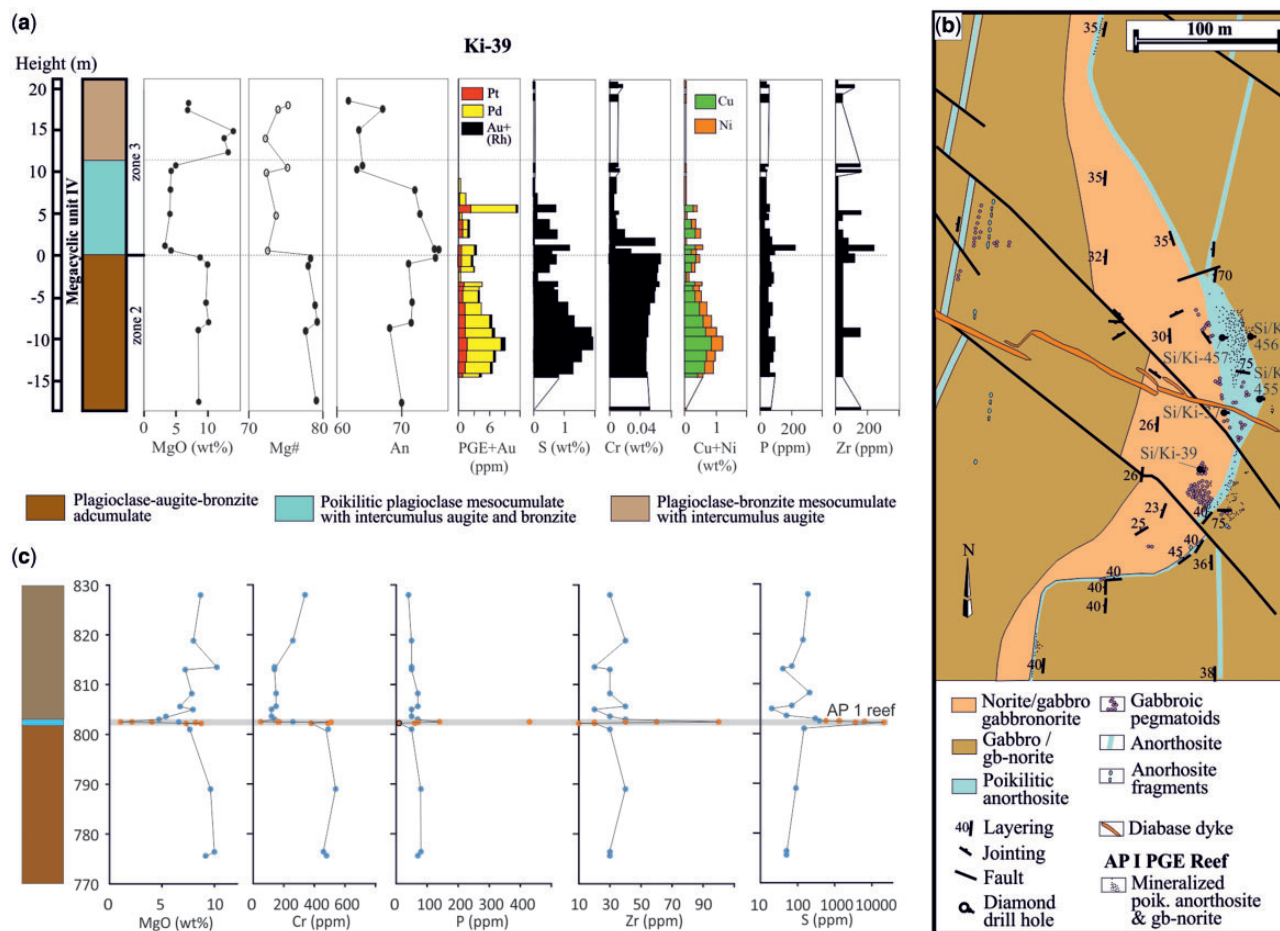


Fig. 8. (a) Stratigraphic variation of selected elements in drillcore SiKi 39 intersecting the AP1 depression structure. It should be noted that in this drillcore PGE-rich sulphides also occur in the gabbro-noritic floor rocks to the pothole. Modified after Halkoaho *et al.* (2005). (b) Map of the large depression structure of the AP1 reef. Cross-cutting relationship of the pothole across several gabbro-norite and anorthosite layers, and thickening of sulphidic anorthosite in the centre of the pothole, should be noted. (c) Compositional profile across non-potholed AP1 reef, based on traverse across the reef sampled 200–400 m to the north of the pothole (data from Halkoaho, 1989). The decrease in Cr above reef, and patchy enrichment of Zr and P in reef, should be noted.

of centimetres (Halkoaho *et al.*, 2005) but peak grades of 49 ppm Pd, 9.8 ppm Pt, and 2.07 ppm Au (gabbro-norite sample 9383–7202, immediately below the anorthosite). It strongly resembles the AP1 reef in terms of host-rock types. The mineralization is again partly located within a laterally continuous, narrow (~5 cm) anorthosite (Fig. 6b) and/or in the underlying gabbro-norite. On average, AP2 contains less base metal sulphides (0.35 wt % S) than AP1, but locally, sulphide-rich patches may contain several tens of ppm PGE. Average metal tenors are 1600 ppm (Halkoaho *et al.*, 2005). The sulphides in both AP reefs have Cu/Ni 1.4–2.7, Pd/Pt 3.7, and Pd/Ir 170–240; that is, the mineralization is of a more differentiated composition than that of the SJ reef.

In the AP reefs, 28 mineral species have been identified (Halkoaho, 1993). The PGM grains investigated vary in diameter from 1 to 65 μm , the mean being 7 μm . The dominant PGM are Pd–Te–(Bi) minerals (39.3% of all grains), sperrylite (20%), Pd–As–Sb minerals (19.7%), Pd–Pt sulphides (5.8%), RhAsS–IrAsS minerals (4.35%),

Pt–Pd–Te minerals (4.35%), Pd–As–Te minerals (2.9%) and Au–Ag minerals (3.6%). About 70% of the PGM grains in the AP1 reef were found to occur in association with silicates, 23% on the edge of base metal sulphide grains and only 7% as inclusions in sulphides. About 87% of the PGMs in the AP2 Reef occur in silicates and 13% in association with sulphides.

The PV (Paasivaara) reef

In contrast to most other PGE reefs globally, the PV reef is located directly beneath the ultramafic basal portion of a cyclic unit (MCU V). The bulk of the mineralization is hosted within an anorthosite layer that is closely associated with pegmatoidal layers or lenses. The rocks beneath and above the PV reef are relatively heterogeneous, displaying strong compositional and lithological variation commonly expressed in the form of a magmatic breccia (the ‘mixed horizon’). The reef interval also contains some of the highest concentrations of incompatible elements in the Penikat intrusion, including

K₂O, P, Pb and Ag, resulting in the occurrence of cumulus apatite and strongly biotite-enriched rocks. At the same time there may be a chromite-enriched zone near the top of the uppermost anorthosite layer (with 1–2 cm sub-rounded patches of chromitite in a 10 cm sample within drillcore SiKi 403). Finally, the PV reef has a much less fractionated PGE signature, with lower Pd/Ir, than the AP reefs, instead resembling that of the ultramafic-hosted SJ reef. Thus, the PV reef displays a remarkable disequilibrium assemblage in terms of lithology and geochemistry.

Although the PV reef has been delineated in most blocks of the intrusion, the drill campaign focused on the Ala-Penikka and Sompujärvi blocks, hence the lateral continuity of grade is less well established than that of the SJ reef (Supplementary Data Electronic Appendix 11). The available data indicate that the PV reef is richest in the Ala-Penikka block, whereas in the Yli-Penikka block it is of lower grade and more heterogeneous. Too few data exist for the Sompujärvi and Kilka blocks to assess the average grade of the reef in these areas.

A detailed profile across the Transition Zone in the Ala-Penikka block, compiled from two drillcores (SiKi 20 and 21) is shown in Fig. 9 and Supplementary Data Electronic Appendix 12. It is apparent that the Transition Zone forms a compositionally distinct package relative to both the footwall and hanging-wall rocks, with a gradational contact to the former and a sharp contact to the latter. The Transition Zone is characterized by strongly enhanced lithological and chemical variation, expressed by interlayering of mela- and leucogabbroic rocks, anorthosite and pegmatoids with highly variable compositions. The abundance of anorthosite is particularly noteworthy. There are three layers within about 35 m of stratigraphy, each 1–2 m wide, whereas in the under- and overlying rocks, anorthosite occurs every 150 m or so. All three anorthosite layers are directly overlain by melanocratic rocks, suggesting a genetic relationship between anorthosite and the melanocratic layers. In general, the rocks of the Transition Zone are less evolved than the footwall rocks (e.g. in terms of Mg# of augite or An of plagioclase), yet more evolved than the hanging-wall rocks. Notably, some of the plagioclase-rich rocks show a strong enrichment in highly incompatible elements K, P and, locally, Zr, and some anorthosites and associated pegmatoids are also enriched in PGE and Cu (Supplementary Data Electronic Appendix 12). The mineralized zones are separated by several metres of unmineralized or poorly mineralized anorthositic and gabbroic rocks. The best PGE grades are found within the uppermost mottled anorthosite (average thickness of mineralization is ~1 m). Average grades of this layer are 2.3 ppm for Pd and 3.9 ppm for Pt and combined Pt + Pd tenors are 280 ppm, somewhat lower than in the SJ and AP reefs (Halkoaho *et al.*, 2005). The Outokumpu Company established a resource of 5 mt at 2.58 ppm Pd, 4.04 ppm Pt, 0.08 ppm Rh, 0.61 ppm Au, 0, 28 wt % Cu, and 0.63 wt % S over a reef thickness of

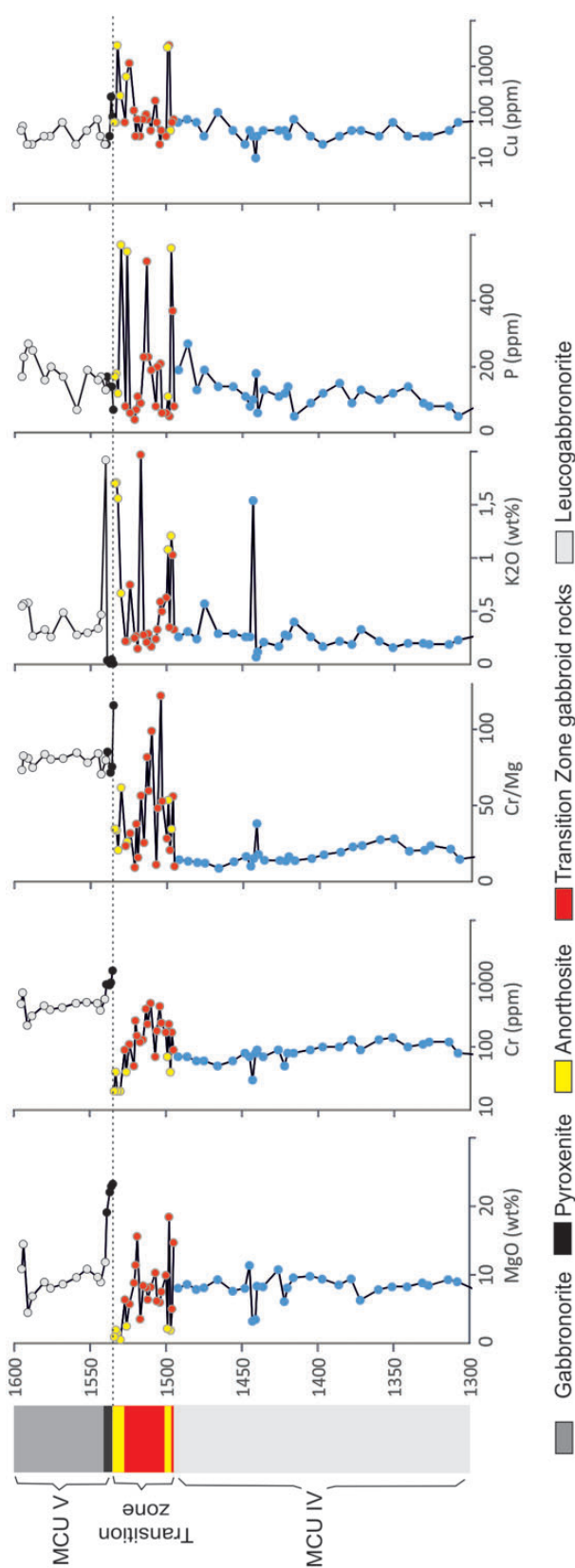


Fig. 9. Compositional variation across the PV reef in the Ala-Penikka block (data from Huhtelin, 1989). It should be noted that the Transition Zone is characterized by a combination of enhanced lithological and compositional variation expressed in layering, as well as enrichment in both compatible and incompatible elements and Cu–Ni–PGE sulphides.

1.09 m (Eerola *et al.*, 1990). Cu/Ni is ~ 1 , Pd/Ir is 28, and Pt/Pd is ~ 2 , the last being the highest in the Penikat intrusion.

In the Yli-Penikka block the PV reef occurs within a broad pegmatoidal zone, with anorthosite forming a less continuous layer. Peak grades are 4 ppm Pt, 2.69 ppm Pd and 0.41 ppm Au over 42 cm. In the Kilkka block the peak grades are Pt 1.50 ppm, Pd 0.87 ppm and Au 0.11 ppm over 48 cm and Pt 1.3 ppm, Pd 2.32 ppm and Au 0.29 ppm over 78 cm. In the Sompujärvi block, exposed by drillcore Ki-403, the Transition Zone is about 25 m thick. There is no mixed rock or pegmatoid at all, and incompatible trace elements are not noticeably enriched. There are several anorthosite layers, including a 6 m seam at the top and several thinner seams (between 10 and 60 cm thick) below this. PGE are concentrated in a 1 m interval towards the top of the main anorthosite, notably in the 10 cm chromite-rich zone at its top contact, with bulk contents of 2.09 ppm Pd, 2.49 ppm Pt and 0.43 ppm Au (Fig. 10).

SAMPLES

Most of the samples used in the present study were collected in outcrop during a field excursion in 2011 to the Ala-Penikka block in the southern portion of the intrusion. In addition, eight samples were collected in 2009, focusing on the SJ and AP reef intervals. Most samples weigh between 1 and 2 kg, and their locations are shown in Fig. 11. To study the ultramafic portion of MCU II, we used outcrop and drillcore samples collected in 1982 in the Sompujärvi block. Additional data for drillcores intersecting the SJ and AP reefs are given in Supplementary Data Electronic Appendix 7.

Four gabbro pegmatoid samples have been previously dated using the conventional U–Pb thermal ionization mass spectrometry (TIMS) method, all yielding discordant results owing to post-magmatic disturbance (Perttunen & Vaasjoki, 2001). Using *in situ* analysis, we re-examined zircon grains from sample A603-Oravikangas, for which Perttunen & Vaasjoki (2001) obtained an imprecise bulk zircon U–Pb age of 2428 ± 35 Ma.

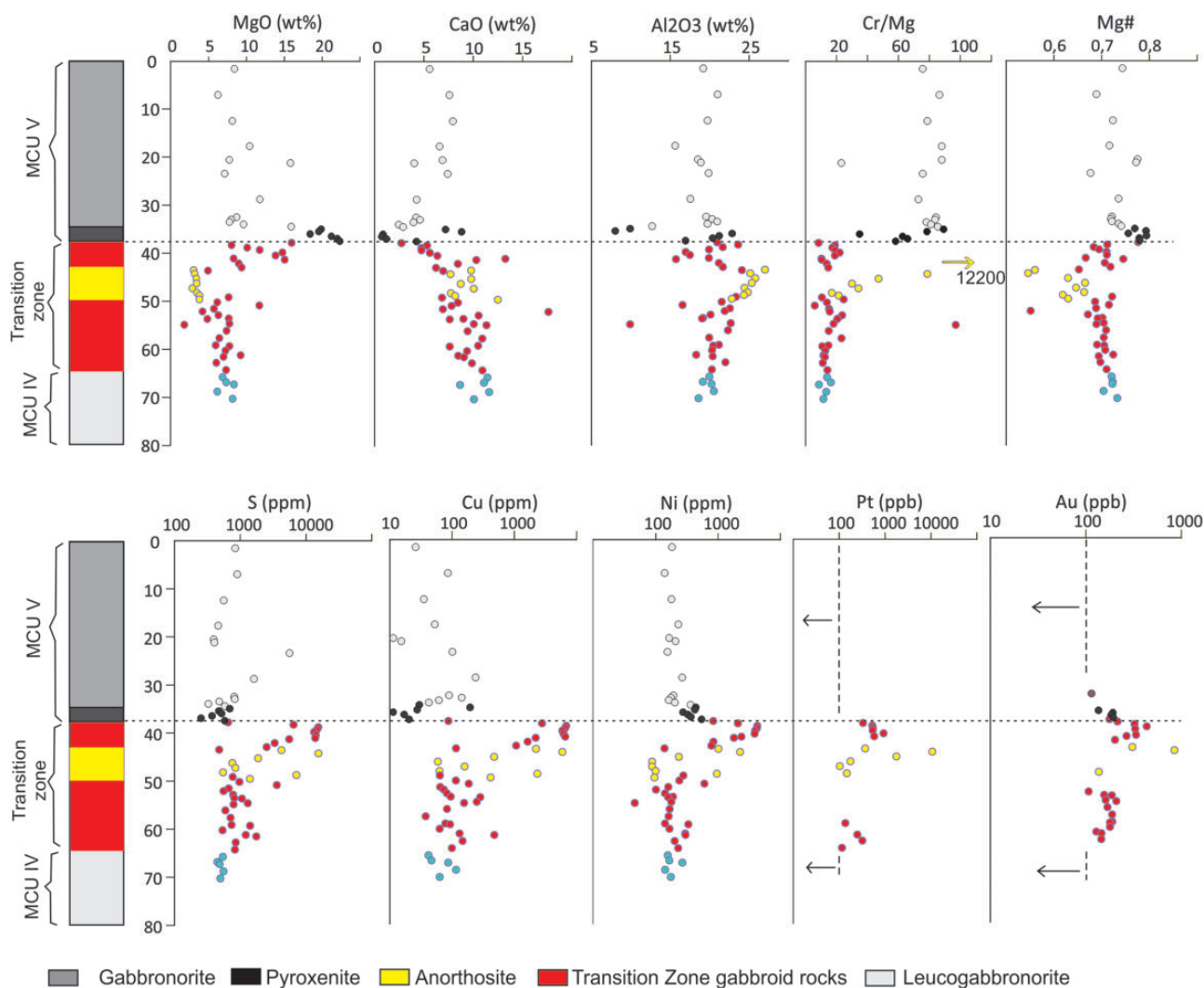


Fig. 10. Drillcore profile SiKi 403 across the Transition Zone and the PV reef in the Sompujärvi block.

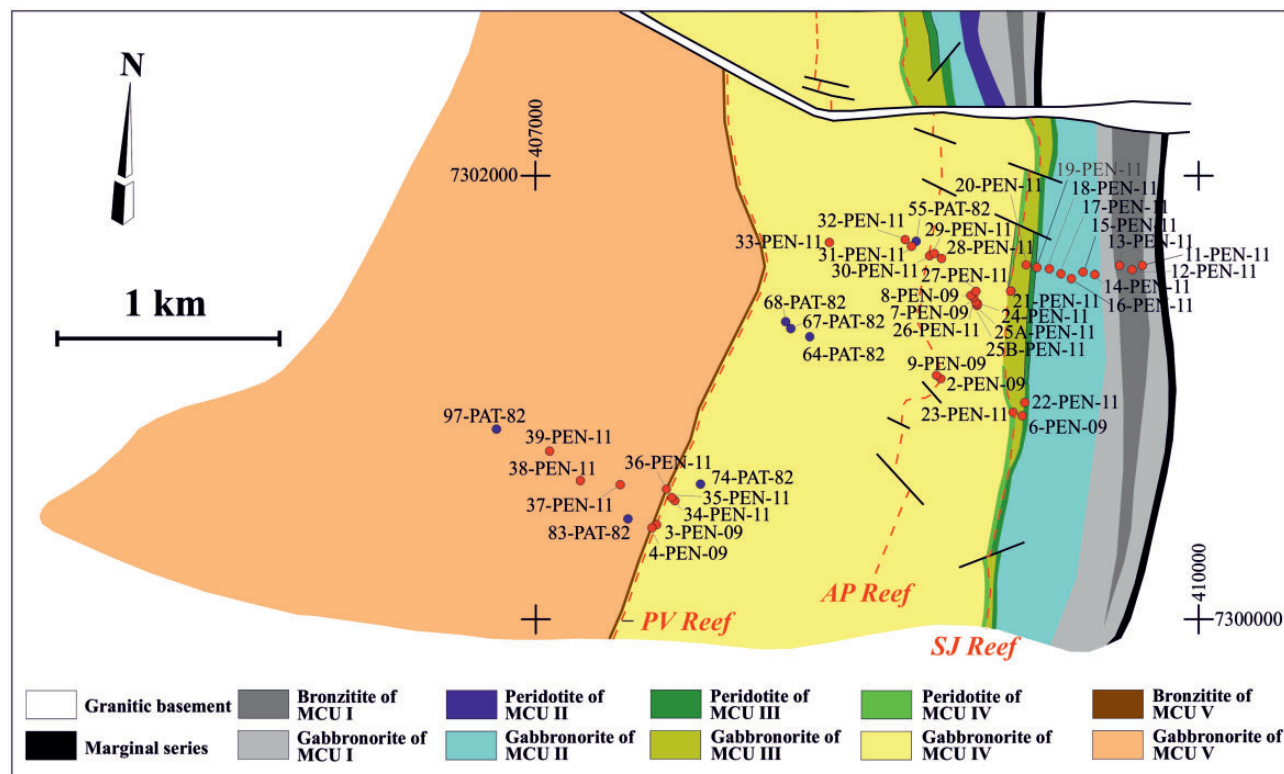


Fig. 11. Geological map of the Ala-Penikka block, showing sample sites for this study. The positions of the PGE reefs are shown by red dashed line.

ANALYTICAL METHODS

After the preparation of thin sections at the University of Oulu, the samples were milled in an alumina vessel. The samples were analysed for major elements and a range of lithophile minor and trace elements including Sr, Rb, Nb, Y, Zr, Ni, Cu, Zn, Co, Cr, Sc, V and REE using inductively coupled plasma optical emission spectrometry (ICP-OES) and inductively coupled plasma mass spectrometry (ICP-MS) at Cardiff University, UK. Full details of the analytical procedures have been given by McDonald & Viljoen (2006). The concentrations of the platinum-group elements were determined at the University of Quebec in Chicoutimi (UQAC), Canada, using ICP-MS after Ni sulphide fire assay and Te co-precipitation [see Savard *et al.* (2010) for analytical details]. Details of analytical accuracy and precision are given in Table 2. Selenium was determined by thiol cotton fibre instrumental neutron activation (TCF-INAA) at UQAC [see Savard *et al.* (2006) for method description]. All data are provided in Table 3.

The Sm–Nd isotope analyses were performed at the Geological Survey of Finland (GTK) in Espoo, using isotope dilution (ID) and TIMS (VG Sector 54). Between 120 and 200 mg of powdered sample were spiked with a ^{149}Sm – ^{150}Nd tracer. The sample–spike mixture was dissolved in HF–HNO₃ in Savillex screw-cap beakers on a hot plate for 48 h. After evaporation of fluorides, the residue was dissolved in 6N HCl and a clear solution was achieved. Samarium and Nd were separated in two

stages using a conventional cation exchange procedure with 7 ml of AG50Wx8 ion exchange resin in a bed of 12 cm length, and a modified version of the Teflon–HDEHP hydrogen diethylhexyl phosphate method developed by Richard *et al.* (1976). The measurements were made in dynamic mode on a VG SECTOR 54 mass spectrometer using Ta–Re triple filaments. The $^{143}\text{Nd}/^{144}\text{Nd}$ ratio was normalized to $^{146}\text{Nd}/^{144}\text{Nd} = 0.7219$. The long-term average $^{143}\text{Nd}/^{144}\text{Nd}$ for the La Jolla standard is 0.511849 ± 0.000013 (standard deviation for 130 measurements during the years 2008–2011). During 2013, the average $^{143}\text{Nd}/^{144}\text{Nd}$ for the La Jolla standard was 0.511851 ± 0.000009 ($n = 85$). The Sm/Nd ratio of the spike was calibrated against the Caltech mixed Sm/Nd standard (Wasserburg *et al.*, 1981). Based on duplicate analyses, the error in $^{147}\text{Sm}/^{144}\text{Nd}$ is estimated to be 0.4%. Initial $^{143}\text{Nd}/^{144}\text{Nd}$ ratios and ϵNd values were calculated using the following parameters: $\lambda^{147}\text{Sm} = 6.54 \times 10^{-12} \text{ a}^{-1}$, $^{147}\text{Sm}/^{144}\text{Nd} = 0.1966$ and $^{143}\text{Nd}/^{144}\text{Nd} = 0.51264$ for present CHUR. Depleted mantle model ages (T_{DM}) were calculated according to DePaolo (1981). Measurements on the rock standard BCR-1 (e.g. Weis *et al.*, 2006) provided the following values: Sm = 6.58 ppm, Nd = 28.8 ppm, $^{147}\text{Sm}/^{144}\text{Nd} = 0.1380$, $^{143}\text{Nd}/^{144}\text{Nd} = 0.51264 \pm 0.00002$. Total procedural blank was <0.5 ng for Nd by mass spectrometry at GTK. All Nd isotope data are shown in Table 4.

The U–Pb analyses were carried out using a Nu Plasma AttoM single-collector ICP-MS system

Table 2: Estimate of accuracy and precision based on results for international reference material determined at UQAC

	OKUM UQAC this run		<i>n</i> = 4 beads RDS%	OKUM Certificate Ontario Geological Survey	
	ng g ⁻¹	SD		ng g ⁻¹	SD
Os	0.5	0.04	8.60	0.98*	0.34
Ir	1.05	0.04	3.87	0.99	0.07
Ru	3.74	0.17	4.62	4.25	0.3
Rh	1.24	0.03	2.77	1.4	0.12
Pt	11.84	0.72	6.12	11.04	0.55
Pd	10.3	0.80	7.81	11.73	0.5
Au	1.01	0.28	28.00	1.5	0.16

*Savard *et al.* (2010).

connected to a Photon Machine Analyte G2 laser ablation (LA) system at the Finnish Isotope Geosciences Laboratory (SIGL) located in the Geological Survey of Finland, Espoo. Samples were ablated in He gas (gas flows = 0.4 and 0.1 l min⁻¹) within a HelEx ablation cell (Müller *et al.*, 2009). The He aerosol was mixed with Ar (gas flow = 0.8 l min⁻¹) prior to entry into the plasma. The gas mixture was optimized daily for maximum sensitivity. Typical ablation conditions were beam diameter 25 µm, pulse frequency 5 Hz and beam energy density 2 J cm⁻². A single U–Pb measurement included a short pre-ablation, 10 s of on-mass background measurement followed by 30 s of ablation with a stationary beam. ²³⁵U was calculated from the signal at mass 238 using a natural ²³⁸U/²³⁵U = 137.88 (Ludwig, 2003). Mass number 204 was used as a monitor for common ²⁰⁴Pb. In an ICP-MS analysis, ²⁰⁴Hg mainly originates from the He supply. The observed background counting-rate on mass 204 was 150–200 c.p.s. The contribution of ²⁰⁴Hg from the plasma was eliminated by on-mass background measurement prior to each analysis. Age-related common lead (Stacey & Kramers, 1975) correction was used when the analysis showed common lead contents above the detection limit. Signal strengths on mass 206 were typically 100 000 c.p.s., depending on the uranium content and age of the zircon.

Two calibration standards were run at the beginning and end of each analytical session, and at regular intervals during sessions. Raw data were corrected for the background, laser-induced elemental fractionation, mass discrimination and drift in ion counter gains, and reduced to U–Pb isotope ratios by calibration to concordant reference zircons of known age, using protocols adapted from Andersen *et al.* (2004) and Jackson *et al.* (2004). The calculations were performed off-line, using an interactive spreadsheet program written in Microsoft Excel/VBA by T. Andersen (Rosa *et al.*, 2009). In-house standard zircons A382 (1877 ± 2 Ma) and A1772 (2712 ± 1 Ma, Huhma *et al.*, 2012) were used for calibration. To minimize the effects of laser-induced elemental fractionation, the depth-to-diameter ratio of the ablation pit was kept low, and isotopically homogeneous segments of the time-resolved traces were calibrated against the corresponding time interval for each mass in the reference zircon. Plotting of the U–Pb isotopic

data and age calculations were performed using the Isoplot/Ex 3 program (Ludwig, 2003). All the ages were calculated with 2σ errors and without decay constants errors. Data-point error ellipses in the figures are at the 2σ level. The ²⁰⁷Pb/²⁰⁶Pb age offset from concordant ID-TIMS ages for several samples does not exceed 0.5%.

RESULTS

Geochronology

To refine the age of sample A603-Oravikangas from the Penikat intrusion, studied earlier by Perttunen & Vaasjoki (2001), 18 single zircon grains were analysed using LA-ICP-MS. The results are shown in Table 5 and plotted in Fig. 12. All measured compositions plot at or close to the concordia curve. Excluding the two most discordant analyses, the data yield an age of 2444 ± 8 Ma (2σ), which is more precise than the TIMS age of 2428 ± 35 Ma proposed by Perttunen & Vaasjoki (2001) based on five analyses of discordant baddeleyite.

Lithophile element geochemistry

In the absence of preserved primary minerals in many of the rocks, the mineralogy of the samples has been deduced based on major element compositions, which are largely controlled by variations in the modal proportions of the major silicate minerals. A plot of CaO vs MgO (Fig. 13a) shows that the analysed ultramafic rocks comprise mainly lherzolites, olivine orthopyroxenites and websterites. Wehrlites are rare and dunites are absent. The Al₂O₃ vs MgO plot (Fig. 13b) indicates that the proportion of intercumulus plagioclase in several of the ultramafic rocks is slightly higher than 10%. The mafic rocks consist of gabbro-norites, norites and anorthosites. Gabbros appear to be rare. Most of the mafic rocks have more than 50% plagioclase, and there are few mesogabbroic rocks, analogous to, for example, the Bushveld Complex, where this was termed the ‘melanorite gap’ by Maier & Eales (1997). Chromite is an accessory phase in many of the samples, irrespective of rock type (Fig. 13c). In the gabbroic rocks, magnetite may account for some of the Cr budget. Assuming that the parental magma was a siliceous high-magnesian basalt (SHMB) containing 70 ppm Zr (as discussed

Table 3: Whole-rock compositional data from Penikat intrusion

Block:	Ala-Pen	Ala-Pen	Ala-Pen	Keski-Pen	Sompuj	Keski-Pen	Sompuj	Sompuj	Sompuj	Ala-Pen
Sample no.:	11 PEN	12 PEN	13 PEN	107B PAT	SiKi7-268-16	108B PAT	SiKi7-209-61	SiKi7-195-9	SiKi7-192-4	14 PEN
Height (above base, m):	50	90	130	165	170	185	200	207	208-5	220
Sample type:	Outcrop	Outcrop	Outcrop	Outcrop	drillcore	Outcrop	drillcore	drillcore	drillcore	Outcrop
Rock type	Opx	Opx	Opx	Webs	Ol-opx	Ol-opx	Webs	Ol-opx	Ol-opx	GN
MCU:	I	I	I	II	II	II	II	II	II	II
<i>wt %</i>										
SiO ₂	51.32	50.45	50.70	46.48	35.76	39.64	50.51	40.93	39.28	50.79
TiO ₂	0.29	0.14	0.25	0.20	0.25	0.09	0.08	0.10	0.07	0.23
Al ₂ O ₃	5.26	6.30	5.58	5.46	5.85	3.26	2.98	5.27	4.45	14.56
Fe ₂ O ₃	10.85	10.95	12.25	8.61	17.83	15.03	8.08	11.29	17.99	7.00
MnO	0.22	0.22	0.23	0.21	0.33	0.16	0.13	0.14	0.15	0.15
MgO	22.90	23.32	21.28	19.49	25.58	29.38	22.49	23.54	20.96	9.79
CaO	4.70	5.57	5.78	16.26	2.59	2.99	10.24	6.95	8.87	14.10
Na ₂ O	0.68	0.69	0.38	0.33	0.09	0.08	0.12	0.10	0.11	1.58
K ₂ O	0.18	0.23	0.08	0.02	0.00	0.00	0.01	0.00	0.00	0.13
P ₂ O ₅	0.05	0.01	0.05	0.00	0.01	0.00	0.01	0.00	0.00	0.02
Cr ₂ O ₃	0.57	0.35	0.34	0.41	6.12	0.54	1.92	0.74	0.39	0.19
LOI	3.15	0.88	3.59	3.04	6.86	9.14	2.20	10.48	7.31	0.60
Total	100.18	99.12	100.50	100.52	101.26	100.32	98.77	99.53	99.58	99.16
<i>ppm</i>										
Sc	29	28	34	42	23	13	25	20	16	34
V	143	79	111	105	262	62	86	77	72	118
Cr	3915	2372	2304	2798	41894	3721	13116	5048	2703	1283
Co	91	90	98	89	161	128	109	99	107	50
Ni	272	271	245	455	502	622	434	509	524	130
Cu	108	150	60	64	26	115	859	26	228	235
Zn	90	73	110	27	251	38	79	51	40	45
Ga	8.1	6.7	7.6	7.1	11.1	5.7	5.7	5.9	6.1	11.3
Rb	7.4	10.0	4.2	2.4	2.3	0.3	0.9	0.4	0.3	2.4
Sr	97	105	25	57	4	12	21	46	46	225
Y	7.5	3.4	7.1	6.0	4.0	3.6	2.5	3.2	4.6	5.8
Zr	32.7	15.5	20.3	14.1	13.9	11.9	8.6	11.1	16.2	20.8
Nb	2.1	4.1	1.7	1.0	0.8	0.7	0.6	0.8	0.7	1.3
Mo	0.56	0.57	0.53	0.56	0.48	0.45	0.62	0.44	0.44	0.55
Sn	0.35	0.52	0.58	0.32	0.36	0.20	0.19	0.30	0.32	0.49
Cs	0.38	0.25	0.53	0.27	0.09	0.05	0.06	0.05	0.04	0.18
Ba	84	79	57	38	2	24	4	7	5	81
La	4.18	1.74	3.22	1.86	0.78	1.76	0.49	1.72	1.28	2.58
Ce	9.04	3.51	6.56	4.29	2.13	3.43	1.01	3.62	3.03	5.82
Pr	1.17	0.44	0.92	0.61	0.31	0.46	0.17	0.45	0.42	0.76
Nd	4.71	1.79	3.79	2.78	1.43	1.86	0.87	1.88	1.91	3.45
Sm	1.09	0.40	0.95	0.80	0.38	0.38	0.28	0.42	0.50	0.88
Eu	0.35	0.21	0.26	0.35	0.11	0.13	0.05	0.15	0.12	0.36
Gd	1.08	0.40	0.96	0.78	0.45	0.47	0.27	0.44	0.49	0.84
Tb	0.17	0.07	0.17	0.15	0.08	0.07	0.05	0.07	0.10	0.14
Dy	1.10	0.48	1.10	0.94	0.52	0.49	0.37	0.46	0.63	0.93
Ho	0.22	0.10	0.22	0.20	0.10	0.09	0.07	0.09	0.12	0.19
Er	0.67	0.32	0.72	0.57	0.33	0.29	0.22	0.28	0.35	0.55
Tm	0.11	0.06	0.12	0.09	0.05	0.05	0.04	0.05	0.06	0.09
Yb	0.71	0.38	0.73	0.58	0.32	0.30	0.23	0.27	0.36	0.54
Lu	0.10	0.05	0.11	0.09	0.05	0.05	0.03	0.05	0.06	0.08
Hf	0.88	0.42	0.60	0.41	0.37	0.32	0.26	0.34	0.39	0.61
Ta	0.14	0.23	0.12	0.07	0.04	0.04	0.03	0.06	0.05	0.08
Th	0.95	0.45	0.74	0.29	0.28	0.28	0.27	0.34	0.26	0.43
U	0.14	0.08	0.13	0.04	0.05	0.05	0.04	0.07	0.06	0.06
C	119	102	194	387	314	2751	290	16945	13645	123
S	52	172	36	182	479	861	1104	1250	2945	708
<i>ppb</i>										
Se	n.d.	n.d.	48.8	n.d.	n.d.	n.d.	n.d.	n.d.	n.d.	n.d.
Os	0.50	0.72	0.30	0.25	1.97	0.65	4.07	0.13	0.17	<0.065
Ir	0.90	1.82	2.27	4.12	43.36	9.62	33.81	3.51	2.27	0.18
Ru	2.35	2.77	1.81	0.80	7.67	2.61	14.46	0.89	0.73	<0.12
Rh	1.71	2.66	5.29	16.64	146.64	28.79	64.54	10.69	7.56	0.43
Pt	5.6	5.6	20.1	88.5	450.6	56.9	56.0	39.3	30.8	4.0
Pd	3.4	5.6	6.3	21.0	226.0	31.5	28.6	77.2	99.1	4.6
Au	1.53	5.02	1.52	0.79	4.33	1.49	0.65	1.45	3.41	0.70
eNd	n.d.	-1.8	n.d.	n.d.	n.d.	n.d.	n.d.	n.d.	n.d.	n.d.

(continued)

Table 3: Continued

Ala-Pen 15 PEN 260 Outcrop GN II	Ala-Pen 16 PEN 305 Outcrop GN II	Ala-Pen 17 PEN 345 Outcrop GN II	Ala-Pen 18 PEN 385 Outcrop GN II	Ala-Pen 19 PEN 425 Outcrop GN II	Ala-Pen 116 PAT 455 Outcrop OI-opx III	Ala-Pen 22 PEN 460 Outcrop OI-opx III	Ala-Pen 6 Pen 465 Outcrop GN III	Ala-Pen 20 PEN 470 Outcrop GN III	Ala-Pen 21 PEN 520 Outcrop GN III	Sompuj SiKi2-160-76 545 drillcore GN III	Ala-Pen 23 PEN 551 Outcrop OI-opx IV
51-00	50-99	49-76	48-62	50-14	45-94	32-65	48-40	51-36	50-90	43-42	46-69
0-13	0-15	0-16	0-10	0-11	0-12	0-19	0-10	0-10	0-25	0-13	0-11
17-33	16-19	18-75	16-91	17-28	5-97	15-02	15-60	16-21	18-87	9-04	5-89
5-61	5-27	4-65	5-94	4-57	10-62	11-50	5-70	5-10	5-82	13-12	8-35
0-12	0-12	0-10	0-12	0-10	0-14	0-11	0-11	0-11	0-10	0-14	0-15
11-27	10-82	9-37	13-94	11-23	27-14	28-93	12-40	10-66	7-42	20-97	25-06
11-64	13-30	13-13	11-33	13-16	10-77	0-81	13-98	14-31	12-72	4-74	6-84
1-76	1-41	1-74	1-15	1-16	0-17	0-10	1-11	1-20	1-93	0-01	0-12
0-16	0-22	0-13	0-11	0-22	<0-01	0-01	0-36	0-09	0-20	0-01	0-01
0-00	0-01	0-01	0-01	0-00	0-02	0-02	<0-01	0-00	0-02	0-02	0-01
0-24	0-22	0-17	0-13	0-12	0-48	0-07	n.d.	0-23	0-07	n.d.	0-93
1-65	0-57	1-26	2-51	1-54	n.d.	10-55	n.d.	0-92	0-86	7-26	4-86
100-91	99-27	99-23	100-86	99-64	101-36	99-98	97-76	100-29	99-14	98-85	99-01
25	32	27	20	24	n.d.	27	29	30	29	12	16
77	83	88	69	72	80	96	90	84	119	44	86
1650	1503	1173	871	842	3280	471	809	1550	483	382	6371
48	47	49	60	49	n.d.	117	43	42	32	109	110
154	136	130	277	142	690	238	244	150	109	1017	1179
109	72	158	95	149	210	55	<20	147	118	32	243
34	24	44	33	22	n.d.	52	n.d.	24	31	46	66
12-8	10-9	12-2	10-9	10-3	n.d.	12-3	n.d.	9-7	14-2	6-7	6-9
3-7	5-7	3-4	1-8	6-1	n.d.	0-5	17-1	1-1	3-3	0-1	0-7
258	236	271	196	198	10	2	n.d.	167	273	1	9
4-5	4-6	4-4	3-1	3-4	n.d.	1-2	3-3	2-8	7-4	2-3	1-8
11-1	14-9	11-4	18-1	8-7	n.d.	17-9	8-0	6-8	18-3	8-1	13-5
1-0	1-2	1-0	1-2	0-7	n.d.	1-3	<0-2	0-7	1-3	0-2	1-6
0-54	0-59	0-59	0-66	0-73	n.d.	0-48	n.d.	0-49	0-50	0-43	0-44
0-52	0-36	0-45	0-47	0-52	n.d.	0-30	n.d.	0-42	0-36	0-30	0-34
0-36	0-25	0-25	0-22	0-28	n.d.	0-05	n.d.	0-14	0-25	0-16	0-02
60	77	65	39	59	n.d.	10	n.d.	23	76	0	30
3-04	1-52	1-98	1-26	1-04	n.d.	0-54	0-89	0-68	3-29	0-34	0-87
6-31	3-43	4-25	2-67	2-37	n.d.	1-01	1-84	1-58	7-55	0-84	1-79
0-81	0-47	0-55	0-36	0-32	n.d.	0-13	0-31	0-23	1-04	0-12	0-21
3-34	2-12	2-39	1-54	1-55	n.d.	0-56	1-28	1-09	4-77	0-63	0-94
0-85	0-60	0-61	0-35	0-42	n.d.	0-12	0-44	0-32	1-17	0-19	0-23
0-41	0-29	0-31	0-23	0-24	n.d.	0-05	0-22	0-20	0-46	0-06	0-07
0-75	0-59	0-63	0-40	0-43	n.d.	0-12	0-43	0-34	1-19	0-22	0-22
0-12	0-11	0-11	0-07	0-08	n.d.	0-02	<0-1	0-06	0-19	0-04	0-04
0-76	0-75	0-73	0-49	0-55	n.d.	0-13	0-58	0-46	1-26	0-29	0-27
0-15	0-14	0-14	0-10	0-11	n.d.	0-03	0-12	0-09	0-24	0-06	0-05
0-44	0-43	0-42	0-29	0-33	n.d.	0-10	0-28	0-28	0-74	0-16	0-17
0-07	0-07	0-07	0-05	0-05	n.d.	0-02	<0-1	0-05	0-12	0-03	0-03
0-44	0-42	0-43	0-29	0-34	n.d.	0-14	0-32	0-28	0-70	0-25	0-17
0-07	0-06	0-06	0-04	0-05	n.d.	0-02	<0-1	0-04	0-11	0-04	0-03
0-36	0-46	0-38	0-47	0-28	n.d.	0-48	<0-5	0-26	0-59	0-15	0-36
0-07	0-08	0-08	0-07	0-05	n.d.	0-09	<0-2	0-05	0-08	0-02	0-12
0-35	0-31	0-46	0-24	0-19	n.d.	0-40	<0-5	0-23	0-33	0-09	0-43
0-05	0-04	0-04	0-02	0-02	n.d.	0-06	<0-2	0-02	0-05	0-01	0-10
72	65	146	171	81	n.d.	331		56	312	494	138
10	81	41	24	16	70	67	<60	20	33	<20	70
n.d.	36-9	26-6	15-6	15-6	n.d.	n.d.	n.d.	n.d.	n.d.	n.d.	n.d.
0-10	0-07	<0-065	<0-065	<0-065	1-02	<0-065	<1	0-10	<0-065	1-47	60-78
1-30	1-10	1-37	0-18	0-06	10-92	0-04	0-23	1-06	0-04	1-67	118-88
0-41	0-19	0-18	<0-12	<0-12	3-40	<0-12	<2	0-32	0-12	4-99	110-53
3-30	4-94	3-16	0-23	0-16	21-87	0-08	<1	2-18	<0-082	1-34	389-70
11-2	27-6	43-5	11-6	3-2	31-9	0-6	2-2	7-8	1-6	9-9	2087-1
12-0	24-1	17-9	6-3	9-4	9-0	1-1	3-6	9-3	0-3	26-1	940-0
0-93	0-22	0-67	0-05	<0-484	1-46	<0-484	0-89	0-83	0-49	<0-484	42-58
-3-1	n.d.	n.d.	n.d.	n.d.	n.d.	n.d.	n.d.	n.d.	n.d.	n.d.	1

(continued)

Table 3: Continued

Sompuj SiKi2- 167-66 551 drillcore Ol-opx IV	Sompuj SiKi2- 176-0 559 drillcore Ol-opx IV	Sompuj SiKi2- 178-65 561-9 drillcore Ol-opx IV	Sompuj SiKi2- 180-75 564 drillcore Webs IV	Ala-Pen 24 PEN 627 Outcrop GN IV	Ala-Pen 25 PEN 631 Outcrop Anorth IV	Ala-Pen 25X PEN 631 Outcrop Anorth IV	Ala-Pen 26 PEN 631.5 Outcrop Webs IV	Ala-Pen 7 Pen 649 Outcrop GN IV	Ala-Pen 27 PEN 651 Outcrop Anorth IV	Ala-Pen 8 Pen 654 Outcrop GN IV	Ala-Pen 28 PEN 760 Outcrop GN IV
40-40	46-50	37-30	50-62	49-79	50-42	49-13	43-50	49-80	48-43	51-00	50-79
0-13	0-14	0-07	0-27	0-21	0-12	0-28	0-11	0-21	0-15	0-44	0-24
5-21	4-36	4-47	2-91	17-04	25-02	24-58	4-95	21-10	23-62	15-80	16-61
14-51	11-23	19-18	8-02	7-31	3-67	4-99	19-22	6-06	4-70	7-97	6-58
0-14	0-16	0-13	0-20	0-12	0-08	0-08	0-16	0-08	0-08	0-13	0-14
27-02	23-30	26-82	23-08	10-60	2-31	5-65	19-97	7-50	3-99	8-88	9-46
1-66	2-83	1-97	8-89	10-43	13-04	9-22	8-09	12-72	13-77	12-61	12-60
0-09	0-04	0-10	0-11	1-85	3-06	2-55	0-11	1-99	2-89	1-90	1-84
0-01	0-02	0-00	0-00	0-16	1-54	1-99	0-00	0-21	0-36	0-20	0-19
0-02	0-01	0-01	0-01	0-02	0-01	0-01	0-01	0-02	0-02	0-03	0-01
0-05	n.d.	0-05	0-15	0-02	0-02	0-01	0-02	n.d.	0-03	n.d.	0-06
10-16	11-46	8-94	4-78	1-67	1-99	2-78	2-98	n.d.	1-90	n.d.	0-91
99-38	100-07	99-04	99-06	99-23	101-29	101-26	99-13	99-69	99-93	98-97	99-43
16	16	15	30	17	8	6	18	20	14	42	30
48	43	40	45	70	38	31	47	94	64	204	101
320	472	369	1037	153	118	44	127	204	191	665	418
141	111	163	98	61	29	62	94	39	39	43	55
1195	1245	1033	667	301	32	196	601	251	62	218	148
35	25	152	1285	180	162	75	107	48	56	61	83
50	49	40	21	28	24	27	29	n.d.	40	n.d.	82
5-4	4-1	5-1	3-2	13-5	19-7	18-3	5-3	n.d.	16-3	n.d.	12-9
0-2	0-4	0-2	0-2	3-2	45-7	56-3	0-0	4-1	11-1	4-3	3-8
7	13	9	7	257	727	436	4	n.d.	367	n.d.	247
3-0	2-6	2-5	3-1	5-0	3-0	2-0	2-3	4-5	8-6	11-8	5-8
15-8	5-7	11-0	28-5	13-7	11-8	10-2	6-0	15-4	10-5	28-5	15-6
1-0	0-5	0-7	1-2	2-0	1-1	1-4	0-8	0-4	0-8	1-1	1-0
0-47	0-46	0-52	0-46	0-57	0-57	0-59	0-47	n.d.	0-51	n.d.	0-51
0-31	1-25	0-27	0-25	0-32	0-44	0-40	0-16	n.d.	0-16	n.d.	0-30
0-04	0-22	0-03	0-03	0-57	0-99	3-23	0-01	n.d.	0-81	n.d.	0-41
7	8	3	1	85	227	362	12	n.d.	100	n.d.	76
1-18	1-51	0-84	0-57	3-04	4-18	3-60	0-57	3-03	7-80	4-65	2-58
2-60	2-84	1-82	1-48	6-37	7-80	6-59	1-17	6-25	16-80	11-60	5-63
0-33	0-34	0-23	0-21	0-78	0-86	0-72	0-24	0-71	2-14	1-59	0-75
1-38	1-39	0-94	1-00	3-31	3-39	2-73	1-05	3-15	9-00	7-33	3-30
0-34	0-32	0-24	0-29	0-75	0-64	0-44	0-27	0-71	2-08	1-92	0-81
0-06	0-09	0-06	0-06	0-44	0-87	0-60	0-08	0-46	1-14	0-47	0-39
0-32	0-28	0-24	0-34	0-76	0-62	0-43	0-24	0-82	1-97	2-39	0-81
0-06	0-05	0-05	0-06	0-13	0-09	0-06	0-05	0-12	0-30	0-34	0-14
0-43	0-32	0-32	0-45	0-81	0-54	0-34	0-31	0-82	1-65	2-19	0-95
0-08	0-07	0-06	0-09	0-16	0-10	0-07	0-06	0-19	0-28	0-46	0-19
0-28	0-18	0-20	0-30	0-47	0-30	0-20	0-20	0-46	0-75	1-25	0-58
0-05	0-03	0-04	0-05	0-08	0-05	0-03	0-04	<0-1	0-10	0-18	0-10
0-28	0-24	0-23	0-30	0-50	0-28	0-20	0-25	0-52	0-57	1-15	0-58
0-05	0-03	0-03	0-05	0-07	0-04	0-03	0-04	<0-1	0-08	0-18	0-08
0-39	0-11	0-31	0-68	0-45	0-36	0-33	0-23	0-50	0-37	0-94	0-49
0-07	0-04	0-04	0-07	0-13	0-09	0-09	0-04	<0-2	0-06	<0-2	0-06
0-35	0-12	0-32	0-33	0-32	0-32	0-25	0-34	<0-5	0-47	<0-5	0-39
0-07	0-02	0-05	0-05	0-07	0-05	0-03	0-04	<0-2	0-33	<0-2	0-07
7243	39	7415	5223	74	493	265	140	150	376	370	118
763	654	2121	2086	104	58	64	239	148	54	368	105
n.d.	n.d.	n.d.	n.d.	n.d.	n.d.	n.d.	n.d.	n.d.	n.d.	n.d.	n.d.
2-12	6-34	6-37	9-80	0-37	0-17	0-09	<0-065	<1	0-08	<1	<0-065
1-49	6-96	10-49	16-48	0-13	0-15	0-11	0-38	<0-1	0-20	<0-1	0-07
5-18	18-40	15-32	36-40	0-18	<0-12	0-14	0-15	<2	0-16	<2	0-16
0-81	8-43	27-82	19-34	0-13	0-21	0-09	0-63	<1	0-36	<1	0-08
4-5	19-2	102-5	82-0	7-1	6-1	5-4	4-6	3-9	4-2	4-3	2-1
7-8	20-1	77-8	116-3	13-6	9-5	6-8	1-6	5-1	2-7	4-3	2-0
1-53	<0-484	4-47	5-92	1-93	0-58	<0-484	1-86	1-26	<0-484	1-51	0-78
n.d.	n.d.	n.d.	n.d.	n.d.	n.d.	n.d.	n.d.	n.d.	n.d.	n.d.	-1-3

(continued)

Table 3: Continued

Ala-Pen 29 PEN 796 Outcrop GN IV	Ala-Pen 2 PEN 802 Outcrop GN IV	Ala-Pen 9 PEN 803 Outcrop Anorth IV	Ala-Pen 30 PEN 804 Outcrop GN IV	Ala-Pen 55 PAT 846 Outcrop GN IV	Ala-Pen 31 PEN 885 Outcrop GN IV	Ala-Pen 32 PEN 913 Outcrop GN IV	Ala-Pen 33 PEN 1100 Outcrop GN IV	Ala-Pen 64 PAT 1158 Outcrop GN IV	Ala-Pen 67 PAT 1220 Outcrop GN IV	Ala-Pen 68 PAT 1240 Outcrop GN IV	Ala-Pen 74 PAT 1440 Outcrop GN IV
51.09	46.60	52.20	49.94	50.86	50.72	51.42	51.50	51.79	50.59	51.93	51.16
0.27	0.20	0.15	0.21	0.31	0.24	0.26	0.23	0.31	0.23	0.22	0.25
19.22	16.20	25.80	18.63	15.69	17.93	16.02	16.62	17.78	17.16	21.43	17.46
5.77	8.55	2.79	6.90	7.09	6.26	6.54	6.20	5.87	6.61	4.83	6.64
0.10	0.10	0.03	0.13	0.13	0.13	0.13	0.12	0.12	0.13	0.09	0.13
6.81	8.69	2.53	8.07	9.45	8.39	8.67	8.51	8.12	8.90	5.42	7.93
14.66	11.96	11.80	11.55	12.75	12.56	12.92	13.51	13.75	12.64	13.27	12.68
2.15	1.80	4.07	2.02	1.63	2.08	1.77	1.76	1.96	1.89	2.58	2.11
0.22	0.22	0.41	0.30	0.14	0.20	0.23	0.21	0.17	0.42	0.33	0.20
0.01	<0.01	<0.01	0.01	0.02	0.01	0.02	0.01	0.01	0.01	0.02	0.02
0.07	n.d.	n.d.	0.02	0.06	0.04	0.04	0.02	0.02	0.01	0.01	0.01
0.74	n.d.	n.d.	1.54	1.11	1.03	1.11	0.79	0.74	1.55	1.06	1.54
101.12	94.31	99.78	99.32	99.25	99.60	99.13	99.49	100.65	100.16	101.19	100.14
31	30	11	20	34	27	30	36	37	33	24	34
115	120	53	72	120	93	110	129	120	108	84	103
455	490	28	145	442	276	293	116	103	82	58	71
35	115	11	47	81	53	55	40	41	38	27	39
102	4300	119	210	144	133	303	131	146	130	88	132
82	8000	40	100	133	97	73	138	88	28	110	92
70	n.d.	n.d.	36	48	52	80	47	39	48	30	37
14.3	n.d.	n.d.	14.3	12.0	13.0	12.8	13.3	13.5	13.6	15.6	13.9
3.5	5.4	9.4	6.3	2.7	3.7	5.1	5.1	5.3	18.1	8.8	4.1
308	n.d.	n.d.	277	226	256	252	269	285	283	353	298
7.1	5.1	1.9	4.7	7.8	5.2	6.4	6.3	6.3	6.0	5.0	6.4
15.7	11.4	13.5	10.4	22.1	16.1	17.9	14.4	20.6	15.6	17.7	17.5
0.7	<0.2	0.2	1.0	1.5	1.4	1.1	1.0	1.9	1.1	1.6	1.1
0.51	n.d.	n.d.	0.49	0.64	0.60	0.48	0.50	0.52	0.46	0.52	0.53
0.36	n.d.	n.d.	0.31	0.42	0.36	0.35	0.51	1.06	0.36	0.39	0.41
0.28	n.d.	n.d.	0.69	0.25	0.53	0.34	0.25	0.26	0.48	0.16	0.22
82	n.d.	n.d.	104	81	83	82	66	66	82	115	68
3.16	1.74	2.86	2.15	3.50	2.87	3.02	2.24	2.41	2.62	3.09	3.23
7.40	4.36	5.39	4.51	7.81	6.11	6.75	5.10	5.45	5.82	6.58	6.93
1.03	0.56	0.61	0.59	1.04	0.76	0.89	0.68	0.74	0.77	0.82	0.89
4.63	3.22	2.10	2.50	4.69	3.22	3.83	3.28	3.28	3.36	3.33	3.80
1.15	0.64	0.39	0.62	1.12	0.77	0.98	0.87	0.89	0.87	0.78	0.96
0.47	0.34	0.51	0.40	0.45	0.38	0.40	0.40	0.42	0.42	0.46	0.44
1.11	0.81	0.34	0.65	1.11	0.78	0.95	0.88	0.89	0.88	0.79	0.95
0.19	0.13	<0.1	0.11	0.18	0.13	0.16	0.15	0.16	0.15	0.13	0.17
1.23	0.74	0.20	0.75	1.20	0.83	1.04	1.06	1.03	0.96	0.80	1.01
0.23	0.19	<0.1	0.15	0.23	0.16	0.20	0.20	0.21	0.19	0.17	0.22
0.69	0.49	0.20	0.47	0.74	0.51	0.61	0.62	0.61	0.60	0.48	0.62
0.11	<0.1	<0.1	0.08	0.12	0.08	0.10	0.10	0.11	0.10	0.08	0.10
0.67	0.47	<0.15	0.50	0.69	0.55	0.63	0.58	0.62	0.61	0.48	0.62
0.10	<0.1	<0.1	0.08	0.11	0.08	0.09	0.09	0.10	0.10	0.08	0.09
0.51	<0.5	<0.5	0.36	0.64	0.48	0.57	0.47	0.62	0.48	0.52	0.53
0.05	<0.2	<0.2	0.07	0.10	0.10	0.08	0.07	0.11	0.07	0.11	0.06
0.32	<0.5	<0.5	0.30	0.56	0.46	0.48	0.33	0.38	0.38	0.45	0.50
0.05	<0.2	<0.2	0.03	0.08	0.08	0.08	0.06	0.06	0.07	0.13	0.09
242	14600	<100	114	318	97	113	127	162	304	277	265
43	14600	<60	87	84	235	173	84	91	140	68	161
n.d.	n.d.	n.d.	n.d.	n.d.	79.3	n.d.	n.d.	n.d.	n.d.	n.d.	n.d.
<0.065	74.60	3.68	0.25	<0.065	<0.065	<0.065	<0.065	<0.065	<0.065	<0.065	<0.065
0.04	137.00	0.69	0.26	0.13	0.09	0.04	0.04	0.03	1.88	2.72	0.66
<0.12	80.20	<2	0.33	<0.12	0.19	<0.12	0.14	0.13	0.14	0.15	0.16
<0.082	510.00	<1	0.19	0.11	0.12	<0.082	<0.082	<0.082	0.33	0.25	1.02
1.9	5550.0	12.9	7.3	5.9	3.2	1.7	1.9	1.6	137.5	219.0	27.9
<0.471	21000.0	1.2	7.6	4.6	1.1	1.3	2.4	1.3	126.4	31.1	30.1
<0.484	1010.00	0.91	1.07	0.62	0.61	0.72	0.73	1.10	3.07	5.55	16.96
n.d.	n.d.	n.d.	n.d.	n.d.	n.d.	n.d.	-1.4	n.d.	n.d.	n.d.	n.d.

(continued)

Table 3: Continued

Ala-Pen 34 PEN 1490 Outcrop GN IV	Ala-Pen 35 PEN 1510 Outcrop GN IV	Ala-Pen 3 Pen 1530 Outcrop Anorth IV	Ala-Pen 36 PEN 1535 Outcrop Webs V	Ala-Pen 4 Pen 1540 Outcrop Norite V	Ala-Pen 83 PAT 1620 Outcrop Norite V	Ala-Pen 37 PEN 1670 Outcrop GN V	Ala-Pen 38 PEN 1795 Outcrop GN V	Ala-Pen 39 PEN 1920 Outcrop Gabbro V	Ala-Pen 97 PAT 2260 Outcrop Gabbro V
49-86	53-58	47-10	51-00	50-30	51-16	52-42	51-88	51-97	53-43
0-20	0-83	0-19	0-37	0-20	0-31	0-26	0-25	0-22	0-40
17-84	21-06	23-70	6-74	19-10	16-97	18-06	18-40	17-73	15-39
6-83	4-49	7-07	12-55	6-54	8-18	7-09	6-14	6-90	8-40
0-13	0-07	0-05	0-22	0-12	0-14	0-13	0-11	0-13	0-17
8-23	4-18	4-60	17-68	9-16	9-17	8-22	8-07	9-04	8-29
13-06	10-95	10-27	7-97	9-62	8-95	8-91	10-12	9-43	7-92
2-23	2-39	2-25	0-12	2-25	2-39	2-20	2-43	2-06	3-20
0-17	0-39	0-59	0-04	0-19	0-55	0-53	0-34	0-44	0-80
0-01	0-10	0-03	0-05	0-02	0-02	0-03	0-04	0-02	0-06
0-01	0-01	n.d.	0-15	n.d.	n.d.	0-05	0-04	0-05	0-05
1-44	1-94	n.d.	3-47	n.d.	1-19	1-35	1-38	1-86	1-91
100-02	99-98	95-86	100-36	97-50	99-03	99-25	99-19	99-83	100-02
32	10	12	35	17	21	19	20	21	33
111	103	68	144	78	89	84	90	99	152
58	74	160	1042	480	436	364	298	350	350
59	33	79	90	37	52	55	43	53	47
139	112	3600	343	240	186	163	134	139	118
152	175	3760	61	40	59	69	116	60	101
55	57	n.d.	67	n.d.	53	62	56	38	72
13-8	17-0	n.d.	7-8	n.d.	15-1	15-3	15-5	14-4	15-9
4-8	11-1	17-9	0-6	4-9	16-3	16-0	9-5	12-0	31-1
344	371	n.d.	8	n.d.	311	343	339	321	295
6-3	8-5	4-2	9-9	3-9	7-2	6-4	6-1	4-9	11-2
18-0	55-6	24-3	34-3	14-8	35-5	28-8	26-0	22-1	46-0
0-9	4-8	0-5	2-4	0-5	2-1	2-9	1-5	1-1	2-3
0-57	0-66	n.d.	0-52	n.d.	0-51	0-79	0-59	0-72	0-55
0-30	0-58	n.d.	0-39	n.d.	0-42	0-46	0-52	0-27	0-59
0-30	0-28	n.d.	0-04	n.d.	0-96	0-85	0-54	0-86	0-59
47	143	n.d.	5	n.d.	152	155	112	126	210
2-94	8-81	4-11	2-89	2-70	5-39	5-35	4-58	3-60	7-10
6-54	18-57	6-81	6-77	5-45	11-10	11-18	9-64	7-47	16-04
0-87	2-18	0-78	1-05	0-63	1-33	1-33	1-18	0-89	2-03
3-85	8-84	3-41	5-28	3-17	5-19	5-45	4-84	3-65	8-30
0-96	1-68	0-70	1-32	0-43	1-13	1-09	1-00	0-77	1-95
0-45	0-63	0-39	0-32	0-32	0-53	0-53	0-46	0-46	0-71
0-93	1-63	0-64	1-33	0-51	1-05	1-08	0-97	0-75	1-86
0-16	0-24	0-12	0-21	0-10	0-17	0-16	0-15	0-12	0-30
1-06	1-44	0-74	1-41	0-67	1-05	1-06	0-94	0-78	1-79
0-21	0-27	0-16	0-28	0-14	0-22	0-20	0-19	0-15	0-36
0-63	0-86	0-42	0-91	0-30	0-72	0-64	0-60	0-49	1-05
0-10	0-13	<0-1	0-16	<0-1	0-12	0-11	0-10	0-08	0-17
0-61	0-78	0-45	0-97	0-49	0-70	0-65	0-57	0-53	1-03
0-09	0-12	<0-1	0-15	<0-1	0-12	0-10	0-09	0-07	0-16
0-56	1-53	0-70	0-89	0-50	0-95	0-82	0-74	0-61	1-18
0-06	0-29	<0-2	0-16	<0-2	0-12	0-20	0-12	0-09	0-16
0-46	1-44	<0-5	0-86	<0-5	1-09	0-88	0-88	0-62	1-61
0-07	0-31	<0-2	0-14	<0-2	0-19	0-19	0-17	0-12	0-29
270	405	9900	206	110	304	334	125	124	613
100	143	9900	154	110	93	154	136	118	166
34-5	n.d.	24600	12-8	n.d.	n.d.	n.d.	n.d.	16-4	n.d.
<0-065	0-16	53-00	<0-065	<1	<0-065	<0-065	<0-065	<0-065	<0-065
0-81	0-44	90-40	0-11	0-52	<0-025	0-04	0-03	0-03	0-04
<0-12	0-26	116-00	<0-12	<2	0-15	<0-12	0-16	<0-12	0-17
0-09	0-59	88-60	0-13	<1	<0-082	<0-082	<0-082	<0-082	<0-082
69-4	19-0	4290-0	3-2	28-0	<0-084	0-3	<0-084	2-0	1-1
9-1	3-3	2210-0	0-6	21-7	<0-471	<0-471	<0-471	<0-471	<0-471
1-02	1-64	471-00	<0-484	1-32	<0-484	0-51	<0-484	<0-484	0-50
n.d.	n.d.	n.d.	n.d.	n.d.	-2-1	n.d.	-2-4	n.d.	n.d.

Ala-Pen, Ala-Penikka; Keski-Pen, Keski-Penikka; Sompuj, Sompujärvi. Opx, orthopyroxenite; OIPx, olivine pyroxenite. GN, gabbro-norite; Anorth, anorthosite; Webs, websterite. Major elements determined by ICP-OES, trace elements by ICP-MS, S and C by elemental infrared analysis, Se by TCF-INAA, and PGE by ICP-MS after Ni sulphide fire assay. n.d., not determined.

Table 4: Sm–Nd isotopic analyses of rocks of the Penikat intrusion

Sample/ analysis no.	Rock type	Sm (ppm)	Nd (ppm)	±0.5%, 0.0050	¹⁴³ Nd/ ¹⁴⁴ Nd	2SE	T (Ma)	eps(T)	T _{DM} (Ma) DePaolo
P12	Bronzite	0.38	1.74	0.0007	0.511499	0.000020	2440	−1.8	2883
P15	Gabbro	1.04	4.48	0.0007	0.511584	0.000010	2440	−3.1	3082
P23 #2	Peridotite– pyroxenite (SJ reef)	0.20	0.67	0.0009	0.512402	0.000013	2440	1.0	
P28	Gabbro	0.96	3.99	0.0007	0.511757	0.000010	2440	−1.3	2924
P33 #2	Gabbro	0.95	3.70	0.0008	0.511912	0.000012	2440	−1.4	3017
P37	Gabbro	1.45	6.76	0.0006	0.511459	0.000010	2440	−2.1	2903
P39	Gabbro	0.91	4.26	0.0006	0.511438	0.000010	2440	−2.4	2922

below), the ultramafic rocks contain mostly between 10 and 20% trapped liquid (Fig. 13d). This suggests that the rocks are meso- and orthocumulates, consistent with the proportion of intercumulus plagioclase in the rocks. Adcumulates, such as those developed in parts of the Lower and Lower Critical Zones of the Bushveld Complex, are not present. For the gabbroic rocks, an estimation of trapped liquid component is not attempted, as many of the rocks probably crystallized from a more evolved liquid and/or reacted with percolating trace element rich melt. However, what can be said is that the Penikat anorthosites tend to have significantly more intercumulus pyroxene than many Bushveld anorthosites, reflected in the fact that none of our anorthosite samples, nor those of Halkoaho *et al.* (1989b), contain less than about 2% MgO and >25% Al₂O₃, whereas in the Bushveld Upper Critical Zone anorthosite adcumulates with <1–2% MgO and >25% Al₂O₃ are common (Maier & Eales, 1997).

Most samples from across the Penikat intrusion have fractionated primitive mantle normalized incompatible element patterns that show strong negative Nb–Ta, P, and Ti anomalies (Fig. 14). One of the samples from MCU I is relatively depleted in most trace elements, but shows a positive Nb–Ta anomaly. Two samples (one each from MCU II and IV) are relatively unfractionated. Several samples from MCU III and the SJ Reef lack negative Nb–Ta and Ti anomalies, and several mineralized SJ reef samples (unlike most samples from the other reefs) are characterized by distinct positive Zr–Hf anomalies. However, these samples tend to be relatively altered and thus it is possible that some of the patterns reflect selective element mobility.

The compositional variation with height through the intrusion is summarized in Fig. 15. Elevated MgO contents are characteristic of the pyroxene- and olivine rich rocks, but concentrations above 30 wt % MgO are confined to MCU II and MCU III and the base of MCU IV. The basal portions of all MCUs are relatively enriched in Cr, resulting from the presence of chromite disseminations, layers or stringers. The remainder of MCU I–III is somewhat less Cr enriched, but still contains >1000 ppm Cr. MCU IV is different; its base is characterized by chromite enrichment located within a relatively thin, highly altered pyroxenite that in most cases also hosts the bulk of the PGE enrichment. However, this is

overlain by ultramafic and mafic rocks that contain <400 ppm Cr, reflected by strong Cr depletion in augite (<0.2 wt % Cr₂O₃ at an Mg# of 0.75–0.8; Halkoaho, 1993; Alapieti & Halkoaho, 1995). There is a marked compositional reversal towards less evolved compositions at the base of MCU V, particularly in terms of the Cr content of the whole-rocks and augite. The modified differentiation index (Fig. 4) also shows a distinct reversal at this stratigraphic level. The mafic rocks of MCU IV and V are characterized by subdued fractionation, analogous to that seen in the Main Zone of the Bushveld Complex and the mafic zone of the Great Dyke (Wilson & Chaumba, 1997; Maier *et al.*, 2013).

Regarding the immobile incompatible trace elements, the analysed profile shows slightly elevated Zr, Th and P contents in the basal samples, followed by relatively low contents throughout MCU II and III, a slight increase through MCU IV, a strong peak in some PV reef samples and then mostly relatively high values in MCU V. The SJ reef is not enriched in incompatible elements relative to its footwall and hanging-wall (Fig. 16), but isolated zircon grains, up to 0.5 mm in width, have been described by Halkoaho *et al.* (1990a) in sample Si/Ki-153/98-75.

Ratios of incompatible elements may also serve as an indicator of differentiation. Ce/Sm shows little systematic variation through the intrusion, plotting in the range of the putative SHMB and tholeiitic parent magmas (Guo & Maier, 2013). However, there is a marked change at the base of MCU V, where Ce/Sm increases from ~8 to 11. Values of εNd are mostly around −2, in the range of Finnish 2.45 Ga layered intrusions and SHMB dykes (Hanski *et al.*, 2001; Hanski, 2012). The analysed SJ reef sample forms an exception in having a higher εNd value (+1) typical of Finnish 2.45 Ga tholeiitic dykes (Vuollo, 1994; Vuollo & Huhma, 2005). However, this sample has very low REE contents and it is possible that the Sm/Nd ratio is not primary.

Variations in ore elements

The Penikat intrusion contains at least six intervals of significant PGE enrichment (Fig. 15b), mostly associated with compositional discontinuities in the igneous stratigraphy, analogous to PGE reefs in many other PGE-mineralized layered intrusions. The SJ and AP reefs occur in rocks of distinctly more evolved

Table 5: LA-ICP-MS analyses on zircon from sample gabbro pegmatoid A603, Oravikangas, Penikat intrusion

Spot no.	ppm		Ratios				Discordance			Ages (Ma)							
	U	Pb	$^{206}\text{Pb}/^{204}\text{Pb}$	$^{207}\text{Pb}/^{206}\text{Pb}$	$^{207}\text{Pb}/^{235}\text{U}^*$	$^{206}\text{Pb}/^{238}\text{U}^*$	$^{206}\text{Pb}/^{238}\text{U}$	Central (%)	$^{207}\text{Pb}/^{206}\text{Pb}$	$^{207}\text{Pb}/^{235}\text{U}$	$^{206}\text{Pb}/^{238}\text{U}$	1σ					
A603-17	214	108	27620	0.1473	0.0021	8.131	0.338	0.4003	0.0157	0.94	-7	2315	24	2246	38	2170	72
A603-7	218	127	56804	0.1513	0.0018	9.214	0.480	0.4416	0.0224	0.97	0	2361	20	2360	48	2358	100
A603-12b	206	123	54110	0.1545	0.0020	9.848	0.389	0.4625	0.0172	0.94	3	2396	21	2421	36	2450	76
A603-12	316	222	34894	0.1551	0.0017	11.542	0.440	0.5397	0.0197	0.96	20	2403	18	2568	36	2782	83
A603-13	469	281	115906	0.1574	0.0014	10.197	0.311	0.4700	0.0138	0.96	3	2428	15	2453	28	2483	60
A603-6	303	201	21489	0.1583	0.0018	11.238	0.374	0.5150	0.0161	0.94	12	2437	19	2543	31	2678	68
A603-18	331	216	169756	0.1583	0.0016	11.349	0.429	0.5199	0.0190	0.97	13	2438	16	2552	35	2699	80
A603-5	266	163	91375	0.1586	0.0014	10.546	0.343	0.4824	0.0151	0.96	5	2440	13	2484	30	2538	66
A603-9	349	240	131407	0.1586	0.0014	11.769	0.402	0.5383	0.0178	0.97	17	2440	15	2586	32	2776	74
A603-15	461	272	137841	0.1590	0.0013	10.177	0.317	0.4642	0.0139	0.96	1	2445	14	2451	29	2458	61
A603-3	269	170	55321	0.1592	0.0014	10.911	0.375	0.4972	0.0165	0.97	8	2447	14	2516	32	2602	71
A603-3b	222	139	50315	0.1593	0.0015	10.768	0.353	0.4904	0.0154	0.96	6	2448	15	2503	30	2572	66
A603-4	222	143	95850	0.1599	0.0015	11.191	0.377	0.5077	0.0165	0.96	10	2454	15	2539	31	2647	70
A603-14	175	108	85648	0.1601	0.0016	10.613	0.337	0.4809	0.0145	0.95	4	2456	17	2490	29	2531	63
A603-8	384	242	160487	0.1601	0.0013	10.968	0.375	0.4968	0.0165	0.97	7	2457	12	2520	32	2600	71
A603-1	350	215	211302	0.1602	0.0014	10.661	0.351	0.4827	0.0153	0.96	4	2458	14	2494	31	2539	66
A603-10	285	170	68284	0.1604	0.0017	10.366	0.338	0.4687	0.0145	0.95	1	2460	17	2468	30	2478	64
A603-11	217	131	63164	0.1604	0.0015	10.483	0.327	0.4741	0.0142	0.96	2	2460	15	2478	29	2501	62

$^{206}\text{Pb}/^{204}\text{Pb}$ calculated from background subtracted counts using program by T. Andersen (for low concentration samples unreliable). $^{206}\text{Pb}_c$ (%) is percentage of common ^{206}Pb in measured ^{206}Pb calculated from the ^{204}Pb signal using age-related common lead after model of Stacey & Kramers (1975). Errors are 1σ absolute. Rho is correlation of Pb/U errors. T. Andersen is acknowledged for providing the program used for data reduction. Two standard samples were used in calibration: A1772 and A382 (Huhma et al., 2012).

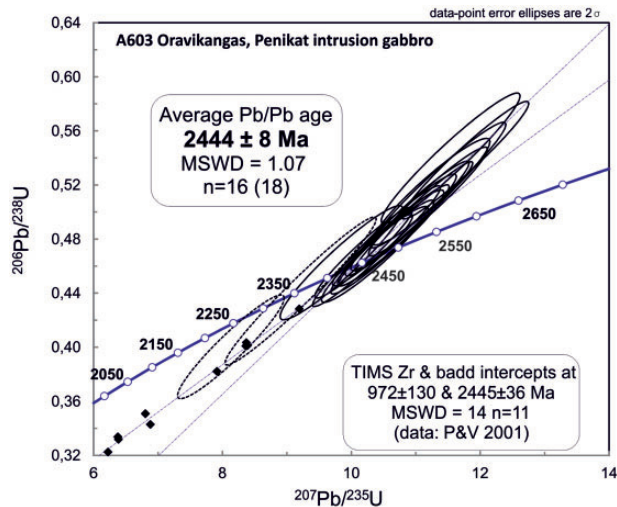


Fig. 12. Concordia diagram showing zircon U–Pb isotope data for gabbro pegmatoid sample A603-Oravikangas from the Penikat intrusion, determined using LA-ICP-MS on zircon. Black diamonds indicate TAMS analyses after Perttunen & Vaasjoki (2001) (P&V 2001). The LA-ICP-MS error ellipses are at 2σ .

composition than their footwall, as discussed in more detail below. In contrast, the PV reef is more ‘primitive’ than its footwall, as reflected by higher whole-rock Cr/V, as well as the Mg# of whole-rocks and augite.

The intrusion displays a general trend of progressive PGE fractionation with height, expressed by increasing (Pt + Pd)/(IPGE + Rh), albeit with several reversals. The lowest values occur in MCU I and at the base of MCU II, III, and IV. Notably, the bulk of the intrusion has higher Cu/(Pt + Pd) than the primitive mantle (i.e. it is PGE depleted). Fertile rocks [i.e. those with Cu/(Pt + Pd) < 3000] mainly occur at the ultramafic base of MCU II, III and IV and in some gabbroic–anorthositic rocks of MCU IV (e.g. in and around the AP and PV reefs). This is in marked contrast to the Bushveld Complex, where the bulk of the Lower Zone and Critical Zone have Cu/(Pt + Pd) ratios below primitive mantle levels (Maier *et al.*, 2013). Cu/Zr ratios are mostly between three and 100 (not shown), significantly higher than in Finnish SHMB and tholeiites (Guo & Maier, 2013). S/Se ratios are broadly around the mantle value

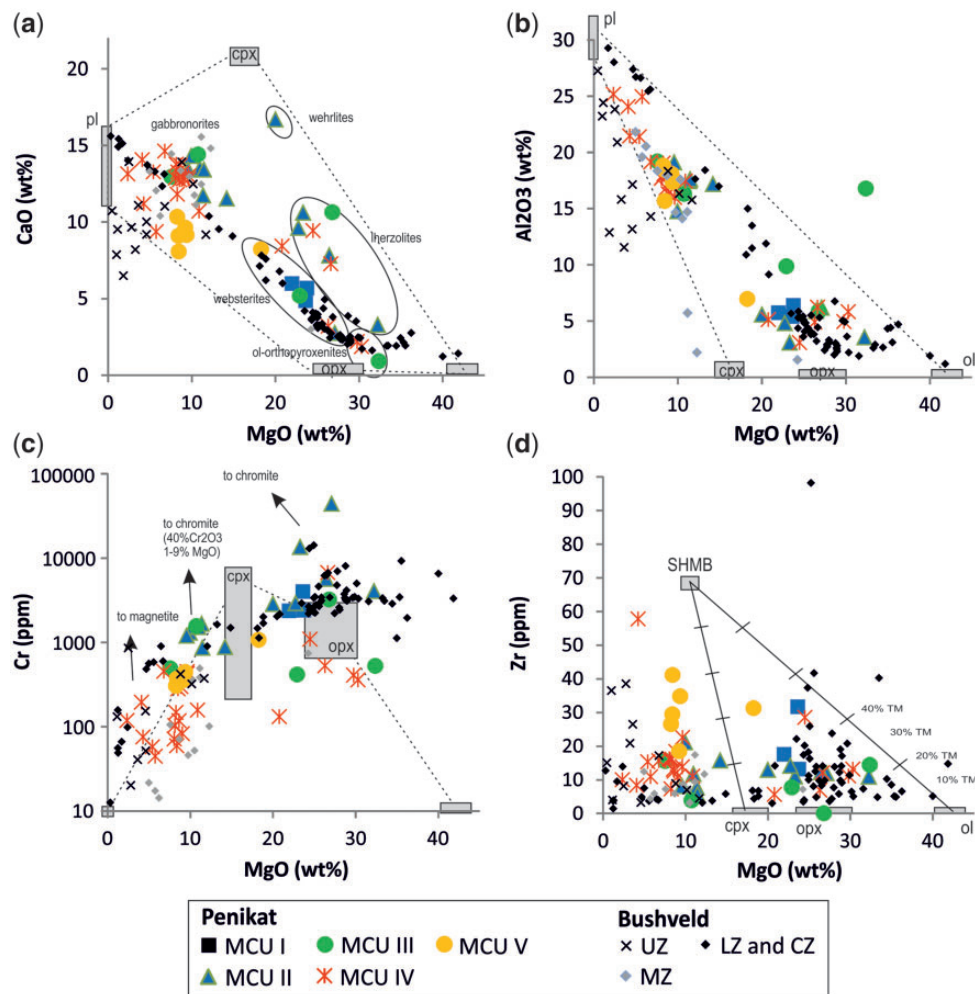


Fig. 13. Binary variation diagrams of major, minor and trace elements plotted vs MgO. (a) CaO vs MgO. (b) Al₂O₃ vs MgO. It should be noted that samples define two distinct fields, one being ultramafic and the other mafic. Intermediate samples are absent. (c) Cr vs MgO. (d) Zr vs MgO. Many of the ultramafic samples contain in excess of 10% trapped liquid.

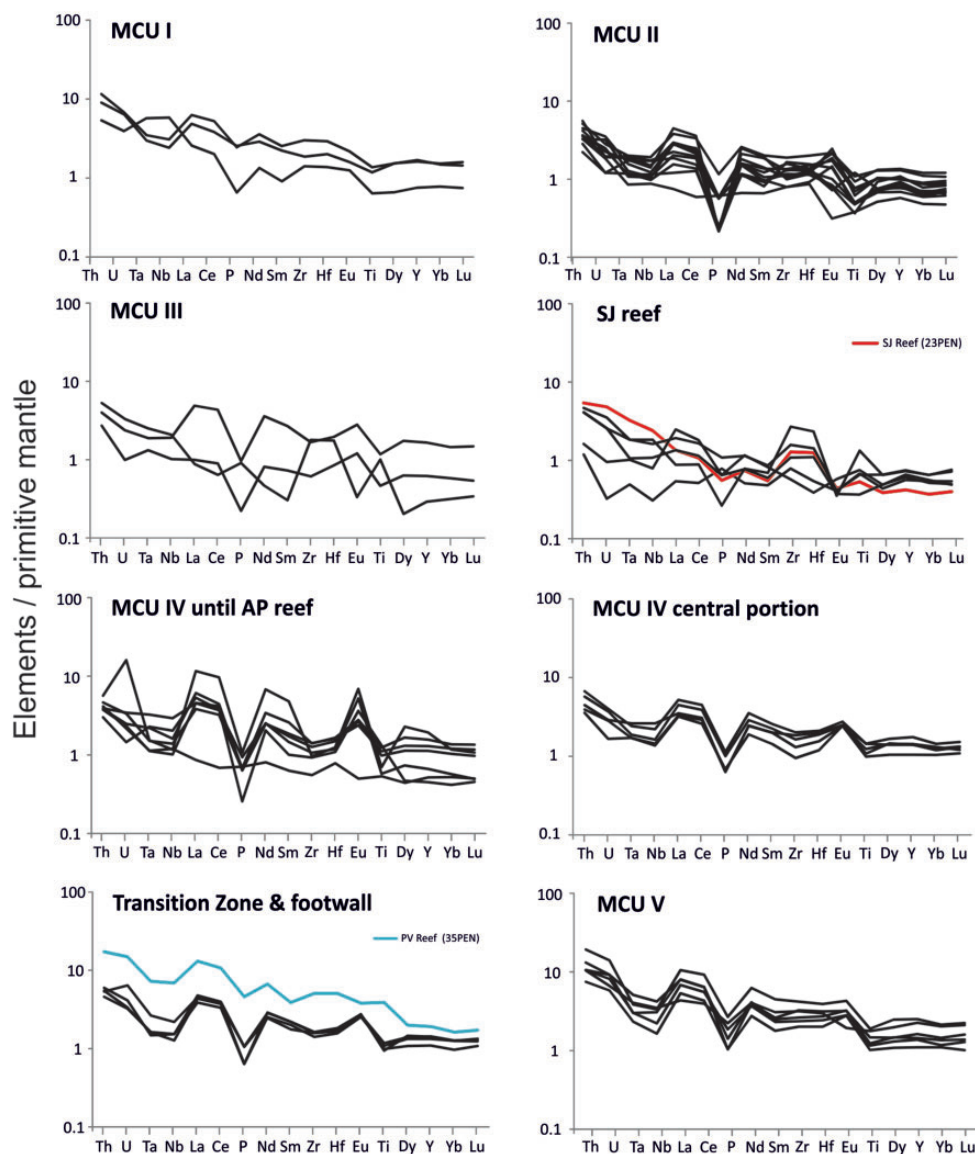


Fig. 14. Primitive mantle normalized incompatible element variation diagrams. Normalisation factors are from Sun and McDonough (1989).

throughout most of the intrusion. However, no samples from the relatively S-poor SJ reef were analysed.

There is generally a good correlation between PPGE and IPGE contents in the intrusion as a whole and in the PGE reefs in particular (Fig. 17), but relatively large scatter in the binary Cu vs Pd plot (Fig. 17d). Figure 18 also illustrates that the AP reefs have a markedly higher Pd/Pt than the SJ and PV reefs, and higher Pd/Ir (Halkoaho *et al.*, 1989a, 1989b, 1994; Huhtelin *et al.*, 1989a, 1990; Halkoaho, 1993).

Primitive mantle normalized chalcophile element patterns are shown in Fig. 18. In MCU I, the patterns are relatively unfractionated, resembling those of Finnish SHMB dykes (Guo & Maier, 2013) and the Loljunmaa dyke, previously suggested to represent a potential parent magma to the Penikat intrusion (Alapieti & Lahtinen, 1989; Halkoaho, 1993). In MCU II and III, as well as the chromitite layers and the SJ reef, the

patterns are bell-shaped, reflecting the PGE enrichment of many samples. Many of the rocks in MCU II–IV have pronounced negative Ru anomalies, as previously noted by Halkoaho *et al.* (1989a, 1989b, 1990a, 1990b). In MCU IV and V, the chalcophile element patterns are trough shaped. The SJ and, in particular, the AP reefs have strong positive Pd anomalies, whereas in many samples from MCU I–III (including the chromitites) this is much less marked, with some samples having higher normalized Pt than Pd values. The PV reef shows positive Pt anomalies.

DISCUSSION

Composition of Penikat parental magma

Knowledge of the composition of the parent magmas to layered intrusions is of key importance in constraining the prospectivity of the intrusions for magmatic ore

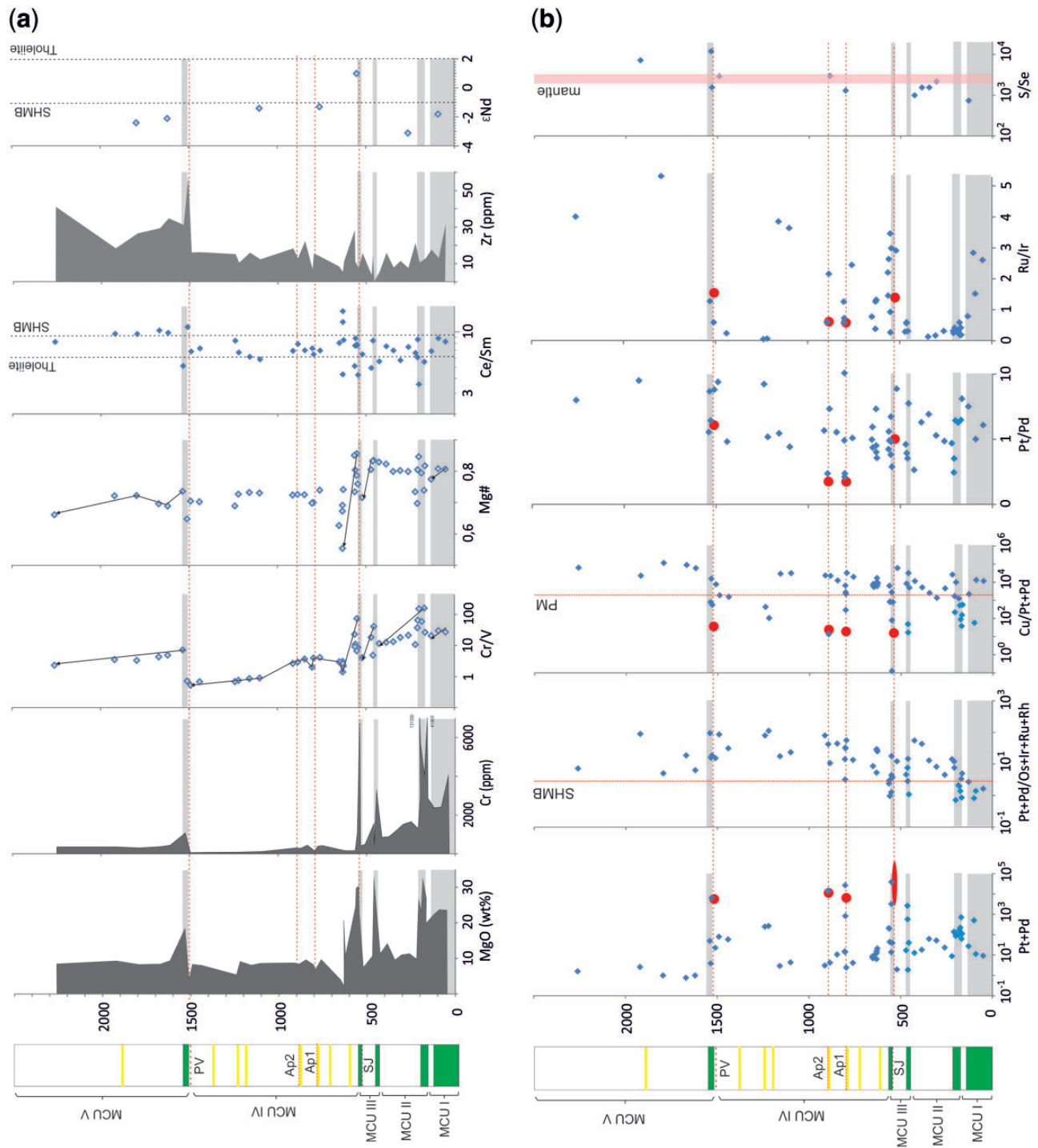


Fig. 15. (a) Compositional variation of lithophile elements with stratigraphic height (in m). (b) Variation in chalcophile elements with height (m). Red circles and ellipsoids represent compositional variation in main reefs. Green, ultramafic rocks; white, gabbroic and noritic rocks; yellow, anorthosite.

deposits. However, for most intrusions, the parental magma composition remains poorly known, with the notable exception of the Bushveld Complex (Sharpe, 1981; Barnes *et al.*, 2010). In the case of the Finnish layered intrusions, including Penikat, a suite of c. 2.45 Ga mafic dykes emplaced in the Archaean basement rocks is generally considered to represent the best candidate

for the parent magmas (Alapieti *et al.*, 1990; Halkoaho, 1993; Saini-Eidukat *et al.*, 1997; Alapieti & Lahtinen, 2002). The dykes are grouped into two main populations, SHMB and tholeiites (Vuollo & Huhma, 2005). The SHMB dykes contain, on average, 11.3 wt % MgO, 960 ppm Cr, and 310 ppm Ni (Table 1). The average initial ϵNd value is around -2 , and the incompatible

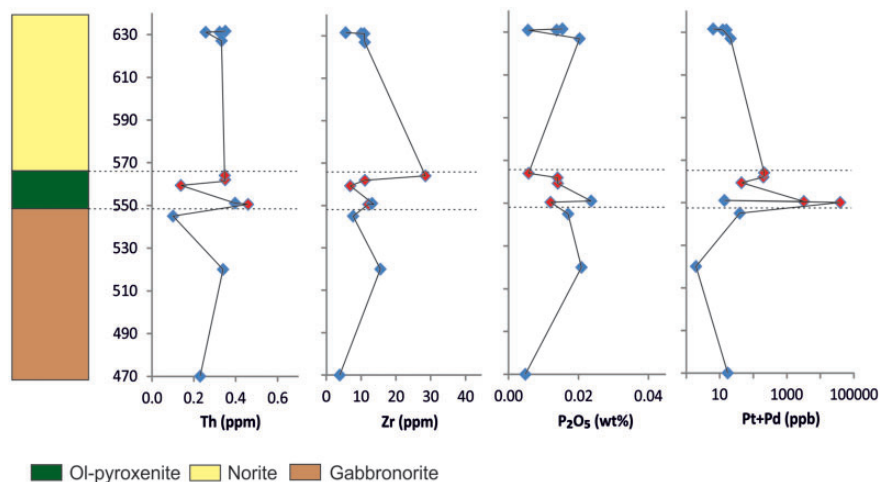


Fig. 16. Compositional profile across the SJ reef, based on outcrop samples. The lack of enrichment in incompatible elements in the reef should be noted.

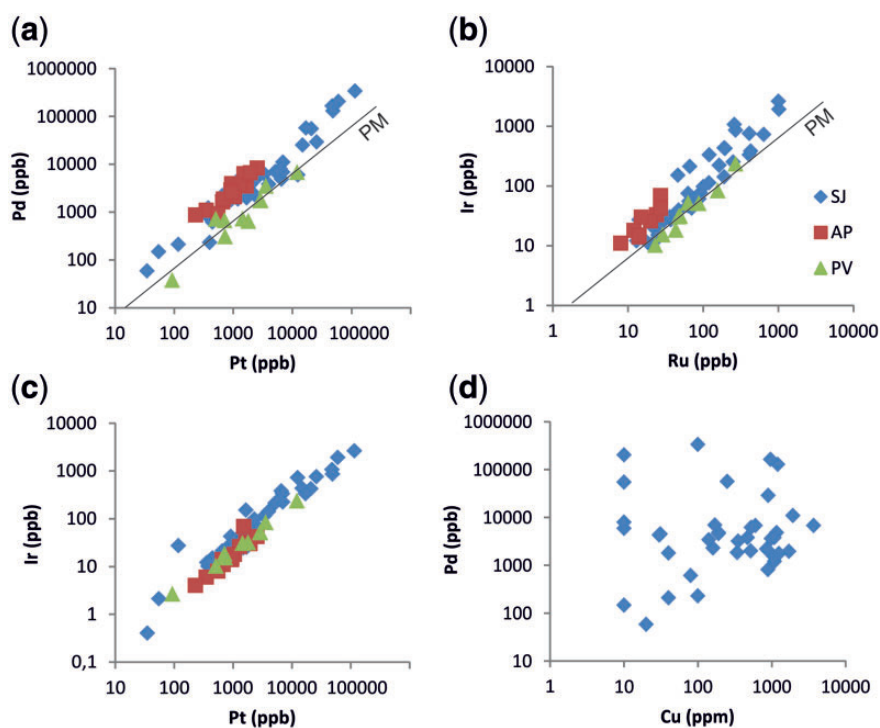


Fig. 17. Binary variation diagrams of PGE. (a) Pd vs Pt. It should be noted that the different reefs have systematically distinct Pt/Pd, with PV higher than SJ and AP. (b) Ru vs Ir. It should be noted that AP has Ru/Ir below that of primitive mantle, whereas PV has Ru/Ir approximately at the level of PM. SJ reef samples form two groups, one with AP-like Ru/Ir and the other with PV-like Ru/Ir. (c) Pt vs Ir. The good correlation between Pt and Ir, suggesting that PGE are concentrated by a magmatic process, should be noted. (d) Cu vs Pd (SJ reef data only). Scatter suggests that Cu was mobile after solidification.

elements are strongly fractionated, with pronounced negative Nb–Ta and Ti anomalies (Fig. 19). In the vicinity of the Penikat intrusion, the SHMB group is represented by the Loljunmaa dyke, located immediately to the east of the intrusion (Fig. 2; Alapieti & Lahtinen, 1989; Alapieti *et al.*, 1990). The dyke has 11.2 wt % MgO, 0.86 wt % TiO₂, 990 ppm Cr, 350 ppm Ni, and 420 ppm S. ϵ Nd is -1.2 (Yang *et al.*, 2016). The Finnish SHMB dykes have a composition that resembles the Bushveld B1

magma in terms of major and compatible trace element contents (Table 1), and the shape of incompatible trace element patterns (Fig. 19). However, the former are somewhat less enriched in REE (e.g. 10 vs 18 ppm La) and have less than half the average PGE contents of Bushveld B1 (7 ppb Pt and 6 ppb Pd vs 19 ppb Pt and 13 ppb Pd; Barnes *et al.*, 2010; Guo & Maier, 2013). The Finnish tholeiite dykes have, on average, 6 wt % MgO, 120 ppm Cr, 70 ppm Ni, and ϵ Nd $+1$, with less

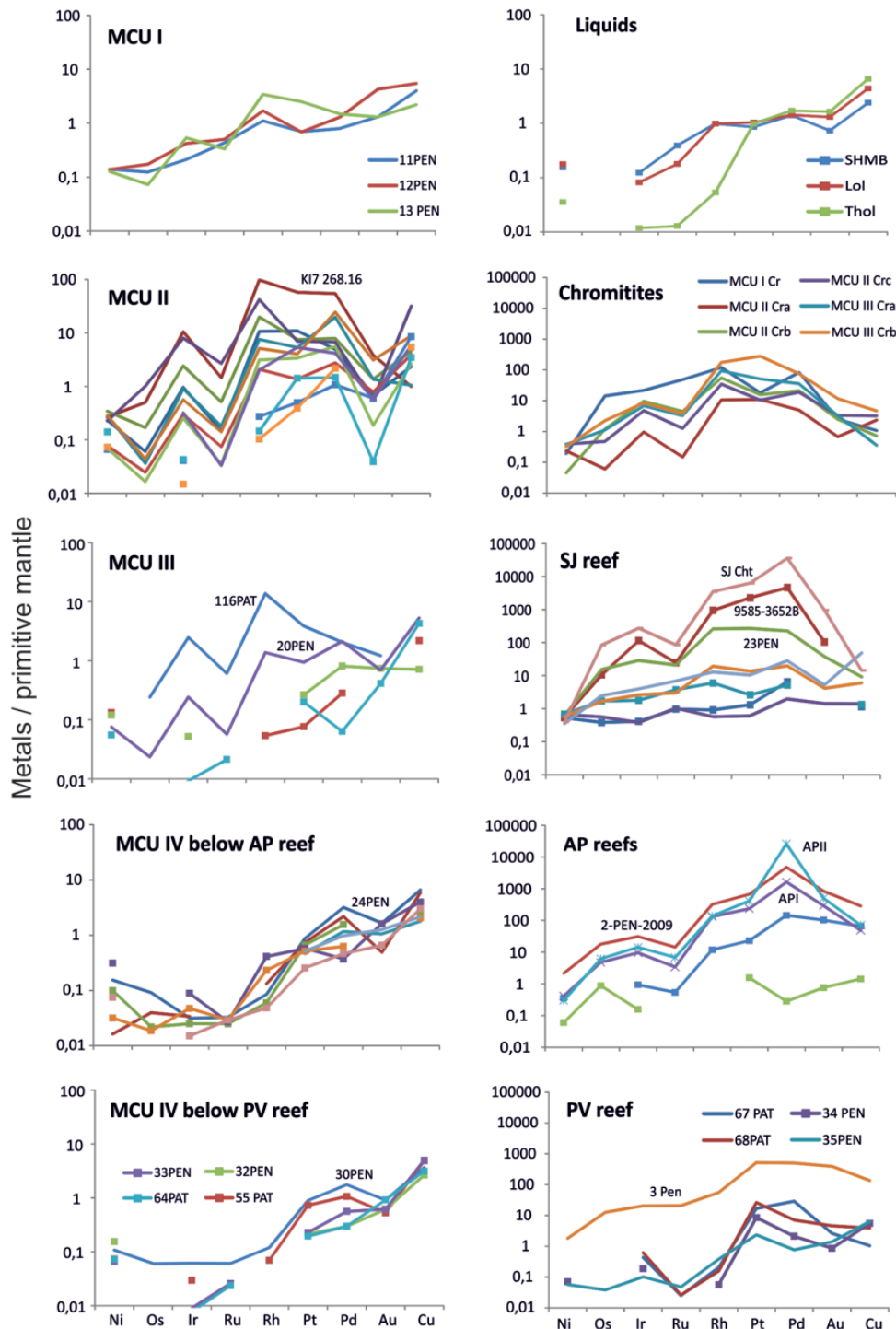


Fig. 18. Primitive mantle normalized multi-element variation diagrams for PGE. Normalization factors are from Barnes & Maier (1999).

fractionated trace element patterns and less prominent negative Nb–Ta and Ti anomalies (Guo & Maier, 2013). They do not show strong compositional overlap with most of the Penikat cumulates.

In addition to the dykes, we could also consider the chilled margins of the Penikat intrusion as representing parental liquids. On average, the chilled margins contain 7.2 wt % MgO and are relatively rich in Cr (around

450 ppm), consistent with an SHMB lineage. However, the rocks have relatively high K_2O contents (4.5–5.7 wt %) suggesting that they are contaminated (Halkoaho, 1993). Notably, they have slightly higher Pd contents (average of 13 ppb Pd) than the average Finnish SHMB, possibly owing to their more evolved nature. Sulphide contents are very low (180–270 ppm S), ruling out the possibility that the relatively high PGE contents are due

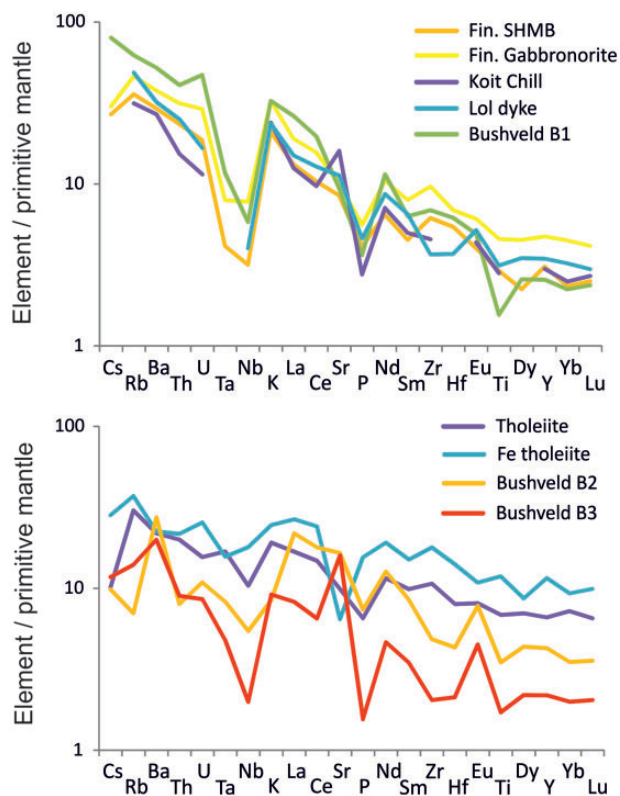


Fig. 19. Multi-element variation diagrams for lithophile elements for Finnish 2.45 Ga dykes (Guo & Maier, 2013) as well as aphanitic marginal rocks of the Bushveld Complex (Bushveld data from Barnes *et al.*, 2010; Koitelainen data from Hanski *et al.*, 2001). The similarities between Finnish SHMB and Bushveld B1 magmas should be noted. Normalization factors from Sun & McDonough (1989).

to the presence of small amounts of sulphide, unless metamorphism has removed some S.

To further constrain whether any of the above magmas may have been parental to the Penikat intrusion, it is first necessary to examine whether the magmas and the cumulates share a similar crystallization sequence. To this effect, we have modelled the crystallization sequence of the dykes using PELE (Boudreau, 1999). At low to intermediate pressure, fO_2 at the quartz–fayalite–magnetite (QFM) buffer, and 0.1 wt % H_2O , Finnish SHMB and the Loljunmaa dyke have a crystallization order of sp–ol–pl–cpx (1 kbar) or sp–ol–opx–pl–cpx (3 kbar), with starting mineral compositions of Fo87 and An 67–69. The crystallization order is broadly similar to that observed in many of the Penikat MCUs (notably II, III and IV) suggesting that the intrusion was emplaced at a moderate depth of <5 km. However, the observed olivine and pyroxene compositions in the least evolved Penikat rocks are less magnesian than the model compositions, and plagioclase has higher An. The low An contents of plagioclase in the crystallization model reflect the relatively high Na contents of the SHMB dykes, possibly resulting from metasomatism during Svecofennian (c. 1.9 Ga) metamorphism. The relatively low Mg# of the Penikat cumulates may reflect 10–15% fractionation of the SHMB prior to final emplacement.

In view of the significant contamination of the Penikat magmas discussed below, it seems plausible to argue that the SHMB must have contained significant water. However, adding 1 wt % H_2O to the magma results in a modelled crystallization order of olivine, followed by the appearance of clinopyroxene (Mg# 84) before orthopyroxene and plagioclase, inconsistent with the observed crystallization order. The composition of the main cumulus phases is little affected by adding 1% H_2O .

MCU IV has significantly lower Mg# and Cr contents in clinopyroxene and whole-rocks than MCU III (Alapieti *et al.*, 1990). Alapieti *et al.* proposed that MCU IV (and V) crystallized from Cr-poor tholeiitic magma as, for example, represented by the chilled margin of the Koillismaa intrusion. However, based on PELE modelling, the Finnish tholeiitic dykes have a crystallization order of pl–cpx–opx and thus seem inappropriate parental magmas for the cyclic units of the Penikat intrusion. The low Cr contents (<400 ppm in the rocks, <0.2 wt % Cr_2O_3 in augite) and Mg# of augite (<80) of MCU IV can instead be explained by crystallization from a more fractionated SHMB magma. For example, after 40% crystallization, the SHMB has 3.8 wt % MgO, 276 ppm Cr, Di 78, En 77 and An 60. This model is more consistent with the relative homogeneity in isotope and trace element signature across the intrusion than a model invoking the presence of several magmas of contrasting lineage. The sharp compositional break between MCU III and IV could reflect emplacement of MCU IV magma from a staging chamber, whereas the reversal at the base of MCU V could reflect replenishment with relatively un-evolved magma, or MCU V could be the residual magma of MCU III, displaced by the voluminous MCU IV influx.

The negative Ru anomalies found in MCU II and III as well as in the SJ, AP and PV reefs are not matched in the potential parent liquids to the intrusion (Fig. 18) and thus appear to have formed within the Penikat magma chamber, or a staging chamber. One possibility is that Ru was removed by fractionating chromite (Arguin *et al.*, 2016); for example, in chromite slurries sliding towards the subsiding centre of the lopolith.

Mantle source to parental magmas and importance of crustal contamination

As has been pointed out by numerous previous researchers, the enriched chemical signature of SHMB (high Ce/Sm, negative ϵNd , negative Ti anomalies, high Si content expressed by appearance of orthopyroxene before clinopyroxene on the liquidus) is consistent with magma derivation either from subcontinental lithospheric mantle (SCLM), or by melting of asthenospheric mantle followed by crustal contamination during magma ascent (Barnes, 1989; Amelin *et al.*, 1995; Amelin & Semenov, 1996; Hanski *et al.*, 2001; Barnes *et al.*, 2010; Yang *et al.*, 2016). For Penikat, the weight of the available evidence is in favour of the latter model,

for the following reasons. (1) The SCLM generally lacks negative Nb and Ta anomalies that are characteristic of the Penikat rocks and the SHMB dykes (Gregoire *et al.*, 2002; Simon *et al.*, 2007; Ionov, 2010; Maier *et al.*, 2012; Arndt, 2013). (2) Coeval basaltic to komatiitic rocks with enriched and broadly similar isotopic and trace element signatures to the Finnish SHMB dykes are exposed in the Vetreny Belt, Russian Karelia. Their compositional variation has been interpreted to result from assimilation of variable amounts of continental crust (Puchtel *et al.*, 1997). (3) The Kemi intrusion has positive initial γ_{Os} that can best be modelled by contamination of asthenospheric magma during ascent through the crust, whereas SCLM derivation is inconsistent with the Os isotope data (Yang *et al.*, 2016).

We have used Nd isotope and trace element data to further constrain the nature of potential crustal contaminants. Figure 20 shows bulk-mixing lines between a komatiitic parental magma and five examples of Finnish granitoids with different isotopic compositions and ages. In reality, contamination probably involved combined assimilation and fractional crystallization (AFC) instead of bulk mixing between magma and crust. Nevertheless, when the crystallized minerals do not significantly change the Sm/Nd ratio of the melt, as can be assumed to be the case in a high-MgO basaltic to komatiitic system crystallizing olivine and clinopyroxene,

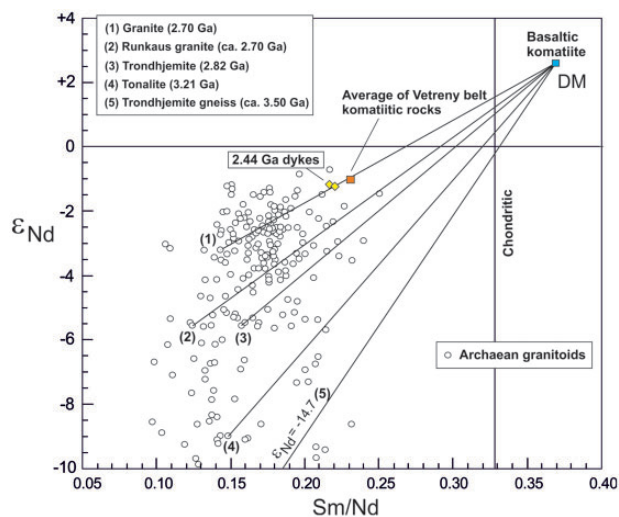


Fig. 20. Sm/Nd vs ϵ_{Nd} for Archaean granitoids from the Karelian craton (literature data) and the 2.44 Ga Loljunmaa and Viianki dykes (Yang *et al.*, 2016). Also shown are mixing lines of basaltic komatiite generated from depleted mantle and five selected examples of different granitoids: (1) 2.70 Ga Surmansuo porphyritic granite (Mikkola *et al.*, 2014); (2) ~2.70 Ga Runkaus K-rich granite, south of the Penikat intrusion, Pudasjärvi block (Huhma *et al.*, 2012); (3) 2.82 Ga Taka-aho trondhjemite from Suomussalmi (Mikkola *et al.*, 2011); (4) 3.21 Ga tonalite from the Vodla block, Russian Karelia (Puchtel *et al.*, 2016); (5) ~3.50 Ga granitic leucosome from the Siurua tonalitic gneiss, Pudasjärvi block (Huhma *et al.*, 2012). Isotopic data for the dykes taken from Yang *et al.* (2016). For comparison, the average Nd isotope composition of Vetreny Belt komatiites from Puchtel *et al.* (1997, 2016) is also plotted. All ϵ_{Nd} values are calculated at 2.44 Ga.

only very slight deviation from the linear trend occurs during AFC.

There are several Neoproterozoic granitoids that can be modelled to produce the isotopic composition of the dykes through AFC, including that of the 2.70 Ga Surmansuo porphyritic granite [(1) in Fig. 20]. It should be noted that the Runkaus granite [(2) in Fig. 20], which forms the footwall to the Penikat intrusion and is cut by the Loljunmaa dyke that may represent a feeder to the intrusion, seems to be an inappropriate contaminant. This is consistent with the trace element and isotope signature of the cumulates that were interpreted largely to reflect contamination in a staging chamber, as discussed above. Mesoarchaeoan or Palaeoarchaeoan granitoids with ages of >3.0 Ga have far too low ϵ_{Nd} (2440 Ma) to have played any role in magma–crust interaction. Assuming a depleted mantle source for the primitive magma, the amount of assimilation required to develop a negative ϵ_{Nd} value of –1.2 for the dyke magma is dependent on the Nd concentration of the komatiitic magma; that is, the degree of fractionation after its generation, and the Nd concentration and isotope composition of the contaminant. In the case of the Surmansuo granite, simple mixing with a basaltic komatiite (MgO 17 wt %) with 2.14 ppm Nd (see Puchtel *et al.*, 1997) simulates the observed isotope composition of the dyke after 12% assimilation, and slightly less contamination if an AFC process is assumed.

Origin of the Penikat PGE reefs

General

The origin of PGE reefs in layered intrusions remains controversial despite nearly 100 years of debate (e.g. Wagner, 1929). The main models generally considered are the following.

Model 1. The reefs formed through mixing of compositionally contrasting resident and replenishing magma triggering sulphide liquid immiscibility in the hybrid magma, followed by segregation of the sulphide melt from, and equilibration with, a large body of hybrid magma to achieve high metal tenors (Irvine, 1975; Campbell *et al.*, 1983; Naldrett & von Gruenewaldt, 1989).

Model 2. The magma from which the PGE reefs crystallized was unusually PGE rich, through assimilation or entrainment of PGE-rich sulphides in a staging chamber (Naldrett *et al.*, 2009; Holwell *et al.*, 2010).

Model 3. The magma in the magma chamber became temporarily supersaturated in sulphide through a sudden increase in pressure; for example, in response to magma replenishment (Cawthorn, 2005). As in model 1, this was followed by segregation of sulphides through a large magma body, to achieve high R factors.

Model 4. The magma reached sulphide melt saturation through contamination within the chamber; for example, with the roof-rocks. As in models 1 and 2, this was followed by segregation of the sulphide melt through, and collection of metals from, the magma body (Kinnaird *et al.*, 2002).

Model 5. The formation of the reefs involved late magmatic fluids ascending through the cooling crystal pile, either introducing PGE from the footwall rocks, or concentrating PGE through recrystallization of rocks containing high *R*-factor magmatic PGE (Nicholson & Mathez, 1991; Boudreau & McCallum, 1992).

Model 6. The PGE in the reefs precipitated from magma that intruded the cumulate sequence as sills (Mitchell & Scoon, 2007; Latypov *et al.*, 2015; Mungall *et al.*, 2016).

Model 7. PGE-rich sulphides were concentrated during hydrodynamic sorting of sulphide-bearing cumulate slurries slumping towards the centre of magma chambers that subsided in response to crustal loading (Maier *et al.*, 2013).

Model 8. Sulphide-bearing magma was mobilized from within the cumulate pile; for example, through tectonic readjustment of the chamber (this study).

In the following, we consider in more detail which of these models is most appropriate to explain the formation of the Penikat PGE reefs. It should be borne in mind that most previous studies of PGE reefs in layered intrusions focused on relatively well-exposed and unaltered or weakly altered intrusions, namely Bushveld, Great Dyke, Skaergaard, Rum and Stillwater. Unravelling the petrogenesis of the Penikat reefs is more challenging, owing to pervasive greenschist to amphibolite metamorphism.

Model 1: magma mixing

This model was originally proposed for the Bushveld and Stillwater intrusions (Irvine, 1975; Campbell *et al.*, 1983; Naldrett & von Gruenewaldt, 1989) in which numerous compositional reversals have been interpreted as a result of frequent magma replenishment and mixing of magmas with distinct compositional lineages. Campbell *et al.* (1983) suggested that particularly vigorous magma mixing resulted when plumes of relatively un-evolved replenishing magma intruded into and through relatively dense and evolved resident magma. If both magmas were nearly saturated in sulphide, an immiscible sulphide melt could have formed (Li & Ripley, 2005). Our new geochemical data do not provide clear constraints on the magma mixing model: although the incompatible trace element and Nd isotope compositions of the Penikat rocks show no evidence for distinct magma lineages, they do not rule out mixing of magmas of similar lineage but different fractionation state. However, a more general criticism of the magma mixing model is that it fails to explain the extremely efficient concentration of sulphide into a narrow layer bounded by rocks that are sulphide- and PGE-poor (< 40 ppb PGE/100 ppm S), as observed at Penikat. To attain the observed high metal tenors of the sulphides (hundreds of ppm), it is normally assumed (within the context of the magma mixing model) that the sulphide droplets must have been swirling within, and equilibrated with a large magma body. One would thus expect that the PGE reefs should be much wider and more

diffuse than what is observed, particularly as the sulphides in the reefs tend to be much smaller (mostly =1 mm, based on petrography) than olivine and pyroxene (mostly >2 mm).

Model 2: intrusion of PGE-rich magmas derived from a staging chamber

Naldrett *et al.* (2009) argued that concentration of PGE into narrow reefs is not feasible from a basaltic magma with 10–20 ppb PGE, for the reasons outlined above. They thus suggested that the reefs crystallized from unusually PGE-rich magma derived from a staging chamber. Mitchell & Scoon (2007) had previously argued for reef crystallization from relatively sulphur-rich magmas, and Holwell *et al.* (2010) found sulphide inclusions within chromite, which they argued indicate entrainment of sulphide from a staging chamber. The main problem with the model is that very few of the dykes or sills that could represent the chilled parent magmas to layered intrusions have been found to be enriched in PGE relative to normal basaltic magmas. This also applies to the 2.45 Ga dyke suite associated with the Finnish layered intrusions (Guo & Maier, 2013).

Model 3: pressure increase

An increase in pressure related to magma replenishment could have triggered sulphide melt saturation throughout the magma chamber (Cawthorn, 2005), but as in Model 1 above, the key challenge is how to achieve rapid and efficient sulphide melt accumulation from a magma body several tens or hundreds of metres in thickness to form the SJ, AP and PV reefs, all of which have widths mostly not exceeding a metre. Pressure changes can potentially explain the formation of the AP and PV anorthosites through pressure release (Cawthorn & Ashwal, 2009) but as pressure release increases the S solubility of the magma (Mavrogenes & O'Neill, 1999), the association of sulphides and anorthosite in the AP and PV reefs is inconsistent with the model.

Model 4: in situ contamination

The PGE reefs could have formed through contamination of replenishing magma pulses with the roof rocks of the magma chamber (Kinnaird *et al.*, 2002). This model would require that replenishing magma pulses intruded the resident magma as a buoyant plume, or that the new magma intruded as a sill between the cumulate pile and the chamber roof. However, the contamination model is inconsistent with our trace element and isotope data that show no significant shift towards more enriched values (as, for example, would be expressed by higher elevated incompatible element contents, LREE/HREE, La/Nb or lower ϵ_{Nd}) across the SJ or the other reefs (Figs 15 and 16).

Model 5: fluid flux

Nicholson & Mathez (1991) and Boudreau (2008) proposed that the Merensky Reef essentially represents a

restite formed at a fluid fluxing front. Specifically, the layered anorthosite–chromitite–pyroxenite interval of the Merensky Reef would have formed in response to recrystallization of an initially relatively poorly layered, sulphide-bearing noritic–pyroxenitic proto-cumulate. Recrystallization would have been triggered by late magmatic fluids ascending through the compacting footwall cumulate pile. The fluids caused partial melting of predominantly pyroxene, peritectic crystallization of olivine, and, owing to the expansion of the phase stability fields of chromite and plagioclase, the formation of a basal (restitic) anorthosite layer and one or several chromitite stringers. If the volatile-rich partial melt could not escape from the melting horizon, a pegmatoidal ultramafic layer would also be produced. Within this model, the PGE-rich sulphides are of magmatic origin, but underwent secondary concentration during the partial melting of the proto-cumulate, which facilitated downward percolation of sulphide melt. Fluid-fluxed partial melting of proto-cumulates could potentially also explain the abundant potholes in the Merensky Reef, interpreted as analogues of seafloor pockmarks by Buntin *et al.* (1985) and Boudreau (1992).

The Penikat reefs share certain lithological features with the Merensky Reef, which could suggest a role for fluid-driven recrystallization in reef formation; namely, the association of PGE with chromitite stringers (SJ, PV reef) and anorthosite layers (AP, PV reefs), the presence of potholes at the base of all reefs, the occurrence of amoeboid (recrystallized) chromite in the footwall of the SJ reef (Halkoaho, 1993), and the localized strong enrichment in incompatible elements Zr, P, Ba and Cl in the reefs (particularly AP and PV, Fig. 8c).

However, models involving fluid-driven recrystallization of the reefs have failed to gain wide support amongst layered intrusion researchers. The main reason may be that current estimates of the composition of Bushveld parent magmas suggest low volatile contents (0.31 wt % H₂O for B1; Barnes *et al.*, 2010) and cumulates from the Bushveld Complex and other PGE mineralized intrusions such as the Great Dyke and Stillwater, including the reef horizons, are relatively poor in hydrous silicates, mostly at < 1 modal %. One could argue that in most of the cumulates, volatiles were efficiently expelled during compaction; Karykowski & Maier (2017) documented up to 5% phlogopite, as well as abundant alkali feldspar, apatite and zircon, concentrated in pods within about 50% of analysed LZ samples and argued that intercumulus liquid is highly mobile in the crystallizing cumulates. Maier *et al.* (2016) suggested that hydrodynamic sorting may result in volatile-rich feldspathic mushes that may act as lubrication planes along which cumulate packages may slide. This in turn may lead to efficient compaction and expulsion of volatile-rich residual liquid.

Some studies of the Bushveld and Stillwater complexes proposed that fluids did not just trigger recrystallization of the cumulates, but additionally introduced PGE from the floor cumulates (Boudreau & McCallum,

1986; Boudreau, 1988; Boudreau & McCallum, 1992; Wilmore *et al.*, 2000). Petrological arguments against the role of fluids in reef formation have been summarized by Cawthorn *et al.* (2005). One of the main criticisms is probably that in some intrusions (Bushveld, Portimo) the reefs may be resting just a few tens of metres above the country-rock floor (Iljina & Hanski, 2005; Van der Merwe, 2007), rendering PGE derivation from the footwall cumulates problematic, unless the footwall was very PGE rich. More importantly, if the PGE were transported by fluids, one would expect to see fractionation between relatively mobile PPGE and largely immobile IPGE, yet the IPGE and PPGE are normally well correlated within the most important PGE reefs, including the Penikat reefs (Fig. 17).

Model 6: emplacement of sills

The model was initially proposed by Lee and Butcher (1990) Mitchell & Scoon (2007) for the Merensky Reef and was further developed and applied to both sulphide reefs and chromitites by Latypov *et al.* (2015). The researchers argued that at the level of the reefs, relatively crystal-poor magma derived from staging chambers injected the semi-consolidated crystal pile in the form of sills. Sulphides were either entrained from a staging chamber or sulphide melt saturation was triggered by *in situ* mixing, and the high *R*-factors required to generate the high metal tenors of the sulphides were achieved when fertile magma streamed laterally within the sills and past sulphides at the crystallization front. This model is difficult to constrain using chemical data, but Mungall *et al.* (2016) presented geochronological data to argue that some Bushveld chromitites postdate their host-rocks. At Penikat, the exposure is not good enough to map and analyse sills and apophyses, but high-precision dating of reefs and their host rocks is in preparation.

Model 7: hydrodynamic sorting of crystal mushes

Maier & Barnes (2008) and Maier *et al.* (2013) proposed that sulphide-bearing crystal mushes at the top of the cumulate pile slump towards the subsiding centre of intrusions, thereby undergoing hydrodynamic sorting to yield layered ultramafic–mafic sequences, consisting of ultramafic and feldspathic cumulates, including anorthosites. The slurries locally intruded into their floor rocks, producing apophyses and sills of chromitite and sulphide-rich silicate rocks. The model is consistent with field and compositional evidence from the Penikat SJ and AP reefs, which are located in intervals characterized by enhanced layering and the presence of magmatic breccias and potholes. The model offers an explanation for the highly efficient concentration of PGE-rich, high *R*-factor sulphides into narrow reefs. Depending on the efficiency of sorting, possibly related to the size and cooling rates of intrusions and the volatile content of the magma, the process may result in the irregular enrichment of chromite and PGE in the reefs

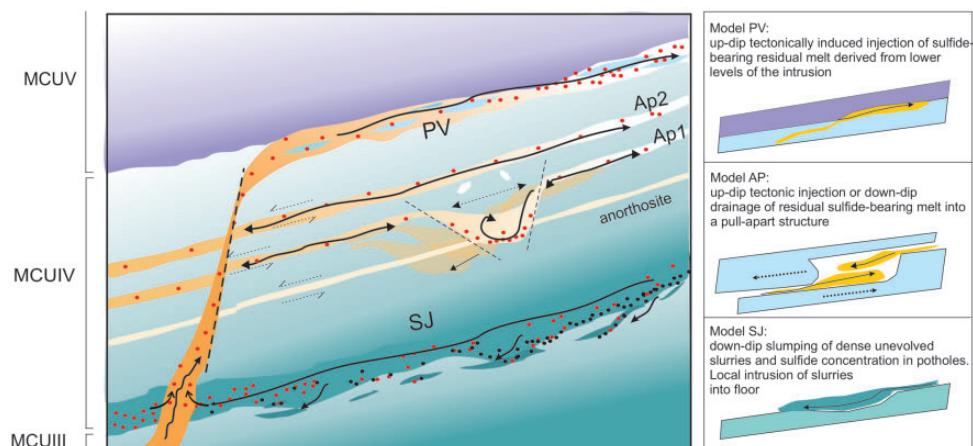


Fig. 21. Schematic model for formation of the Penikat PGE reefs. The SJ reef formed by hydrodynamic sorting of the MCU IV magma influx, leading to concentration of chromite, sulphide and olivine–pyroxene. The abundance of potholes and localized injections into the floor should be noted. The AP reefs formed by hydrodynamic sorting of sulphides emplaced with new magma pulses injecting into MCU IV. This replenishment event also resulted in pull-apart structures expressed in the large AP1 pothole, filled with sulphidic cumulates. The PV reef represents the residual liquid of the SJ reef, displaced upwards owing to intrusion of MCU IV. All three reefs were variably affected by late-stage partial melting induced by late magmatic fluids dammed up below the well-compacted reef rocks, triggering the formation of anorthosite and pegmatoids, notably in the AP and PV reefs. Red dots, sulphide; black dots, chromite; continuous-line arrows, direction of movement of crystal slurries; fine dotted-line arrows, direction of movement of solid rocks; dashed black line, fault.

along-strike, with bonanza-style enrichments in potholes such as within the SJ reef at Kirakkajuppura and the AP1 pothole of the Ala-Penikka block (Fig. 8). The potholes may have formed through a combination of magmatic erosion and faulting facilitating localized collapse of mushes into dilatational (pull-apart) structures. Notably, the abundant pegmatoidal patches associated with the AP pothole and the anorthosite fragments confined to the roof rocks of the pothole suggest that at the time of pull-apart, the AP1 reef was covered by further cumulates (Fig. 21). The hydrodynamic sorting model has been tested by fully scaled tank experiments (Forien *et al.*, 2015), but these need to be extended using non-spherical crystal analogues and variable volatile contents, given that gas bubbles may dramatically alter the flow behaviour of mushes (Leshar & Spera, 2015).

Model 8: mobilization of PGE-rich magmas from the lower portions of intrusions

Large layered intrusions are likely to undergo significant tectonism during emplacement and growth (Uken & Watkeys, 1997). This process could trigger mobilizations of PGE-rich magmas or slurries from within the semi-consolidated cumulate package, ascending through the pile and intruding either as sills within, or as flows on top of the pile. Evidence supporting the model could include features such as intrusive relationships of layers characterized by knife-sharp and transgressive contacts with the hanging-wall and footwall rocks, dykes extending into the roof and floor of layers and possibly containing magmatic breccias, and disequilibrium assemblages characterized by, for example, reversed zoning of minerals. However, the good three-

dimensional exposure necessary to make many of these observations is rarely available.

A strong case for sill emplacement can be made for the PV reef in the Penikat intrusion (Fig. 21), characterized by a reversal to relatively un-evolved metal signatures, disequilibrium assemblages characterized by the coexistence of chromite and sulphides showing unfractionated PGE contents with evolved phases such as apatite, alkali feldspar and quartz, strong enrichments in incompatible elements and volatiles relative to the floor and roof rocks, the presence of magmatic breccias, and a knife-sharp contact to the barren roof rocks. These observations are consistent with a model whereby the PV reef formed through intrusion of fractionated, volatile-rich magma along the contact between the largely solidified MCU IV and V. The relatively 'primitive' Pt/Pd, Pd/Ir and Cu/Ni ratios of the PV reef suggest that magma assimilated and entrained sulphide melt from one of the PGE reefs in the lower portion of the intrusion; that is, MCU II or III, or the SJ reef.

SUMMARY AND CONCLUSIONS

The Penikat intrusion contains several PGE-enriched zones or reefs, analogous to many other PGE mineralized layered intrusions. Poor outcrop and pervasive alteration make interpretation of the data more difficult than elsewhere, and thus much of the evidence has to be gathered from drillcore, complemented by a test pit in the Sompujärvi block and clearing (from lichen) of key outcrops across the intrusion conducted in the 1980s. The evidence suggests that the Penikat reefs formed through a combination of processes. All Penikat rocks have elevated Cu/Zr, suggesting that the magma was S-saturated or close to S-saturation during much of

Table 6: Major and trace element and Sm–Nd isotope data for five types of granitoids used in Fig. 20

Sample:	1	2*	3	4	5
Region:	A2126	R4, 93001822	A1906	K13	A1602
Area:	Eastern Finland	Pudasjärvi	Suomussalmi	Russian Karelia	Pudasjärvi
Rock type:	Surmansuo	Runkaus	Taka-aho	Vodla Block	Siurua
	porphyritic granite	granite	trondhjemite	tonalite	trondhjemite gneiss
SiO ₂	71.82	67.2	72.30	68.5	70.30
TiO ₂	0.34	0.467	0.28	0.37	0.45
Al ₂ O ₃	14.08	15.8	14.80	16.6	15.6
FeO _t	1.99	3.34	2.60	3.26	2.33
MnO	0.02	0.042	0.04	0.05	0.020
MgO	0.79	1.24	0.64	1.32	0.92
CaO	2.03	2.3	2.78	3.94	3.17
Na ₂ O	4.16	4.16	4.57	4.74	4.48
K ₂ O	3.89	4.2	1.85	1.01	1.83
P ₂ O ₅	0.13	0.229	0.12	0.12	0.03
Ba	1115	2817	524	n.a.	503
Bi	n.a.	<0.04	<30	n.a.	n.a.
Cl	128.00	110	121	n.a.	170.00
Co	4.6	7.6	4.0	n.a.	5.6
Cr	<30	25	<30	15	<30
Cu	n.a.	<17	<20	20.1	<5
Ga	23	28	26	20.2	15
Hf	n.a.	3.82	3.42	4.11	6.90
Mo	n.a.	<2.6	<10	n.a.	n.a.
Nb	4.89	4.05	4.59	4.1	5.20
Ni	29	<14	<20	5	8
Pb	24.0	35	<30	n.a.	32
Rb	159.0	91	67.1	n.a.	57
S	32	<70	<60	n.a.	n.a.
Sc	5.10	n.a.	4.02	6.92	3.6
Sr	370	854	248	n.a.	311
Ta	0.42	n.a.	0.40	n.a.	<0.2
Th	18.59	n.a.	7.24	2.8	46
U	3.60	n.a.	0.94	0.256	2
V	31.5	44.5	19.8	58	32
Y	6.03	7.31	7.16	6.92	7.5
Zn	55	70	65	n.a.	22
Zr	188	162	127	151	294
La	52.0	74.4	23.5	23.7	123.0
Ce	95.9	131	42.9	39.4	213.0
Pr	10.1	13.1	4.4	4.65	22.2
Nd	34.6	41.1	13.8	16.2	75.8
Sm	5.01	4.94	2.06	2.41	10.0
Eu	1.05	1.26	0.51	0.811	1.35
Gd	3.42	3.53	2.01	1.97	6.77
Tb	0.37	0.37	0.27	0.242	0.59
Dy	1.69	1.34	1.30	1.34	1.90
Ho	0.23	0.22	0.23	0.26	0.27
Er	0.53	0.55	0.63	0.739	0.60
Tm	0.07	0.08	<0.10	0.106	<0.1
Yb	0.48	0.49	0.62	0.695	0.55
Lu	0.1	0.07	<0.10	0.105	<0.1
<i>Isotopic data</i>					
Sm	4.41	4.24	2.38	2.41	10.44
Nd	30.76	34.08	15.09	16.23	78.18
¹⁴⁷ Sm/ ¹⁴⁴ Nd	0.0866	0.0752	0.0955	0.08975	0.0807
¹⁴³ Nd/ ¹⁴⁴ Nd	0.510707	0.510404	0.510731	0.510464	0.510025
εNd(2440 Ma)	-3.2	-5.6	-5.5	-9.0	-14.7
Age (Ma)	2695	2700	2824	3213	3500

References: 1, Mikkola *et al.* (2014); 2, Huhma *et al.* (2012), Geological Survey of Finland (GTK); 3, Mikkola *et al.* (2011); 4, Puchtel *et al.* (2016); 5, Mutanen & Huhma (2003), Huhma *et al.* (2012).

*For 2, we used isotopic data on sample R4, major and trace elements on sample 93001822 (GTK's litho geochemistry database).

the crystallization history. All reefs occur in intervals of enhanced layering and compositional reversals, suggesting that magma replenishment played an important role in reef formation. Whether mixing of magmas and temporary increases in pressure resulting from replenishment contributed to driving the magmas to sulphide

saturation remains unclear. Although all Penikat reefs have been traced along much of the strike length of the intrusion, they show less continuity, albeit broadly similar overall grade, compared with, for example, the Bushveld or Great Dyke reefs, possibly owing to faster cooling as a result of the relatively smaller size of the

intrusion. Bonanza-style PGE enrichments in SJ and AP potholes suggest that hydrodynamic sorting was important in reef formation. The PV reef is unusual in that it possibly formed from magmas that cannibalized sulphides from the lower portion of the intrusion and then intruded into, rather than flowed on top of the cumulate package. All three major PGE reefs were affected by late magmatic recrystallization triggered by fluids or volatile-rich melts ascending during cooling and compaction of the footwall rocks. This was of relatively minor importance in the case of the SJ reef, but was more significant in the AP and PV reefs, generating abundant pegmatoidal pods, and localized pods and stringers of chromitite. However, in none of the reefs is there evidence for mobilization of PGE by fluids.

ACKNOWLEDGEMENTS

Yann Lahaye, Hugh O'Brien, Leena Järvinen and Arto Pulkkinen are thanked for assistance during ICP-MS analyses. Constructive reviews by Alan Boudreau, Jim Miller and Markku Iljina provided much added insight.

FUNDING

W.M.'s research is supported by the Renlund Foundation and E. Hanski's research by an Academy of Finland grant (No. 281859).

SUPPLEMENTARY DATA

Supplementary data for this paper are available at *Journal of Petrology* online.

REFERENCES

- Alapieti, T. T. & Halkoaho, T. A. A. (1995). Cryptic variation of augite in the Penikat layered intrusion, northern Finland, with reference to megacyclic units and PGE-enriched zones. *Mineralogy and Petrology* **54**, 11–24.
- Alapieti, T. T. & Lahtinen, J. J. (1986). Stratigraphy, petrology and platinum-group element mineralization of the early Proterozoic Penikat layered intrusion, Northern Finland. *Economic Geology* **81**, 1126–1136.
- Alapieti, T. T. & Lahtinen, J. J. (1989). Early Proterozoic layered intrusions in the northeastern part of the Fennoscandian Shield. In: Alapieti, T. (ed.) *5th International Platinum Symposium, Guide to the Post-Symposium Field Trip, Geological Survey of Finland, Guide* **29**, 3–41.
- Alapieti, T. T. & Lahtinen, J. J. (2002). Platinum-group element mineralization in layered intrusions of northern Finland and the Kola peninsula. In: Cabri, L. J. (ed.) *The Geology, Geochemistry, Mineralogy and Mineral Beneficiation of Platinum-Group Elements. Canadian Institute of Mining, Metallurgy and Petroleum, Special Volume* **54**.
- Alapieti, T. T., Kujanpää, J., Lahtinen, J. J. & Papunen, H. (1989). The Kemi stratiform chromitite deposit, northern Finland. *Economic Geology* **84**, 1057–1077.
- Alapieti, T. T., Filén, B. A., Lahtinen, J. J., Lavrov, M. M., Smolkin, V. F. & Voitsekhovskiy, S. N. (1990). Early Proterozoic layered intrusions in the northeastern part of the Fennoscandian Shield. *Mineralogy and Petrology* **42**, 1–22.
- Amelin, Y. V. & Semenov, V. S. (1996). Nd and Sr isotopic geochemistry of mafic layered intrusions in the eastern Baltic shield: implications for the evolution of Paleoproterozoic continental mafic magmas. *Contributions to Mineralogy and Petrology* **124**, 255–272.
- Amelin, Y. V., Heaman, L. M. & Semenov, V. S. (1995). U–Pb geochronology of layered mafic intrusions in the eastern Baltic Shield; implications for the timing and duration of Paleoproterozoic continental rifting. *Precambrian Research* **75**, 31–46.
- Andersen, J. C. Ø., Thalhammer, O. A. R. & Schoenberg, R. (2006). Platinum-group element and Re–Os isotope variations of the high-grade Kilvenjärvi platinum-group element deposit, Portimo Layered Igneous Complex, Finland. *Economic Geology* **101**, 159–177.
- Andersen, T., Griffin, W. L., Jackson, S. E., Knudsen, T.-L. & Pearson, N. J. (2004). Mid-Proterozoic magmatic arc evolution at the southwest margin of the Baltic Shield. *Lithos* **73**, 289–318.
- Arguin, J.-P., Pagé, P., Barnes, S.-J., Yu, S.-Y. & Song, X.-Y. (2016). The effect of chromite crystallization on the fractionation of osmium, iridium, ruthenium and rhodium in picritic magmas: an example from the Emeishan Large Igneous Province, south-western China. *Journal of Petrology* **57**, 1019–1048.
- Barnes, S. J. (1989). Are Bushveld U-type parent magmas boninites or contaminated komatiites? *Contributions to Mineralogy and Petrology* **101**, 447–457.
- Barnes, S.-J. & Maier, W. D. (1999). The fractionation of Ni, Cu and the noble metals in silicate and sulfide liquids. In: Keays, R. R., Leshner, C. M., Lightfoot, P. C. & Farrow, C. E. G. (eds) *Magmatic Ore Deposits and their Application in Mineral Exploration. Geological Association of Canada, Short Course Volume* **13**, 69–106.
- Barnes, S.-J., Maier, W. D. & Curl, E. (2010). Composition of the marginal rocks and sills of the Rustenburg Layered Suite, Bushveld Complex, South Africa: implications for the formation of the platinum-group element deposits. *Economic Geology* **105**, 1491–1511.
- Boudreau, A. E. (1992). Volatile fluid overpressure in layered intrusions and the formation of potholes. *Australian Journal of Earth Sciences* **39**, 277–287.
- Boudreau, A. E. (2008). Modeling the Merensky Reef, Bushveld Complex, Republic of South Africa. *Contributions to Mineralogy and Petrology* **156**, 431–437.
- Boudreau, A. E. & McCallum, I. S. (1986). Investigations of the Stillwater Complex. Part III. The Picket Pin Pt–Pd deposit. *Economic Geology* **81**, 1953–1975.
- Boudreau, A. E. & McCallum, I. S. (1992). Concentration of platinum-group elements by magmatic fluids in layered intrusions. *Economic Geology* **87**, 1830–1848.
- Buntin, T. J., Grandstaff, D. E., Ulmer, G. C. & Gold, D. P. (1985). A pilot study of geochemical and redox relationships between potholes and adjacent Merensky Reef on the Bushveld Complex. *Economic Geology* **80**, 975–987.
- Campbell, I. H., Naldrett, A. J. & Barnes, S. J. (1983). A model for the origin of the platinum-rich sulfide horizons in the Bushveld and Stillwater Complexes. *Journal of Petrology* **24**, 133–165.
- Cawthorn, R. G. (2005). Pressure fluctuations and the formation of the PGE rich Merensky and chromitite reefs, Bushveld Complex. *Mineralium Deposita* **40**, 231–235.
- Cawthorn, R. G. & Ashwal, L. D. (2009). Origin of anorthosite and magnetite layers in the Bushveld Complex, constrained by major element compositions of plagioclase. *Journal of Petrology* **50**, 1607–1637.

- DePaolo, D. J. (1981). Neodymium isotopes in the Colorado Front Range and crust–mantle evolution in the Proterozoic. *Nature* **291**, 193–687.
- Eales, H. V. & Reynolds, I. M. (1986). Cryptic variations within chromitites of the upper critical zone, northwestern Bushveld Complex. *Economic Geology* **81**, 1056–1066.
- Eales, H. V., Field, M., de Klerk, W. J. & Scoon, R. N. (1988). Regional trends of chemical variation and thermal erosion in the Upper Critical Zone, western Bushveld Complex. *Mineralogical Magazine* **52**, 63–79.
- Eerola, P., Reino, J., Vaajoensuu, K. & Seppänen, A. (1990). *On the potential to utilize the PGE–Au–Cu–Ni occurrences in the Kivalot area. Outokumpu Mining Services, Report 090/2543,2544,3613/90* (in Finnish).
- Ernst, R. & Bleeker, W. (2010). Large igneous provinces (LIPs), giant dyke swarms, and mantle plumes: significance for breakup events within Canada and adjacent regions from 2.5 Ga to the Present. *Canadian Journal of Earth Sciences* **47**, 695–739.
- Forien, M., Tremblay, J., Barnes, S.-J., Burgisser, A. & Page, P. (2015). The role of viscous particle segregation in forming chromite layers from slumped crystal slurries: insights from analogue experiments. *Journal of Petrology* **56**, 2425–2444.
- Guo, F. & Maier, W. D. (2013). Geochemistry of ~2.45 Ga mafic dykes in Northern Finland: constraints on the origin of PGE mineralization in coeval layered intrusions. 12th SGA Biennial Meeting, Uppsala, Sweden.
- Halkoaho, T. A. A. (1989). *Ala-Penikka platinum mineralisations in the Penikat layered intrusion (Ala-Penikan platinametallimineralisaatiot Penikkain kerrosintruusiassa). Report 2 of the PGE research project, University of Oulu*, 173 pp. (in Finnish).
- Halkoaho, T. A. A. (1993). *The Sompujärvi and Ala-Penikka PGE reefs of the Penikat Layered Intrusion, northern Finland—implications for PGE-reef forming processes. Acta Universitatis Ouluensis, Series A, Scientiae Rerum Naturalium* **249**, 122 pp.
- Halkoaho, T. A. A., Alapieti, T. T. & Lahtinen, J. J. (1989a). The Sompujärvi PGE mineralization in the Penikat layered intrusion, Northern Finland. In: Alapieti, T. (ed.) *5th International Platinum Symposium, Guide to the Post-Symposium Field Trip, Geological Survey of Finland, Guide* **29**, 71–92.
- Halkoaho, T. A. A., Alapieti, T. T. & Lahtinen, J. J. (1989b). The Ala-Penikka PGE mineralizations in the Penikat layered intrusion, Northern Finland. In: Alapieti, T. (ed.) *5th International Platinum Symposium, Guide to the Post-Symposium Field Trip, Geological Survey of Finland, Guide* **29**, 93–122.
- Halkoaho, T. A. A., Alapieti, T. T. & Lahtinen, J. J. (1990a). The Sompujärvi PGE reef in the Penikat layered intrusion, northern Finland. *Mineralogy and Petrology* **42**, 39–55.
- Halkoaho, T. A. A., Alapieti, T. T., Lahtinen, J. J. & Lerssi, J. M. (1990b). The Ala-Penikka PGE reefs in the Penikat layered intrusion, northern Finland. *Mineralogy and Petrology* **42**, 23–38.
- Halkoaho, T. A. A., Alapieti, T. & Huhtelin, T. (2005). The Sompujärvi, Ala-Penikka and Pasivaara PGE reefs in the Penikat layered intrusion, northern Finland. In: Alapieti, T. T. & Kärki, A. J. (eds) *Field Trip Guidebook. Geological Survey of Finland, Guide* 51a, 110 pp.
- Hanski, E. (2012). Evolution of the Palaeoproterozoic (2.50–1.95 Ga) non-orogenic magmatism in the eastern part of the Fennoscandian Shield. In: Melezhik, V. A., Prave, A. R., Fallick, A. E., Kump, L. R., Strauss, H., Lepland, A. & Hanski, E. J. (eds) *Reading the Archive of Earth's Oxygenation, Volume 1: The Palaeoproterozoic of Fennoscandia as Context for the Fennoscandian Arctic Russia—Drilling Earth Project*. Berlin: Springer, doi:10.1007/978-3-642-29682-6_6.
- Hanski, E. & Huhma, H. (2005). Central Lapland Greenstone Belt. In: Lehtinen, M., Nurmi, P. & Rämö, O. T. (eds) *Precambrian Bedrock of Finland—Key to the Evolution of the Fennoscandian Shield*. Amsterdam: Elsevier, pp. 139–194.
- Hanski, E. J. & Melezhik, V. A. (2012). Litho- and chronostratigraphy of the Karelian Formations. In: Melezhik, V. A., Prave, A. R., Hanski, E. J., Fallick, A. E., Lepland, A., Kump, L. R. & Strauss, H. (eds) *Reading the Archive of Earth's Oxygenation. Volume 1: The Palaeoproterozoic of Fennoscandia as Context for the Fennoscandian Arctic Russia—Drilling Early Earth Project*. Berlin: Springer, pp. 39–110.
- Hanski, E., Walker, R. J., Huhma, H. & Suominen, I. (2001). The Os and Nd isotopic systematics of the 2.44 Ga Akanvaara and Koitelainen mafic layered intrusions in northern Finland. *Precambrian Research* **109**, 73–102.
- Heltz, R. (1985). Compositions of fine-grained mafic rocks from sills and dikes associated with the Stillwater Complex. In: *The Stillwater Complex, Montana: Geology and Guide, Montana Bureau of Mines and Geology, Special Publication* **92**, 97–117.
- Holwell, D. A., McDonald, I. & Butler, I. B. (2010). Precious metal enrichment in the Platreef, Bushveld Complex, South Africa: evidence from homogenized magmatic sulfide melt inclusions. *Contributions to Mineralogy and Petrology* doi: 10.1007/s00410-010-0577-0.
- Huhma, H., Cliff, R. A., Perttunen, V. & Sakko, M. (1990). Sm–Nd and Pb isotopic study of mafic rocks associated with early Proterozoic continental rifting: the Peräpohja schist belt in northern Finland. *Contributions to Mineralogy and Petrology* **104**, 369–379.
- Huhma, H., Mänttari, I., Peltonen, P., Kontinen, A., Halkoaho, T., Hanski, E., Hokkanen, T., Hölttä, P., Juopperi, H., Konnunaho, J., Layahe, Y., Luukkonen, E., Pietikäinen, K., Pulkkinen, A., Sorjonen-Ward, P., Vaasjoki, M. & Whitehouse, M. (2012). The age of the Archaean greenstone belts in Finland. *Geological Survey of Finland, Special Paper* **54**, 74–175.
- Huhma, H., Hanski, E., Kontinen, A., Vuollo, J., Mänttari, I. & Lahaye, Y. (2018). Sm–Nd and U–Pb isotope geochemistry of the Palaeoproterozoic mafic magmatism in eastern and northern Finland. *Geological Survey of Finland, Bulletin* **405**, 150.
- Huhtelin, T. (1989). *Paasivaaran platinamineralisaatio Penikkain kerrosintruusiassa. Report 1 of the PGE Research Project, University of Oulu*, 70 pp. (in Finnish).
- Huhtelin, T. A., Alapieti, T. T. & Lahtinen, J. J. (1989a). The Paasivaara PGE mineralization in the Penikat layered intrusion, Northern Finland. In: Alapieti, T. (ed.) *5th International Platinum Symposium, Guide to the Post-Symposium Field Trip, Geological Survey of Finland, Guide* **29**, 123–144.
- Huhtelin, T. A., Alapieti, T. T., Lahtinen, J. J. & Lerssi, J. (1989b). Megacyclic Units I, II and II in the Penikat layered intrusion. In: Alapieti, T. (ed.) *5th International Platinum Symposium, Guide to the Post-Symposium Field Trip, Geological Survey of Finland, Guide* **29**.
- Huhtelin, T. A., Alapieti, T. T. & Lahtinen, J. J. (1990). The Paasivaara PGE reefs in the Penikat layered intrusion, northern Finland. *Mineralogy and Petrology* **42**, 57–70.
- Ilijina, M. (1994). *The Portimo Layered Igneous Complex with emphasis on diverge sulphide and platinum-group element deposits. Acta Universitatis Ouluensis, Series A, Scientiae Rerum Naturalium* **258**, 158 pp.

- Iljina, M. & Hanski, E. (2005). Layered mafic intrusions of the Tornio-Näränkäväära Belt. In: Lehtinen, M., Nurmi, P. A. & Rämö, O. T. (eds) *Precambrian Geology of Finland—Key to the Evolution of the Fennoscandian Shield*. Amsterdam: Elsevier, pp. 101–138.
- Iljina, M. & Salmirinne, H. (2011). *Suhanko seismic reflection profile and integrated geological-geophysical model of the Portimo area*. Geological Survey of Finland, Report of Investigation **189**.
- Irvine, T. N. (1975). Crystallization sequences in the Muskox intrusion and other layered intrusions—II. Origin of chromitite layers and similar deposits of other magmatic ores. *Geochimica et Cosmochimica Acta* **39**, 991–1020.
- Irvine, T. N. (1982). Terminology for layered intrusions. *Journal of Petrology* **23**, 127–162.
- Jackson, S. E., Pearson, N. J., Griffin, W. L. & Belousova, E. A. (2004). The application of laser ablation-inductively coupled plasma-mass spectrometry to *in-situ* U–Pb zircon geochronology. *Chemical Geology* **211**, 47–69.
- Karinen, T. (2010). *The Koillismaa Intrusion, northeastern Finland—evidence for PGE reef forming processes in the layered series*. Geological Survey of Finland Bulletin **404**, 176 pp.
- Karinen, T., Hanski, E. & Taipale, A. (2015). The Mustavaara Fe–Ti–V oxide deposit. In: Maier, W., O'Brien, H. & Lahtinen, R. (eds) *Mineral Deposits of Finland*. Amsterdam: Elsevier, pp. 179–194.
- Karykowski, B. & Maier, W. D. (2017). Microtextural characterisation of the Lower Zone in the western limb of the Bushveld Complex, South Africa: Evidence for extensive melt migration within a sill complex. *Contributions to Mineralogy and Petrology* **172**, 60.
- Kukkonen, I., Heikkinen, P., Elo, S., Heinonen, S. & Laitinen, J. & HIRE Working Group of the Geological Survey of Finland (2010). *HIRE Seismic Reflection Survey in the Sompujärvi PGE Exploration Area, Northern Finland*. Geological Survey of Finland, Report **Q23/2010/23**, 43 pp.
- Latypov, R., Chistyakova, S., Page, A. & Hornsey, R. (2015). Field evidence for the *in situ* crystallization of the Merensky Reef. *Journal of Petrology* **56**, 2341–2372.
- Lee, C. A. & Butcher, A. R. (1990). Cyclicity in the Sr isotope stratigraphy through the Merensky and Bastard Reefs, Atok Section, eastern Bushveld Complex. *Economic Geology* **85**, 877–883.
- Lerssi, J. (1990). Geophysical investigations. In: Alapieti, T., Halkoaho, T., Huhtelin, T., Iljina, M. & Lerssi, J. (eds) *Final Report of the Peräpohja Platinum Project. PGE Research Project, University of Oulu, Report 3*, pp. 122–149 (in Finnish).
- Li, C. & Ripley, E. M. (2005). Empirical equations to predict the sulfide content of mafic magmas at sulfide saturation and applications to magmatic sulfide deposits. *Mineralium Deposita* **40**, 218–230.
- Linkermann, S. A. (2011). Emplacement of the 2.44 Ga ultramafic layered Kemi intrusion, Finland: PGE, geochemical and Sm–Nd isotopic implications. MSc thesis, Rhodes University, Grahamstown, South Africa.
- Ludwig, K. R. (2003). *User's manual for Isoplot/Ex, Version 3.00. A geochronological toolkit for Microsoft Excel*. Berkeley Geochronology Center Special Publication **4**.
- Maier, W. D. & Barnes, S.-J. (2008). Platinum-group elements in the UG1 and UG2 chromitites and the Bastard reef at Impala platinum mine, western Bushveld Complex. *South African Journal of Geology* **111**, 159–176.
- Maier, W. D. & Eales, H. V. (1997). *Correlation within the UG2–Merensky Reef interval of the Western Bushveld Complex, based on geochemical, mineralogical and petrological data*. Geological Survey of South Africa Bulletin **120**, 56 pp.
- Maier, W. D., Peltonen, P., McDonald, I., Barnes, S. J., Barnes, S.-J., Hatton, C. & Viljoen, F. (2012). The platinum-group element budget of the Kaapvaal and Karelian sub-continental lithospheric mantle: implications for mantle evolution. *Chemical Geology* **302–303**, 119–135.
- Maier, W. D., Barnes, S.-J. & Groves, D. I. (2013). The Bushveld Complex, South Africa: formation of platinum–palladium, chrome and vanadium-rich layers via hydrodynamic sorting of a mobilized cumulate slurry in a large, relatively slowly cooling, subsiding magma chamber. *Mineralium Deposita* **48**, 1–56.
- Maier, W. D., Barnes, S.-J. & Karykowski, B. T. (2016). A chilled margin of komatiite and Mg-rich basaltic andesite in the western Bushveld Complex, South Africa. *Contributions to Mineralogy and Petrology* doi:10.1007/s00410-016-1257-5.
- McDonald, I. & Viljoen, K. S. (2006). Platinum-group element geochemistry of mantle eclogites: a reconnaissance study of xenoliths from the Orapa kimberlite, Botswana. *Transactions of the Institution of Mining and Metallurgy* **115**, 81–93.
- Mikkola, P., Huhma, H., Heilimo, E. & Whitehouse, M. (2011). Archean crustal evolution of the Suomussalmi district as part of the Kianta Complex, Karelia: Constraints from geochemistry and isotopes of granitoids. *Lithos* **125**, 287–307.
- Mikkola, P., Heilimo, E. & Huhma, H. (2014). Relationships between sanukitoids and crust-derived melts and their implications for the diversity of Neoproterozoic granitoids: a case study from Surmansuo and nearby areas, Eastern Finland. *Bulletin of the Geological Society of Finland* **86**, 23–40.
- Naldrett, A. J. & von Gruenewaldt, G. (1989). Association of platinum-group elements with chromitite in layered intrusions and ophiolite complexes. *Economic Geology* **84**, 180–187.
- Naldrett, A. J., Wilson, A., Kinnaird, J. & Chunnnett, G. (2009). PGE tenor and metal ratios within and below the Merensky Reef, Bushveld Complex: implications for its genesis. *Journal of Petrology* **50**, 625–659.
- Nicholson, D. M. & Mathez, E. A. (1991). Petrogenesis of the Merensky Reef in the Rustenburg section of the Bushveld Complex. *Contributions to Mineralogy and Petrology* **107**, 293–309.
- Perttunen, V. & Vaasjoki, M. (2001). U–Pb geochronology of the Peräpohja Schist Belt, northwestern Finland. In: Vaasjoki, M. (ed.) *Radiometric Age Determinations from Finnish Lapland and their Bearing on the Timing of Precambrian Volcano-sedimentary Sequences*. Geological Survey of Finland, Special Paper **33**, 45–84.
- Pripachkin, P. V., Rundkvist, T. V., Miroshnikova, Y. A., Chernyavsky, A. V. & Borisenko, E. S. (2018). Geological structure and ore mineralization of the South Sopchinsky massif (Monchegorsk area, Kola Peninsula, Russia). *Mineralium Deposita*, in press.
- Puchtel, I. S., Haase, K. M., Hofmann, A. W., Chauvel, C., Kulikov, V. S., Garbe-Schönberg, C. D. & Nemchin, A. A. (1997). Petrology and geochemistry of crustally contaminated komatiitic basalts from the Vetreny Belt, southeastern Baltic Shield: evidence for an early Proterozoic mantle plume beneath rifted Archean continental lithosphere. *Geochimica et Cosmochimica Acta* **61**, 1205–1222.
- Puchtel, I. S., Touboul, M., Blichert-Toft, J., Walker, R. J., Brandon, A. D., Nicklas, R. W., Kulikov, V. S. & Samsonov, A. V. (2016). Lithophile and siderophile element systematics of Earth's mantle at the Archean–Proterozoic boundary: evidence from 2.4 Ga komatiites. *Geochimica et Cosmochimica Acta* **180**, 227–255.

- Puritch, E., Ewert, W., Brown, F. H., Rickard, J. & King, D. (2007). *Technical report, mineral resource estimate, and preliminary economic assessment (scoping study) of the Suhanko project northern Finland NI-43-101 & 43-101F1, Technical Report and Scoping Study, Report 135*.
- Richard, P., Shimizu, N. & Allègre, C. J. (1976). $^{143}\text{Nd}/^{146}\text{Nd}$, a natural tracer: an application to oceanic basalts. *Earth and Planetary Science Letters* **31**, 269–278.
- Rosa, D. R. N., Finch, A. A., Andersen, T. & Inverno, C. M. C. (2009). U–Pb geochronology and Hf isotope ratios of magmatic zircons from the Iberian pyrite belt. *Mineralogy and Petrology* **95**, 47–69.
- Saini-Eidukat, B., Alapieti, T. T., Thalhammer, O. A. R. & Iljina, M. J. (1997). Siliceous, high-magnesian parental magma compositions of the PGE-rich Early Paleoproterozoic layered intrusion belt of northern Finland. In: Pei, R. (ed.) *Proceedings of the 30th International Geological Congress, Beijing, China, 4–14 August 1996. Vol. 9, Energy and Mineral Resources for the 21st Century, Geology of Mineral Deposits, Mineral Economics*. VSP, pp. 177–197.
- Savard, D., Bedard, L. P. & Barnes, S.-J. (2006). TCF selenium preconcentration in geological materials for determination at sub $\mu\text{g g}^{-1}$ with INAA (Se/TCF-INAA). *Talanta* **70**, 566–571.
- Savard, D., Barnes, S.-J. & Meisel, T. (2010). Comparison between nickel–sulfur fire assay Te co-precipitation and isotope dilution with high-pressure asher acid digestion for the determination of PGE Re and gold. *Geostandards and Geoanalytical Research* **34**, 281–291.
- Sharpe, M. R. (1981). The chronology of magma influxes to the eastern compartment of the Bushveld Complex, as exemplified by its marginal border group. *Journal of the Geological Society, London* **138**, 307–326.
- Stacey, J. S. & Kramers, J. D. (1975). Approximation of terrestrial lead isotope evolution by a two-stage model. *Earth and Planetary Science Letters* **26**, 207–221.
- Sun, S.-S. & McDonough, W. F. (1989). Chemical and isotopic systematics of oceanic basalts: implications for mantle composition and processes. In: Saunders, A. D. & Norry, M. J. (eds) *Magmatism in the Ocean Basins. Geological Society, London, Special Publications* **42**, 313–345.
- Turner, A. R., Wolfgram, D. & Barnes, S. J. (1985). Geology of the Stillwater county sector of the J-M Reef, including the Minneapolis adit. In: Czamanske, G. K. & Zientek, M. L. (eds) *Stillwater Complex, Montana: Geology and Guide. Montana Bureau of Mines and Geology, Special Publication* **92**, 210–231.
- Uken, R. & Watkeys, M. K. (1997). Diapirism initiated by the Bushveld Complex, South Africa. *Geology* **25**, 723–726.
- Van der Merwe, M. (2007). The occurrence of the critical zone along the exposed southeastern sector of the eastern Bushveld Complex. *South African Journal of Geology* **110**, 617–630.
- Vuollo, J. (1994). Palaeoproterozoic basic igneous events in Eastern Fennoscandian shield between 2.45 and 1.97 Ga, studied by means of mafic dyke swarms and ophiolites in Finland, 47 + 67 pp.
- Vuollo, J. & Huhma, H. (2005). Paleoproterozoic mafic dykes in NE Finland. In: Lehtinen, M., Nurmi, P. A. & Rämö, O. T. (eds) *Precambrian Geology of Finland—Key to the Evolution of the Fennoscandian Shield*. Amsterdam: Elsevier, pp. 195–236.
- Wagner, P. A. (1929). *The Platinum Deposits and Mines of South Africa*. Edinburgh: Oliver & Boyd, 326 pp.
- Wasserburg, G. J., Jacobsen, S. B., DePaolo, D. J., McCulloch, M. T. & Wen, T. (1981). Precise determination on Sm/Nd ratios, Sm and Nd isotopic abundances in standard solutions. *Geochimica et Cosmochimica Acta* **45**, 2311–2324.
- Weis, D., Kieffer, B., Maerschalk, C., Barling, J., de Jong, J., Williams, G. A., Hanano, D., Pretorius, W., Mattielli, N., Scoates, J. S., Goolaerts, A., Friedman, R. M. & Mahoney, J. B. (2006). High-precision isotopic characterization of USGS reference materials by TIMS and MC-ICP-MS. *Geochemistry, Geophysics, Geosystems* **7**, Q08006.
- Wilson, A. H. & Chaumba, J. B. (1997). Closed system fractionation in a large magma chamber: mineral compositions of the websterite layer and lower mafic succession of the Great Dyke, Zimbabwe. *Mineralogical Magazine* **61**, 153–173.
- Yang, S. H., Hanski, E., Li, C., Maier, W. D., Huhma, H., Mokrushin, A. V., Latypov, R., Lahaye, Y., O'Brien, H. & Qu, W. J. (2016). Mantle source of the 2.44–2.50 Ga mantle plume-related magmatism in the Fennoscandian Shield: evidence from Os, Nd and Sr isotope compositions of the Monchepluton and Kemi intrusions. *Mineralium Deposita* doi:10.1007/s00126-016-0673-9.